Project name:
Characterizing the Baseline Hydrogeochemistry of a Shallow Groundwater System in the Peace Region, Northeast BC

From:
Matt Martinolich M.Sc.
Dirk Kirste Ph.D.

To:
The BC Oil and Gas Research and Innovation Society (BCOGRIS)

Date:
December 3, 2022

Executive Summary

This report summarizes part of the M.Sc. Thesis completed by Matt Martinolich at Simon Fraser University (SFU) under the direct technical supervision of Dr. Dirk Kirste, Dr. Diana Allen, Dr. Laurie Welch, and external supervision of Dr. Dan Alessi (Martinolich, 2022).

In most areas that support resource development, such as the Peace Region (PR) of northeast BC, the natural (i.e., baseline) groundwater quality is poorly understood, limiting our ability to identify and assess groundwater quality impacts. This research utilized a paired multivariate/descriptive statistical–numerical hydrogeochemical modeling approach to characterize the baseline hydrogeochemistry the shallow (i.e., < 600 m BGS) groundwater system in the PR. Here, we discuss the PR's regional hydrochemical baselines, primary groundwater types, the regional distribution of groundwater types, and the results of a regionally extensive mineralogical XRD/SEM analysis. At the end of this report, an assessment of groundwater quality in a subregion of the PR (Lone Prairie) is presented, demonstrating the use of the hydrochemical baselines as a water quality assessment tool.

K-means cluster analysis was used to identify three primary water types in the unconsolidated groundwater system and three water types in the bedrock groundwater system. Water types in the unconsolidated groundwater system include Ca-HCO_3, Ca-Mg-HCO_3, and Ca-Mg-HCO_3-SO_4 types, with Ca-HCO_3 groundwater found in recharge areas, Ca-Mg-HCO_3 groundwater found throughout the entire region, and Ca-Mg-HCO_3-SO_4 groundwater found in and around paleovalleys and likely where groundwater from the bedrock mixes with groundwater in the sediments. Water types in the bedrock groundwater system include Na-Ca-Mg-HCO_3-SO_4, Na-HCO_3, and Na-SO_4-HCO_3 types, with Na-Ca-Mg-HCO_3-SO_4 likely occurring near the upper surface of the bedrock and in recharge areas, Na-HCO_3 groundwater occurring throughout the region, and Na-SO_4-HCO_3 groundwater occurring predominantly in the eastern part of the study area where gypsum is prevalent.

The XRD/SEM-EDS analysis determined that the regional mineralogy is dominated by quartz and illite/muscovite. Carbonate minerals, including magnesian calcite and dolomite, are relatively abundant in the sediments, and siderite is more abundant in the bedrock. XRD indicates that gypsum is present in relatively impermeable materials,

including diamicton mud, silt/clay, and mudstone/shale. During SEM, gypsum was only observed in a single shale sample collected near the upper surface of the bedrock, adjacent to pyrite crystals. Pyrite crystals are predominantly intragranular or coated by secondary minerals, implying that pyrite has little influence on the groundwater quality. Ultimately, the regional mineralogy is consistent among bedrock and sediment samples.

Comparing groundwater quality data collected in Lone Prairie to the PR's regional hydrochemical baselines showed that the baselines are robust and unlikely to change considerably after more hydrochemical data is added to the dataset. The baselines indicate that the groundwater quality in Lone Prairie is typical of the PR, with few anomalous groundwater quality parameters and relatively low to moderate major ion concentrations.

Contents

Executive Summary **1**
1. Introduction **4**
2. Background **4**
2.1. Hydrochemical Baselines 4
2.2. Multivariate Statistical Analysis 5
3. Study Area Description **5**
3.1. Physiography 5
3.2. Surficial Geology 7
3.3. Bedrock Geology 8
3.4. Hydrogeology 8
4. The SFU-EERI-FLNRORD Dataset **9**
5. Methodology **12**
5.1. Groundwater Quality Analysis 12
5.2. Characterizing the Regional Mineralogy 13
5.2.1. X-Ray Diffraction (XRD) Mineralogical Analysis 13
5.2.2. Scanning Electron Microscopy (SEM) Mineralogical Analysis 14
5.3. Defining Hydrochemical Baselines 14
5.4. Defining Primary Water Types and Mapping their Distribution 15
5.4.1. K-Means Cluster Analysis 15
5.4.2. Mapping Water Types in the Unconsolidated Groundwater System 17
5.4.3. Mapping Water Types in the Bedrock Groundwater System 18
6. Results **19**
6.1. Regional Mineralogy 19
6.2. Hydrochemical Baselines and Water Types in the Unconsolidated Groundwater System 24
6.3. Hydrochemical Map of the Unconsolidated Groundwater System 27
6.4. Hydrochemical Baselines and Water Types in the Bedrock Groundwater System 30
6.5. Hydrochemical Map of the Bedrock Groundwater System 33
7. Conceptual Hydrogeochemical Model of the Peace Region, Northeast BC **35**
8. Assessment of Groundwater Quality in Lone Prairie, Northeast BC **37**
9. Conclusions **41**
9.1. Regional Hydrochemical Baselines 41
9.2. Hydrochemical Mapping 42
10. Limitations **43**
10.1. The SFU-EERI-FLNRORD Dataset 43
10.2. K-Means Cluster analysis and Hydrochemical Mapping 43
11. Recommendations **44**
12. References **45**

13. Appendix A – XRD Mineralogy Results 48
14. Appendix B – The Hydrochemical Baselines of the Unconsolidated Groundwater System 50
14.1. Chemical Properties 50
14.2. Major and Minor Ion Concentrations 54
14.3. Isotopic Composition 68
14.4. Gas Concentrations 71
15. Appendix C – The Hydrochemical Baselines of the Bedrock Groundwater System 73
15.1. Chemical Properties 73
15.2. Major and Minor Ion Concentrations 77
15.3. Isotopic Composition 91
15.4. Gas Composition 94

1. Introduction

This report summarizes the M.Sc. Thesis completed by Matt Martinolich at Simon Fraser University (SFU) under the direct technical supervision of Dr. Dirk Kirste, Dr. Diana Allen, Dr. Laurie Welch, and external supervision of Dr. Dan Alessi. This research utilized a paired multivariate/descriptive statistical – numerical hydrogeochemical modeling approach to characterize the baseline hydrogeochemistry of a shallow (i.e., < 600 m BGS) groundwater system in the Peace Region (PR) of northeast BC. Here, we discuss the PR's regional hydrochemical baselines, primary groundwater types, the regional distribution of groundwater types, and the results of a regionally extensive mineralogical XRD/SEM analysis. Furthermore, a regional hydrogeochemical conceptual model is presented, as well as an assessment of groundwater quality in a subregion of the PR (Lone Prairie), demonstrating the use of the baselines defined in this research as a water quality assessment tool. This research was funded by the BC Oil and Gas Research and Innovation Society (BCOGRIS) and supported by the BC Oil and Gas Commission (BCOGC), the BC Ministry of Forests (BCMF; formerly known as the BC Ministry of Forests, Lands, Natural Resources, and Rural Development; BCFLNRORD), and the University of British Columbia's Energy and Environment Research Initiative (UBC-EERI). The numerical hydrogeochemical modeling and multivariate statistical components of this research are available in the full thesis located at the SFU library (Martinolich, 2022).

2. Background

2.1. Hydrochemical Baselines

Hydrochemical baselines are the chemical characteristics of a groundwater system, reflecting natural gas-water-rock interactions in the environment. Important baseline characteristics include chemical properties such as redox potential and pH, natural solute and gas concentration ranges, and the isotopic composition of groundwater. Furthermore, it is important to consider the regional mineralogy, as water-rock interactions often impart primary control over hydrochemical baselines. Hydrochemical baselines are defined by ranges rather than individual values because groundwater chemistry varies both spatially and temporally in the natural environment (Hem,

1989; Holland and Turekian, 2004; Appelo and Postma, 2005). The purpose of defining hydrochemical baselines is to establish guidelines for evaluating groundwater quality and detecting groundwater perturbed from its natural chemical state.

Defining hydrochemical baselines has been the focus of hydrogeochemical research throughout Europe and eastern Canada (e.g., Edmunds and Shand, 2008; Hamilton et al., 2011), but limited research has focused on defining the baseline hydrogeochemistry in areas that support oil and gas development. Research has shown that oil and gas activities can impact shallow groundwater quality (e.g., Jackson et al., 2013; Vengosh et al., 2014), and it is difficult to identify groundwater quality impacts without an understanding of the regional hydrochemical baselines. Ideally, a hydrogeochemical investigation will have been performed in a region prior to any resource development or land-use change, thereby allowing comparison of current and historical data during a groundwater quality assessment. Alternatively, hydrochemical baselines can be determined using statistical analyses and supported by numerical hydrogeochemical models. Ultimately, hydrochemical baselines aid groundwater monitoring, remediation, and reclamation programs, and government agencies use hydrochemical baselines to address groundwater quality concerns.

2.2. Multivariate Statistical Analysis

Multivariate statistical analysis (MSA) is a powerful tool for interpreting groundwater quality data because groundwater chemistry is often controlled by multiple chemical variables, and MSA allows for analysis of multiple chemical variables simultaneously. Many researchers have utilized multivariate statistical analyses such as linear discriminant analysis, principal component analysis, and variety of cluster analyses to reduce the complexity and allow for in-depth analysis of regional hydrochemical datasets (e.g., Steinhorst and Williams, 1985; Guler et al., 2002; Guler and Thyne, 2004; Cloutier et al., 2006; 2008). Cluster analyses have been used specifically to segregate large hydrochemical datasets, define primary water types, and construct hydrochemical maps. Cluster analysis is a broad group of multivariate statistical classification methods used to categorize objects defined by multiple independent variables (Davis, 1985).

3. Study Area Description

3.1. Physiography

The PR is situated east of the Rocky Mountains, between the BC-Alberta boundary and the Rocky Mountain Foothills (RMF). The PR spans the Alberta Plateau, Rocky Mountain Foothills, and the Interior Plains physiographic subdivision of BC (Church and Ryder, 2006). The study region consists of rolling hills, plains, and deeply incised river valleys (Mathews, 1978; Clague and Hartman, 2008). The study area is approximately 35,000 km^2 (**Figure 1**), and ground elevations range from approximately 400 to 1100 m ASL. The north study area boundary follows the border of the Beatton River watershed, and the southeast study area boundary runs along the border of the Kiskatinaw River watershed. The east study area boundary is the BC-Alberta border, and the west study area boundary follows the mapped extent of the Fort St. John Group, Dunvegan, and Kaskapau

formations adjacent to the RMFs. Near Chetwynd, the west study area boundary cuts across a small area of the Fort St. John Group.

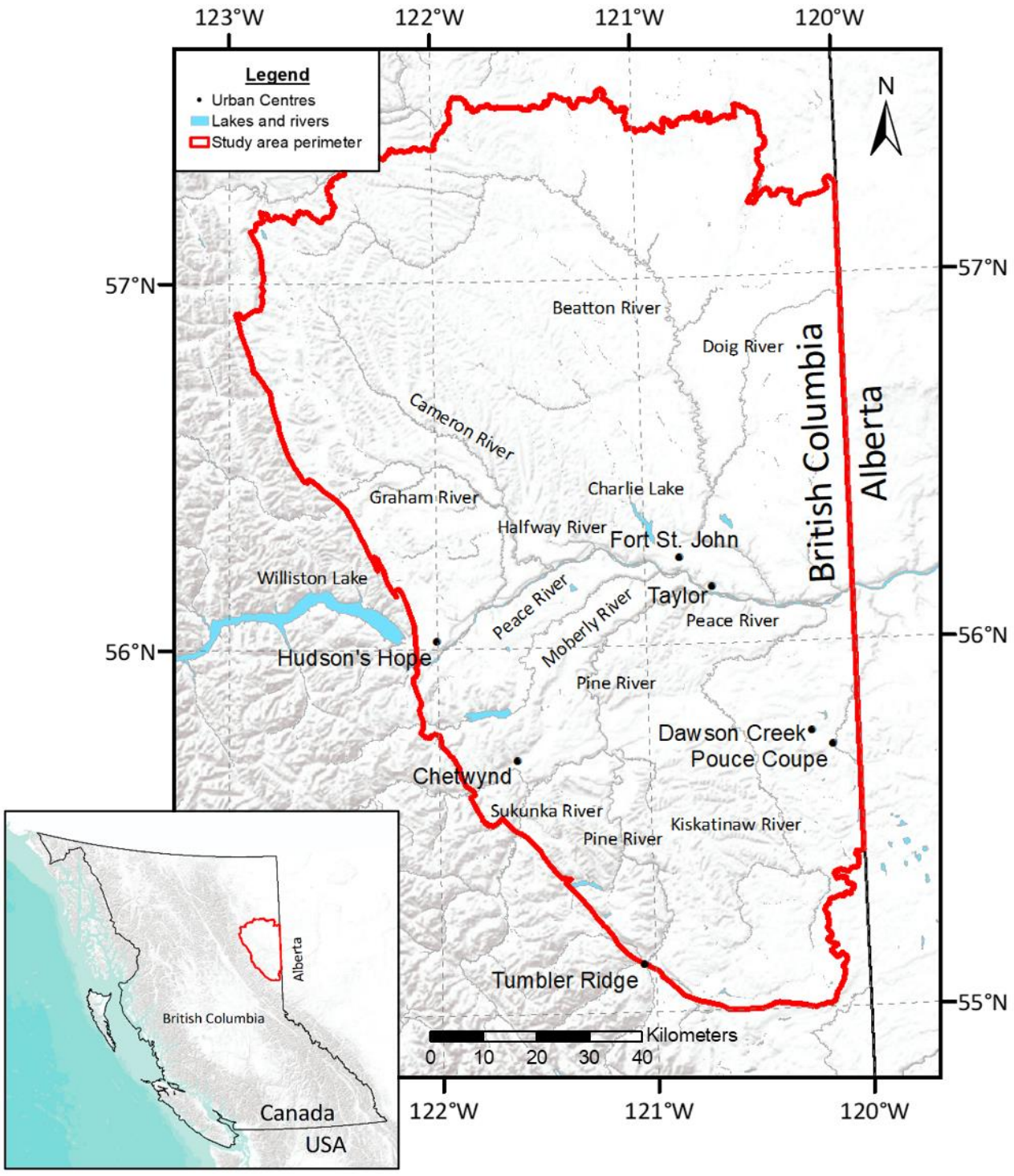

Figure 1. The study area, located in the Peace Region, northeast BC. The study area boundaries are delineated in red.

Population centers include Fort St. John, Dawson Creek, Pouce Coupe, Tumbler Ridge, Hudson's Hope, and Chetwynd. Three climate stations have recorded long-term climate data in the study region. These stations are in Chetwynd, Dawson Creek, and Fort St. John (Environmental Canada Climate Station IDs: 1181513, 1182289, and 1183001, respectively). The climate of the PR is continental, and the average daily temperature ranges from approximately -13 to 16°C. Winters are relatively long, cold, and dry, and rainfall peaks during relatively short summers. The region receives approximately 470 mm of precipitation annually; most of which occurs in the summer. The Peace River is the region's major river, flowing from Williston Lake into the Alberta Interior Plains. Rivers that converge with the Peace River include the Halfway, Moberly, Pine, Kiskatinaw, and Doig rivers.

3.2. Surficial Geology

Clague and Hartman (2008) describe the PR as a gently rolling plateau with complex glacial and interglacial surficial stratigraphy. Mathews (1978) suggests three distinct surficial features dominate the terrain:

1. Uplands with steep to rolling ridges, where the underlying bedrock controls the topography.
2. Flat river valleys and narrow river valleys that deeply incise the uplands.
3. Benches of low relief adjacent to incised valleys, which are distinguished from the uplands by their level topography.

Surficial strata in the PR are comprised of till, glaciofluvial and fluvial gravel, alluvium, colluvium, aeolian sand and silt, glaciolacustrine, and minor organic limestone deposits (Mathews, 1978; Catto, 1991; Hickin and Fournier, 2011; 2016; Clague and Hartman, 2008). Alluvial, glaciofluvial, and colluvial deposits are situated primarily in modern river valleys and lack interconnectivity at a regional scale. Aeolian deposits are situated mostly along the edges of modern river valleys but extend beyond the valley edges in some areas by several kilometers. Glaciolacustrine and till deposits are prevalent at the surface throughout most of the region.

A network of paleovalleys that predate the last three glaciations has been mapped and delineated (Clague and Hartman, 2008; Hickin, 2011; Hickin et al., 2016). The paleovalley fill consists of advance-phase glaciolacustrine sediments from glacial Lake Mathews, glacial sediments from the Late Wisconsinan glaciation, and retreat-phase glaciolacustrine sediments from glacial Lake Peace (Hickin et al., 2016). The paleovalley sediments are massive, and grain sizes vary substantially (Levson, 2015; Hicken et al., 2016). Paleovalley fill ranges in thickness up to approximately 500 m (Hickin, 2011). Core logging and results from shallow seismic reflection, ground-based electromagnetic, borehole gamma-ray, and airborne electromagnetic geophysical surveys indicate that permeable units in the paleovalleys are discontinuous and separated by thick confining layers (Hickin et al., 2016; Morgan et al., 2018).

Two Cordilleran and three Laurentide glacial advances have been interpreted in the Quaternary strata (Clague and Hartman, 2008), and the orientation/geomorphology of glacial landforms suggests that Laurentide and Cordilleran ice coalesced in the PR during the most recent glaciation (Hickin et al., 2016). Laurentide glacial drift deposits in the PR contain abundant pyrite because Laurentide ice advanced over pyrite-rich Mesozoic shale in the Western Canadian Sedimentary Basin (WCSB) (Grasby et al., 2010). Cordilleran till is abundant in carbonates

and contains minor anhydrite because Cordilleran ice advanced over Devonian carbonate and evaporite deposits in the Rocky Mountains (Grasby and Hutcheon, 2000; Grasby et al., 2010).

3.3. Bedrock Geology

The regional bedrock geology has been mapped and delineated (**Table 1**) (e.g., Jones, 1966; Stott, 1982; McMechan, 1994; Cowen, 1998). The bedrock consists of sedimentary rock deposited from the Paleozoic Era to the Tertiary Period, overlying Precambrian crystalline basement rock (BC Ministry of Natural Gas Development, 2011). Near-surface bedrock units include the Fort St. John Group, the Dunvegan Formation, and the overlying Smokey Group (Stott, 1982; McMechan, 1994). These bedrock units were deposited in the Cretaceous, along the western margin of the Western Interior Seaway (McMechan, 1994; Riddell, 2012). The depositional environment of the bedrock ranges from marginal marine to marine or deltaic, and bedrock units range in thickness from centimetres to tens of metres (Rutherford, 1930; Stott, 1982). Except for the Dunvegan Fm., near-surface bedrock units are defined by transgressive and regressive sequences. The Dunvegan Formation is a heterogenous deltaic complex that includes shale, fine-grained to conglomeratic sandstone, and pebble to boulder conglomerate (Stelck and Wall, 1955; Stott, 1982; Bhattacharya and Walker, 1991; Plint, 2003). Non-marine sandstone and conglomerate in the Dunvegan Fm. are prevalent in the northwest, whereas fine-grained sandstones and shale are more common in the southeast (Stott, 1982).

Table 1. Shallow bedrock substrates in the Peace Region, northeast BC.

Period	Group	Formation	[1] Lithology
Upper Cretaceous	Smokey	Wapiti	Sandstone, mudstone
		Puskwaskau	Marine shale, siltstone
		Badheart/Marshybank	Sandstone, shale
		Muskiki	Marine shale
		Cardium	Sandstone
		Kaskapau	Marine shale, interbedded shale, and sandstone
	Dunvegan Formation		Conglomerate, sandstone, shale, siltstone
	Fort St. John	Sulley (north of the Peace River), Shaftesbury (south of the Peace River)	Marine and non-marine shale, siltstone
Lower Cretaceous			

[1]Lithological descriptions were obtained from Stott (1982) and Cowen (1998).

3.4. Hydrogeology

The PR is situated in BC's Western Plains Hydrogeological Region, supporting both a bedrock groundwater system and an unconsolidated groundwater system. Surficial aquifers are composed of fluvial, colluvial, and alluvial gravel deposits in modern river valleys and discontinuous lenses of sand and gravel in the uplands. The paleovalley

network accommodates buried valley and inter-till aquifers composed primarily of glaciofluvial/fluvial sediments (Lowen, 2011). Glaciolacustrine and till/diamicton confining layers are regionally extensive at the surface, ranging from metres to tens of metres in thickness (Hickin and Fournier, 2011; Cummings et al., 2012; Baye et al., 2016). Such confining layers limit recharge to approximately 2-33 mm/year (Holding and Allen, 2016).

The bedrock groundwater system consists of heterogeneous sandstone aquifers and shale confining units (Baye et al., 2016). Moreover, Nastev et al. (2005) estimate that the upper 30 to 50 m of the bedrock has considerable secondary porosity, and Lowen (2011) and Riddell (2012) believe the fractured upper surface of the bedrock supports a regional-scale aquifer. Compared to surficial aquifers in the PR, the bedrock aquifers are more laterally extensive and provide a more reliable groundwater despite being incised in several areas by major rivers. Most bedrock aquifers are situated in the Dunvegan and Kaskapau formations, and the Fort St John Group consists mainly of shale confining layers.

Allen (2021) used the bulk chemistry of geologic materials in the PR to define seven hydrostratigraphic units (HSUs), summarized in **Table 2**. Allen (2021) indicates that all HSUs have similar bulk compositions despite variations in grain size.

Table 2. Hydrostratigraphic Units (HSUs) in the PR (Allen, 2021).

Groundwater system	HSU	
Unconsolidated	Aquifers	Silty sand
		Sandy gravel
	Confining Units	Clayey silt
		Diamicton
Bedrock	Aquifers	Sandstone
	Confining Units	Shale
		Shale and mudstone

4. The SFU-EERI-FLNRORD Dataset

Before this research, 397 groundwater samples, 61 stream samples, and 85 rain and snow samples were collected throughout the PR, during the Private Wells Network Sampling Program (PWNSP). The water samples were collected by researchers at SFU, the UBC-EERI, and the BCMF (formerly BCFLNRORD). The “SFU-EERI-FLNRORD dataset” consists of 252 groundwater samples collected from bedrock aquifers and 145 samples collected from unconsolidated aquifers. In total, groundwater samples were collected from 315 unique locations.

Groundwater samples collected from the sediments were referred to as “NEBC 1” samples, whereas groundwater samples collected from the bedrock were referred to as either “NEBC 2’ and “NEBC 3” samples depending on their $\delta^{2}H$-$\delta^{18}O$ stable isotopic composition; groundwater samples with depleted stable isotopic signatures (i.e., <

185 ‰ δ^2H and < -23.5 ‰ $\delta^{18}O$ VSMOW) were classified as NEBC 3 samples. It is important to note that there is very little well depth information available in the SFU-EERI-FLNRORD and BC GWELLS datasets, so groundwater samples collected from the bedrock and sediments were differentiated primarily by their sodium concentrations. In some cases, they were differentiated based on available drilling logs. The distribution of groundwater samples collected throughout the PR is shown in **Figure 2**.

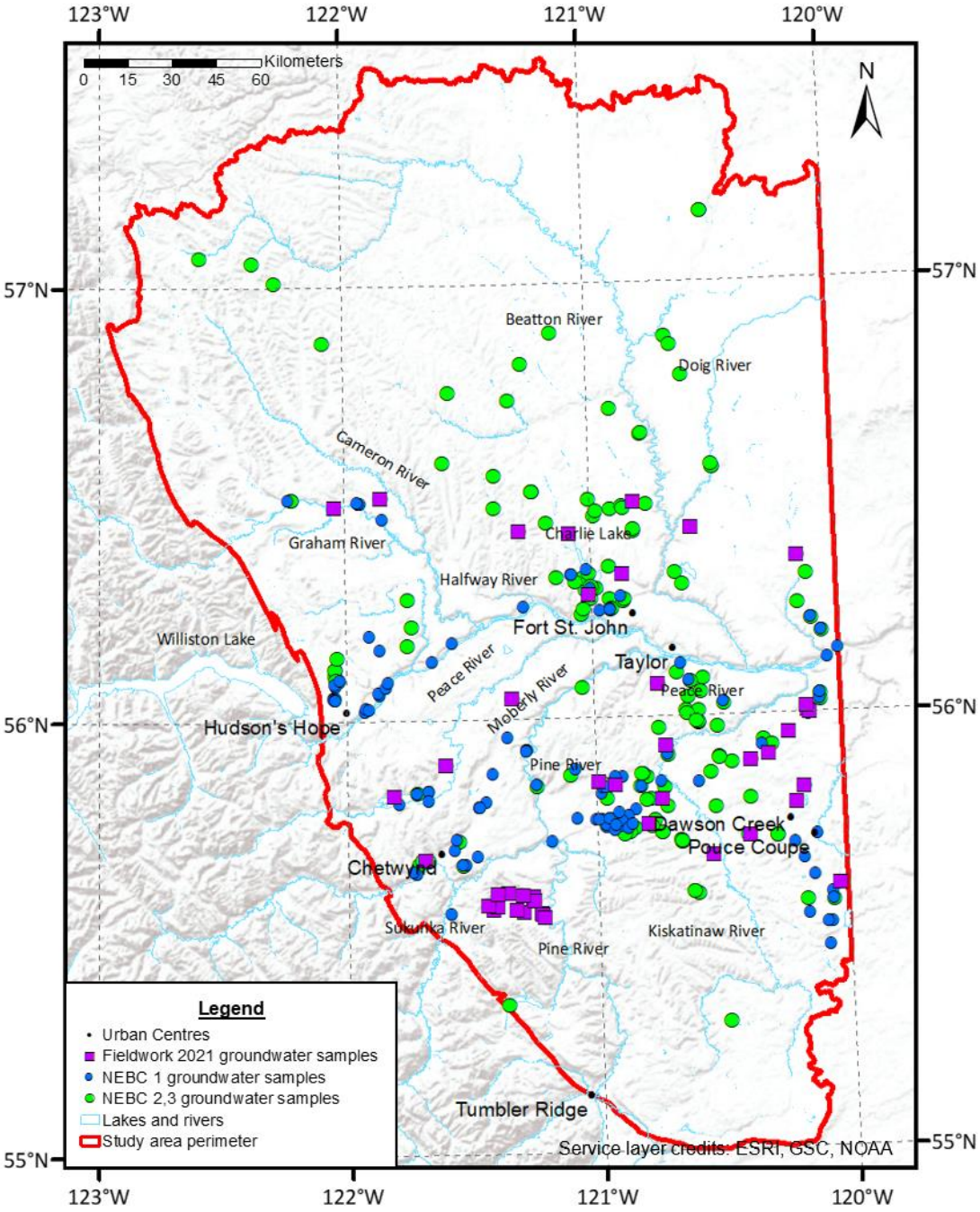

Figure 2. The regional distribution of groundwater samples in the SFU-EERI-FLNRORD dataset collected in the PR from 2011 to 2022.

For this research, fieldwork was conducted from July 26th to August 11th, 2021, and 44 groundwater samples were collected (see **Figure 2**). Of the 44 samples, 43 were collected from unique locations, and 25 were collected from the EERI Groundwater Monitoring Well Network. The remaining 19 samples were collected from domestic wells. Fifteen of the 19 groundwater samples were collected in Lone Prairie (LP), approximately 25 km southeast of Chetwynd (**Figure 3**). An effort was made to collect groundwater samples in LP because no groundwater samples were collected there in the past, and few oil and gas wells are situated there.

An additional 24 groundwater analytical results were sourced from the Provincial Groundwater Observation Well Network (PGOWN), and 14 groundwater analytical results were acquired from the BCOGC. Four groundwater analytical results were sourced from the Northern Health database (NH). Groundwater data sourced from the PGOWN, BCOGC, and NH were collected between 1985 and 2018 and only contain major ion concentration data.

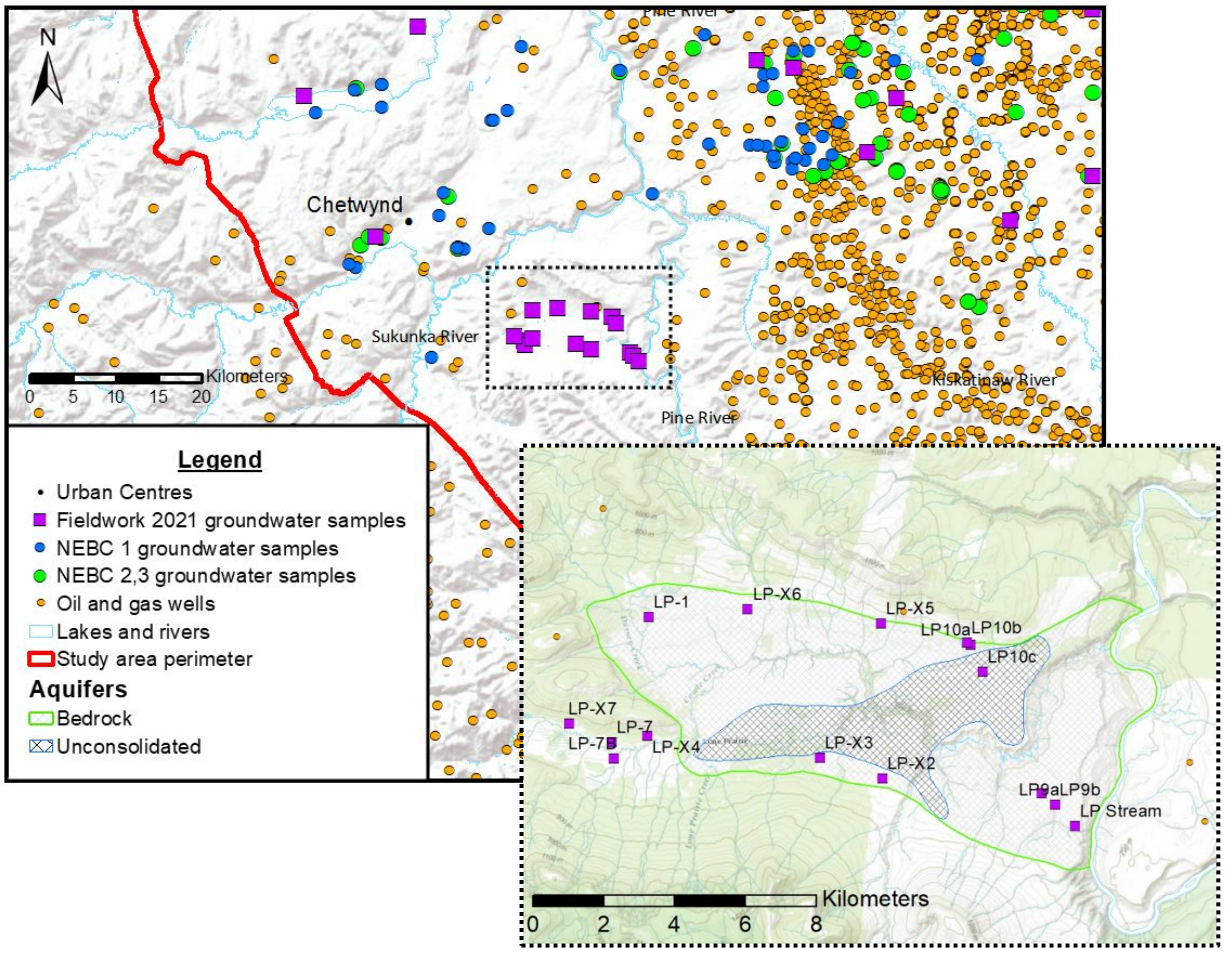

Figure 3. The distribution of oil and gas wells, aquifers, and groundwater samples collected in Lone Prairie, northeast BC.

5. Methodology

5.1. Groundwater Quality Analysis

Most groundwater samples in the SFU-EERI-FLNRORD dataset were collected from domestic wells, and some were collected from the EERI Groundwater Monitoring Well Network. Private well water samples were collected from taps or access points as close to the source well as possible. Water treatment systems (e.g., filters, reverse osmosis, etc.) were avoided by collecting the sample from a pre-treated access point. Groundwater samples collected from EERI monitoring wells were collected using a Grundfos 3-inch submersible pump or a Geotech Series II peristaltic pump. At each sample site, in-situ parameters were measured with Thermo-Orion Star A325 and A329 Multimeters and probes suspended in an Eijkelkamp flow-through cell. Groundwater samples were collected after the oxidation-reduction potential (ORP), dissolved oxygen (DO), pH, electrical conductivity (EC), and temperature of the groundwater stabilized. All groundwater samples were filtered through a Waterra 0.45 µm inline filter and collected in four triple-rinsed Nalgene bottles ranging in volume. Alkalinity titrations were performed in triplicate at each sample site, using 0.1 molar HCl, a Hach digital pipette, and methyl orange pH indicator. Sample volumes and preservation methods are summarized in **Table 3**. The four bottles of groundwater were used for six separate analyses. Data collected from each sample and the analytical equipment used for each analysis are summarized in **Table** 4.

Table 3. Sample volumes and post-filtering preservation methods.

Sample volume	Analysis	Preservation method	Purpose
1.0 L	Tritium	None	
0.5 L	Carbon and oxygen isotopes	~ 2 mL NaOH, ~1.0 g $SrCl{\cdot}6H_2O$	Increase pH, so any dissolved CO_2 forms bicarbonate acid, then $SrCl{\cdot}6H_2O$ is added to precipitate strontium carbonate for the analysis.
0.25 L	Anions and stable isotopes	None	
0.125 L	Cations	~ 2 mL 70% reagent grade HNO3	Prevent any material from precipitating.

Table 4. Groundwater analytical methods.

Data (collected from 2011-2022)		Method of analysis
Physical properties	UTM coordinates, ground elevation, limited hydraulic head data	GPS, Water level probe
Chemical properties	Temperature, pH, EC, redox potential (Eh), dissolved oxygen (DO), Bicarbonate alkalinity	Thermo-Orion Star A325 and A329 Multimeters, Digital alkalinity titration
Ammonia	NH_4^+	Hach DR2800 Spectrophotometer
Major and minor anions	F^-, Cl^-, NO_3^-, PO_4^{-2}, SO_4^{-2}	Dionex ICS-3000 Chromatography System (anions) (SFU)

Major and minor elements	Ca, Mg, Na, K, Si, Fe, Mn, Mg, B, Ba, Li, Mo, S, Sr, Zn	Horiba Jobin Yvon Ultima 2 Inductively Coupled Plasma Atomic Emission Spectrometer (SFU), Thermo Scientific iCAP Inductively Coupled Plasma Mass Spectrometer (ICP-MS) (SFU)
Minor and trace elements	Li, Be, Al, Sc, V, Cr, Co, Ni, Zn, Ga, As, Se, Rb, Sr, Zr, Ag, Cd, Sb, Cs, Ba, La, Ce, Pr, Nd, Sm, Eu, Gd, Tb, Dy, Ho, Er, Tm, Yb, Lu, Tl, Pb, Bi, Th, U	
Major, minor, and trace elements	Limited: Li, Be, B, Na, Mg, Al, Si, S, K, Ca, Sc, V, Cr, Mn, Fe, Co, Ni, Cu, Zn, Ga, As, Se, Rb, Sr, Zr, Ag, Cd, Sb, Cs, Ba, La, Ce, Pr, Nd, Sm, Eu, Gd, Tb, Dy, Ho, Er, Tm, Yb, Lu, Tl, Pb, Bi, Th, U	Agilent 8800 Triple Quadrupole ICP-MS Trent University Water Quality Centre
Stable isotopes	$\delta^{18}O$, $\delta^{2}H$, $\delta^{13}C$, ^{13}C-CO_2, ^{13}C-CH_4 Limited: ^{34}S, ^{18}O-SO_4, ^{15}N	LGR DLT-100 Liquid Water Laser Isotope Analyzer (SFU Geochemistry Lab, Isotope Science Lab of the University of Calgary), Thermo-Finnigan Delta V Isotope Ratio Mass Spectrometer (Isotope Science Lab of the University of Calgary, Ján Veizer Stable Isotope Laboratory University of Ottawa), Enrichment and Liquid Scintillation Counting (AE Lalonde AMS Laboratory University of Ottawa), Accelerator Mass Spectrometry (AE Lalonde AMS Laboratory University of Ottawa), Enrichment and Low-Level Gas Proportional Counting (The Tritium Laboratory University of Miami)
Radionuclides	^{14}C, ^{3}H	
Gas composition	He, O_2, N_2, CO_2, CH_4, C_2H_6, C_3H_8	Gas Chromatography (Applied Geochemistry Lab University of Calgary)
[1]Aquifer Materials data	Bedrock formation, screened interval materials	BC WELLS database, Northeastern Water Tool (NEWT)

[1]Relatively high uncertainty in aquifer materials data.

5.2. Characterizing the Regional Mineralogy

Mineralogical data were sourced from X-ray diffraction analysis (XRD), petrographic optical microscopy, scanning electron microscopy (SEM-EDS), and whole-rock analysis (WR). The WR analysis was performed by Allen (2021). Geological materials used in the mineralogical analysis were sourced from drill cuttings during sonic and rotary drilling of the EERI Groundwater Monitoring Well Network. Sediment and bedrock samples were collected in 5 ft. intervals.

5.2.1. X-Ray Diffraction (XRD) Mineralogical Analysis

Sixty-three rock (21) and sediment (42) samples were sent to the University of British Columbia Electron Microbeam & X-Ray Diffraction Facility (EMXDF) for XRD analysis. The rock and sediment samples were segregated into seven categories: clay/silt, diamict-mud, diamict-sand, mudstone, sandstone, sandy gravel, and silt/sand. Shale samples were lumped with mudstone samples, and sand samples were lumped with silt/sand. The rock and sediment samples were mounted as-is into Bruker back-loading specimen holders. Continuous-scan X-ray powder-diffraction data were collected over a range 3-80°2θ with CoKα radiation on a Bruker D8 Advance

Bragg-Brentano diffractometer equipped with an Fe filter foil, 0.6 mm (0.3°) divergence slit, incident- and diffracted-beam Soller slits and a LynxEye-XE detector. The long fine-focus Co X-ray tube was operated at 35 kV and 40 mA, using a take-off angle of 6°". The X-ray diffractograms were analyzed using the International Centre for Diffraction Database PDF-4 and Search-Match software by Bruker. Moreover, the X-ray powder diffraction data of the samples were refined with the Rietveld program, Topas 4.2 (Bruker AXS).

5.2.2. Scanning Electron Microscopy (SEM) Mineralogical Analysis

An FEI Explorer scanning electron microscope (SEM) with energy-dispersive X-ray spectroscopy (EDS) was used to investigate the solid-solution chemistry of minerals in 23 resin pucks and four polished thin sections constructed from geological materials recovered during drilling of the EERI Groundwater Monitoring Well Network. The SEM-EDS analysis was performed at 4DLabs, in SFU, Burnaby, BC. Sediment samples were used to construct the resin pucks, and four bedrock core samples (three sandstone and one mudstone) were used to construct polished thin sections. Resin pucks were constructed from clay/silt, diamict-mud, diamict-sand, sandy gravel, and silt/sand samples. Geologic materials used for SEM were dried for 24 hours at ~50°C, then the dried material was sieved to extract sand, silt, and clay grains. The resin pucks and polished thin sections were constructed at Precision Petrographics Ltd., in Langley, BC.

An effort was made to perform SEM on the same geologic materials analyzed via XRD and WR, but many samples were consumed entirely for the XRD and WR analyses. If a sample had been consumed for XRD and WR analysis, geological materials from the nearest sampled interval were selected for SEM analysis, on the condition that the material in the adjacent interval matched the geological description of the target interval. The SEM electron beam can induce a charge in polished thin sections, interfering with the electron beam, diminishing image quality, so the polished thin sections were carbon-coated using 4DLabs Leica EM ACE600 high vacuum coating system. Each sample was coated with approximately 8-10 nm of carbon. Resin pucks were constructed with a carbon-rich epoxy to prevent charging, but some charging is evident in SEM images at relatively high magnification. High-resolution images were collected using the SEM's gaseous analytical detector (GAD).

5.3. Defining Hydrochemical Baselines

Edmunds and Shand (2008) recommend quantifying hydrochemical baselines using cumulative distribution plots (CDPs) and/or boxplots. Here, "Martinolich plots" that consist of a CDP and boxplot merged into one figure are used to illustrate the full range of chemical component values, their range excluding outliers, their interquartile range (IQR), and their median values. Edmunds and Shand (2008) suggest that hydrochemical baselines should be quantified using non-outlying data (2.5^{th} to 97.5^{th} percentiles), but the CDPs show the full range of data for reference. The boxplots show values between the 2.5^{th} and 97.5^{th} percentiles, median values, and the IQR. Median values are reported because many chemical component distributions are log-normal, exponential, or follow a power function. For such distributions, the median better approximates the data center (Davis, 1985).

Groundwater samples collected from the bedrock and sediments were separated to characterize the baseline hydrochemistry of the unconsolidated and bedrock groundwater systems independently. In the case of duplicate

samples, the most recently collected samples were analyzed, and the rest were excluded. Using the Anderson-Darling goodness-of-fit test, the data distributions were tested for goodness-of-fit to four distributions: normal, log-normal, exponential, and a power function. The tested distribution that resulted in the highest p-value was reported, and a respective trendline is plotted in each CDP.

Arsenic concentrations in groundwater in the sediments and bedrock are only represented with boxplots because the range of arsenic concentrations varies over five orders of magnitude and cannot be displayed effectively in a CDP. For the same reason, only a boxplot is shown for methane concentrations in the bedrock.

5.4. Defining Primary Water Types and Mapping their Distribution

5.4.1. K-Means Cluster Analysis

Cluster analysis is a broad group of multivariate statistical classification methods used to categorize objects defined by multiple independent variables (Davis, 1985). Cluster analysis is a powerful tool because it can analyze the similarity of several chemical constituents and properties simultaneously. For this research, K-means clustering (KMC) was used to categorize groundwater samples collected from the sediments and bedrock independently. KMC is a form of cluster analysis that utilizes machine learning and is built upon the concept of Expectation-Maximization. KMC utilizes Euclidean Distance as a statistical distance metric and requires the user to select the number of groups/clusters to categorize data. The KMC algorithm segregates objects (e.g., water samples) into clusters by minimizing the sum of the squared “distances” between the objects and cluster centroids. The KMC algorithm operates by 1) randomizing the dataset and constructing centroids based on the predefined number of clusters, 2) adding each object to the cluster with the “nearest” centroid, and 3) iterating steps (1) and (2) with new centroid cluster positions until the same centroids form repeatedly. The KMC objective function is as follows (Sharma, 2019):

Equation 5-1:
$$J = \sum_{j=1}^{k} \sum_{i=1}^{n} \left\| x_i^j - \mu_j \right\|^2$$

where:

- J is the objective function.
- k is the number of clusters.
- n is the number of objects.
- X_i^j is object i of cluster j.
- μ_j is the centroid of cluster j.

Because KMC uses a statistical distance metric, before performing the analysis, the data need to be standardized to z-scores. This step is performed so that data with relatively large magnitudes, such as EC, do not dominate the

analysis. In other words, converting the data into z-scores allows variables with different units can be included in the same analysis. Z-scores are calculated by subtracting each variable by the variable mean and dividing by the standard deviation.

There is no statistical metric for determining the optimal number of clusters. However, the cluster analysis results can be evaluated based on knowledge of the study area or a conceptual hydrogeochemical model and supported by hydrochemical plots such as Piper plots (Piper, 1944) and Stiff diagrams (Bach, 1961). For example, the mean/median major ion concentrations of each cluster can be used to construct Stiff diagrams, thereby providing a visual indication of how the clusters differ chemically. Based on understanding of the regional geology and the variability in average cluster compositions, it can be inferred if more or fewer water types are appropriate. Alternatively, the ideal number of clusters can be inferred by using GIS to interpolate the spatial distribution of cluster analysis results in order to compare the regional water type distribution to the hydrogeological features of the study area (Guler et al., 2002; Guler and Thyne, 2004).

Compared to the total number of groundwater analytical results in the SFU-EERI-FLNRORD dataset, the number of analytical results included in the KMC analysis was relatively low. Of the 316 groundwater samples collected from the bedrock; 105 samples were included in the cluster analysis. Of the 171 groundwater samples collected from the sediments, 89 were included. The relatively low number of samples is due to duplicate samples and outliers that were excluded.

Because cluster analysis requires a complete dataset (no missing variable values) and several groundwater samples were not measured for trace elements, gas, and minor ion concentrations, most chemical variables were excluded. Ultimately, one chemical property (EC) and six chemical components, including calcium, sodium, sulphate, bicarbonate, magnesium, and potassium, were included in the KMC analysis. Chloride was excluded from the KMC analysis because it shows no spatial patterns in the study area, and there is no geological source of chloride in the unconsolidated groundwater system. Additionally, the chloride data contain an exceptionally high number of outliers. pH was excluded from the analysis because it shows relatively low variability throughout the study area. Eh was excluded because it is sensitive to changes in depth and often exhibits disequilibrium. Temperature was excluded from the analysis because it is influenced by depth and varies seasonally. Ten groundwater samples included in the analysis were missing EC data, but the missing EC values were calculated in GWB using the major ion chemistry and TDS of the samples.

Outliers were detected using JMP 16's "Robust Fit Outliers" function, which distinguishes outliers as data situated "far" from the center of a column of data based on the range of data in the column (SPS Institute, 2019). The Robust Fit Outliers function utilizes Huber M-Estimation (Huber and Ronchetti, 2009) to estimate the center and variability of the data. The user selects a "K-value" multiplied by the estimated spread value to define the cut-off for outlying samples. The default K-value (4) was used for the analysis. Using a K-value of 3 resulted in a relatively high number of outliers. Samples containing an outlier were excluded from the analysis, however, in one case, an outlying groundwater sample (MM-EERI-9) that exhibited highly elevated sulphate concentrations and was

removed from the analysis, but its sampling location was considered when constructing the hydrochemical map of the unconsolidated groundwater system.

5.4.2. Mapping Water Types in the Unconsolidated Groundwater System

Delineating areas in the unconsolidated groundwater system with distinct groundwater chemistry relied on interpretation of the following:

- Regional topography
- Groundwater divides, i.e., topographic divides and major rivers
- The total number of samples in each group/cluster
- Sample distribution and density
- The distribution of surficial materials
- The paleovalley network

A goal of the mapping objective was to extrapolate the results to areas with limited data density so the maps can be used as predictive tools. As such, the water type characterized by the cluster attributed the most groundwater samples was extrapolated throughout the region, and areas with water types characterized by the remaining clusters were delineated manually.

Groundwater sample density throughout the region is very low (approximately 1 sample per 110 km^2), so drawing polygons that contain groundwater samples belonging to a single water type/cluster was not possible. Moreover, there is very little well depth information available in the SFU-EERI-FLNRORD dataset, which makes understanding the distribution of water types very challenging. For example, in some areas, the map shows relatively evolved groundwater upstream of less evolved (more dilute) groundwater, and what could falsely be interpreted as a chemical evolution, may just be groundwater samples collected from wells completed in different aquifers. Ultimately, there is significant uncertainty in the distribution of the polygons, so it is emphasized that the maps produced in this research are interpretive.

Polygons of relatively permeable sedimentary units (e.g., alluvium, colluvium, etc.) and confining materials such as glaciolacustrine and till deposits were clipped from the regional surficial geology map available on the BC Data Catalogue. and integrated into the hydrochemical map because they likely influence groundwater flow. The relatively permeable units were coloured to match the water types in each area because they are likely aquifers. The paleovalleys shapefile was also included in the map because the structure of the paleovalleys is inferred to influence the groundwater flow regime in both the sediments and bedrock. This interpretation is supported by groundwater flow modeling, which indicated that buried valley aquifers (at the base of the paleovalleys) receive 99% of their recharge from the underlying and adjacent bedrock (Goetz et al., 2021). Relatively saline groundwater from the bedrock is likely to migrate into the paleovalley sediments, producing an evolved groundwater chemical signature in the sediments.

5.4.3. Mapping Water Types in the Bedrock Groundwater System

Delineating areas in the bedrock groundwater system with distinct groundwater chemistry relied on interpretation of the following:

- Regional bedrock topography (where the upper surface of the bedrock has been mapped/interpolated
- The paleovalley network
- The hydrogeochemical conceptual model
- Sample distribution and density
- The glacial history and mineralogy of glacial drift deposits in the PR

The regional bedrock topography was considered because it has been weathered mechanically during several glaciations, exhibits secondary porosity, and likely permits relatively rapid groundwater flow. The bedrock is comprised predominantly of tilted, interbedded shale and sandstone units, which may impart a structural control over groundwater flow patterns where the bedrock is still competent. However, the paleovalley network incises the bedrock, producing potentiometric lows in hydraulic connection with the bedrocks fractured upper surface.

Because the bedrock groundwater system is paleomarine, Na-HCO_3 groundwater can likely be found anywhere in the region if a well is completed deep enough into the bedrock. Groundwater near the upper surface of the bedrock is more likely to be mixed with groundwater from the sediments and is also more likely to exhibit elevated sulphate due to the presence of authigenic gypsum. Conceptually, it is logical to extrapolate an Na-HCO_3 groundwater type throughout the region. Additionally, the glacial history and mineralogy of glacial drift deposits in the PR impacted the delineation of the hydrochemical polygons, as Laurentide glacial drift deposits are predominant in the eastern PR and are known to produce authigenic gypsum via pyrite oxidation. Gypsum mineral dissolution results in elevated sulphate concentration, so delineating a high-sulphate groundwater type in the eastern PR is also supported by conceptual understanding of the PR.

The hydrochemical map of the bedrock was constructed in the same qualitative way as the map of the unconsolidated groundwater system. In some areas, all water types occur within close lateral proximity, likely reflecting the depth dependence of the groundwater chemistry. Ultimately, an Na-HCO_3 water type was extrapolated throughout the region, and polygons were delineated in areas relatively abundant in other water types. As described above, it is emphasized that the maps produced in this research are interpretive, and a different water type may be encountered in an area where a non-representative hydrochemical polygon was delineated. The maps are likely to evolve over time, as more hydrogeological infrastructure is developed, and more groundwater samples are collected.

6. Results

6.1. Regional Mineralogy

The average regional mineral abundances determined via XRD are plotted in **Figure 4**, and the full list of results are tabled in **Appendix A**. The XRD results indicate that quartz is the dominant mineral among each rock/sediment type, followed by illite/muscovite. The most common silicates are clinochlore (a magnesium-rich chlorite mineral), k-feldspar, plagioclase, and potentially muscovite. XRD cannot resolve muscovite from illite, but petrographic microscopy confirmed the presence of abundant mica grains (Martinolich, 2022). Common aluminosilicates include illite and kaolinite. Carbonate minerals including calcite, dolomite, and ankerite, are considerably more abundant in the sediments (**Figure 4**), and siderite is relatively abundant in the bedrock. Pyrite is slightly more abundant in the bedrock, particularly in mudstone/shale, ranging as high as high as 5.1 wt.%. Gypsum was not observed in sandstone and is more common in mudstone/shale.

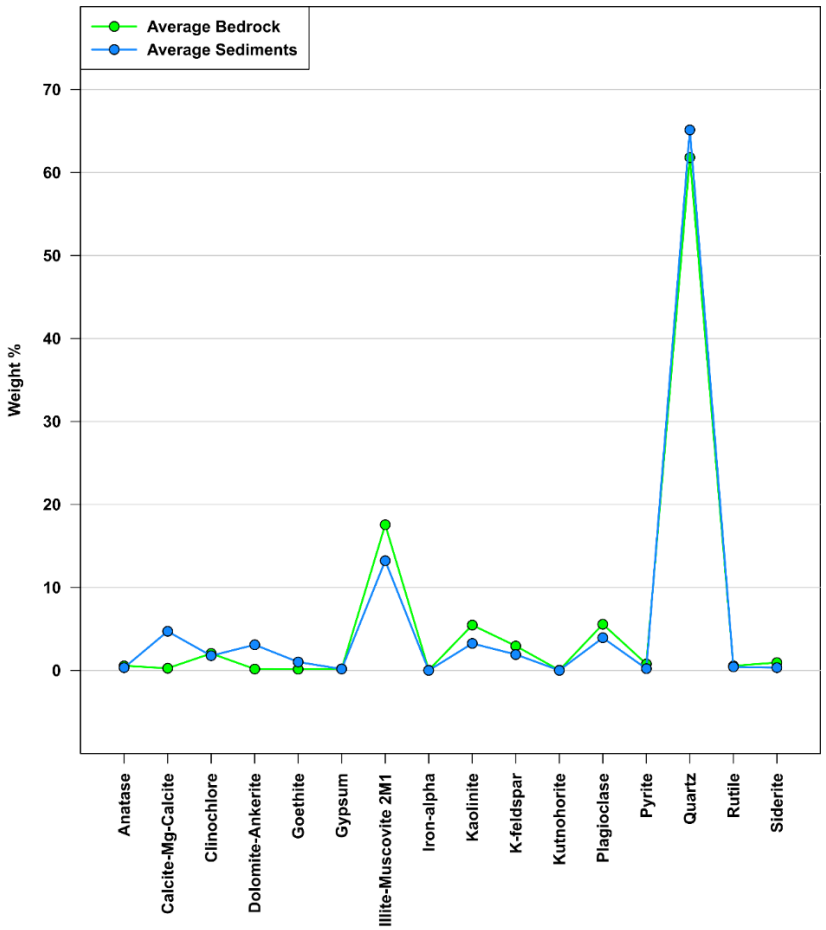

Figure 4. Average XRD results by weight %. Average weight % values were calculated from XRD analysis of 42 sediment samples and 21 rock samples

SEM results indicate that carbonate minerals often contain magnesium, iron, potassium, and silica. **Figure 5** shows an SEM-EDS image of a magnesian calcite crystal. The EDS spectra shows a relatively large magnesium peak, confirming the presence of magnesium in the calcite crystal structure. Calcite grains of this composition were commonly observed in the sediment samples. Another spectral peak is visible for silica, indicating silica is in a solid solution with calcium and magnesium. A small spectral peak is visible to the right of the silica peak and may indicate the presence of strontium.

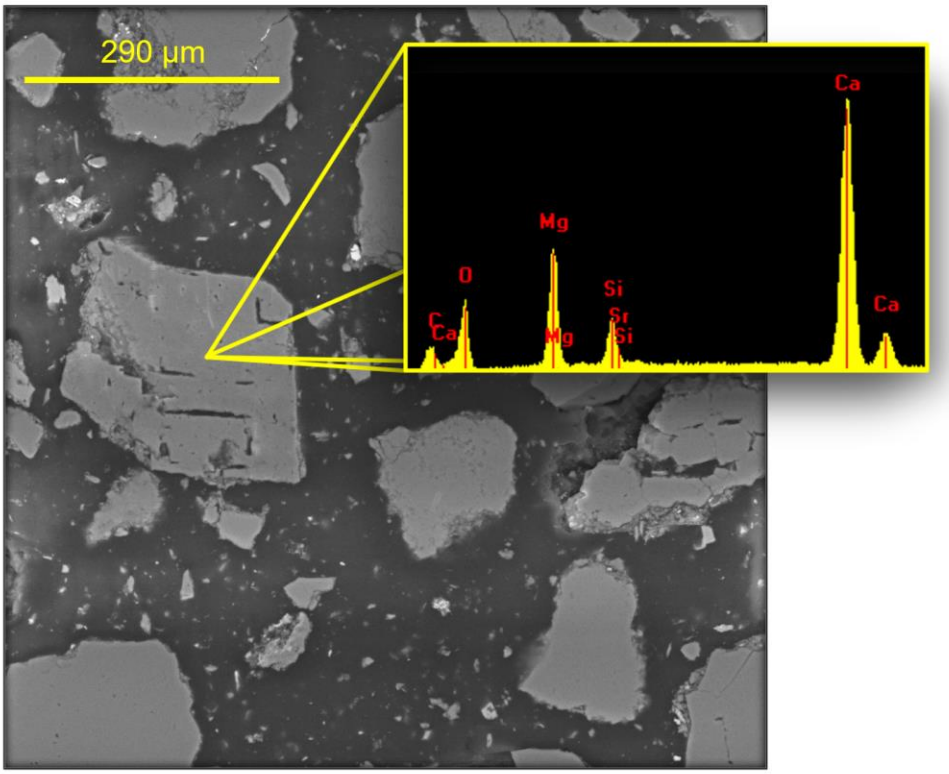

Figure 5. SEM-EDS image of magnesian calcite (250x magnification). The yellow inset shows the EDS spectra from a rhombic magnesian calcite crystal. Spectral peaks are shown for calcium oxygen, magnesium, silica, and potentially strontium.

The SEM-EDS analysis indicated that chlorite often exhibits elevated iron and magnesium, and plagioclase grains often contain calcium. Many plagioclase minerals have sodium/calcium ratios in the range of andesine/oligoclase. Moreover, the SEM images show that pyrite is abundant in the sediments but is mainly intragranular with respect

to siderite, calcite, magnesian calcite, or feldspar crystals (

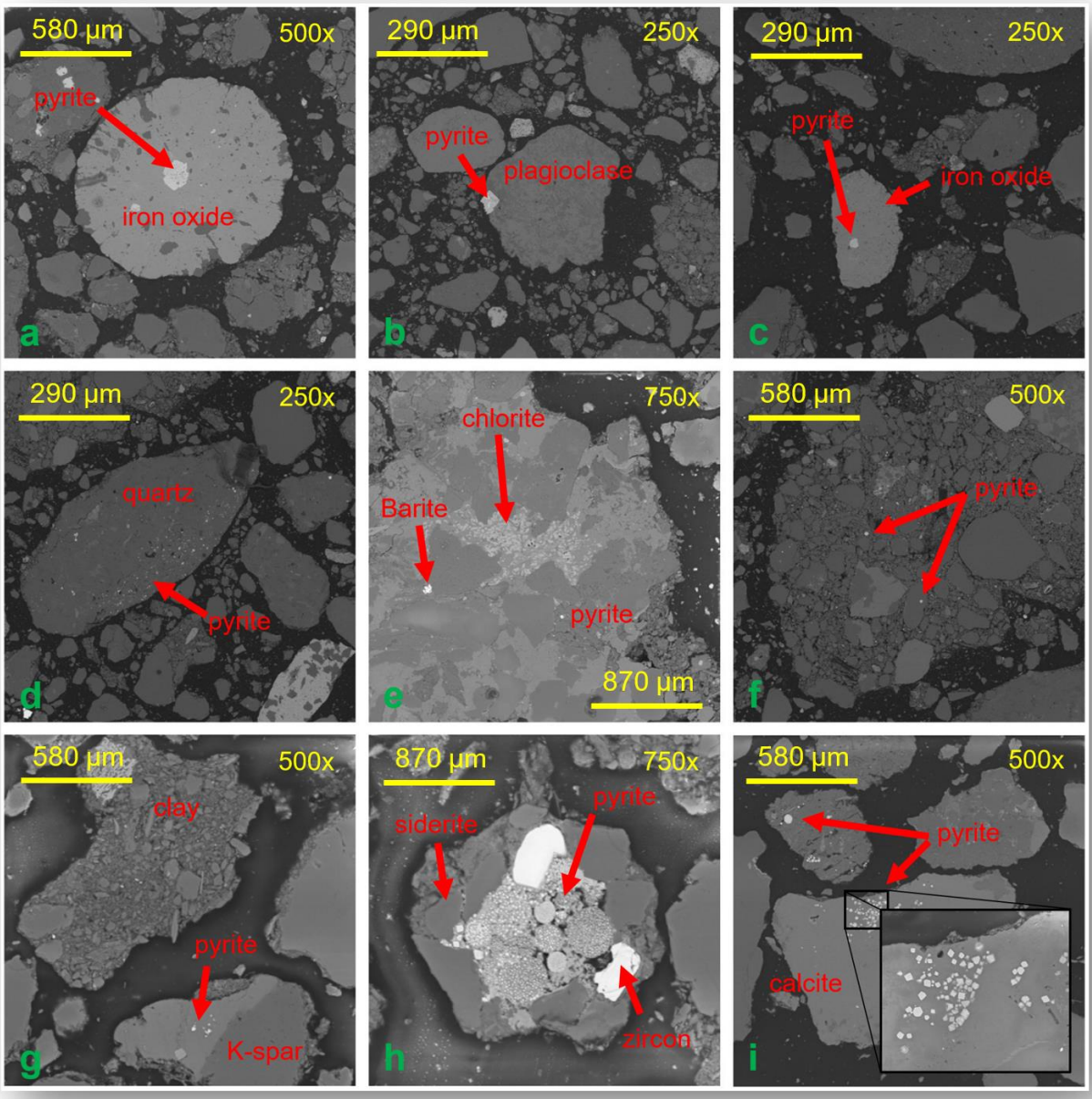

Figure 6). Isolated pyrite grains typically exhibit secondary mineral coatings primarily consisting of ferrihydrite. Ultimately, pyrite is abundant in the shallow groundwater system, but it was hypothesized that pyrite has a minor to negligible impact on the groundwater quality due to its low available reactive surface area.

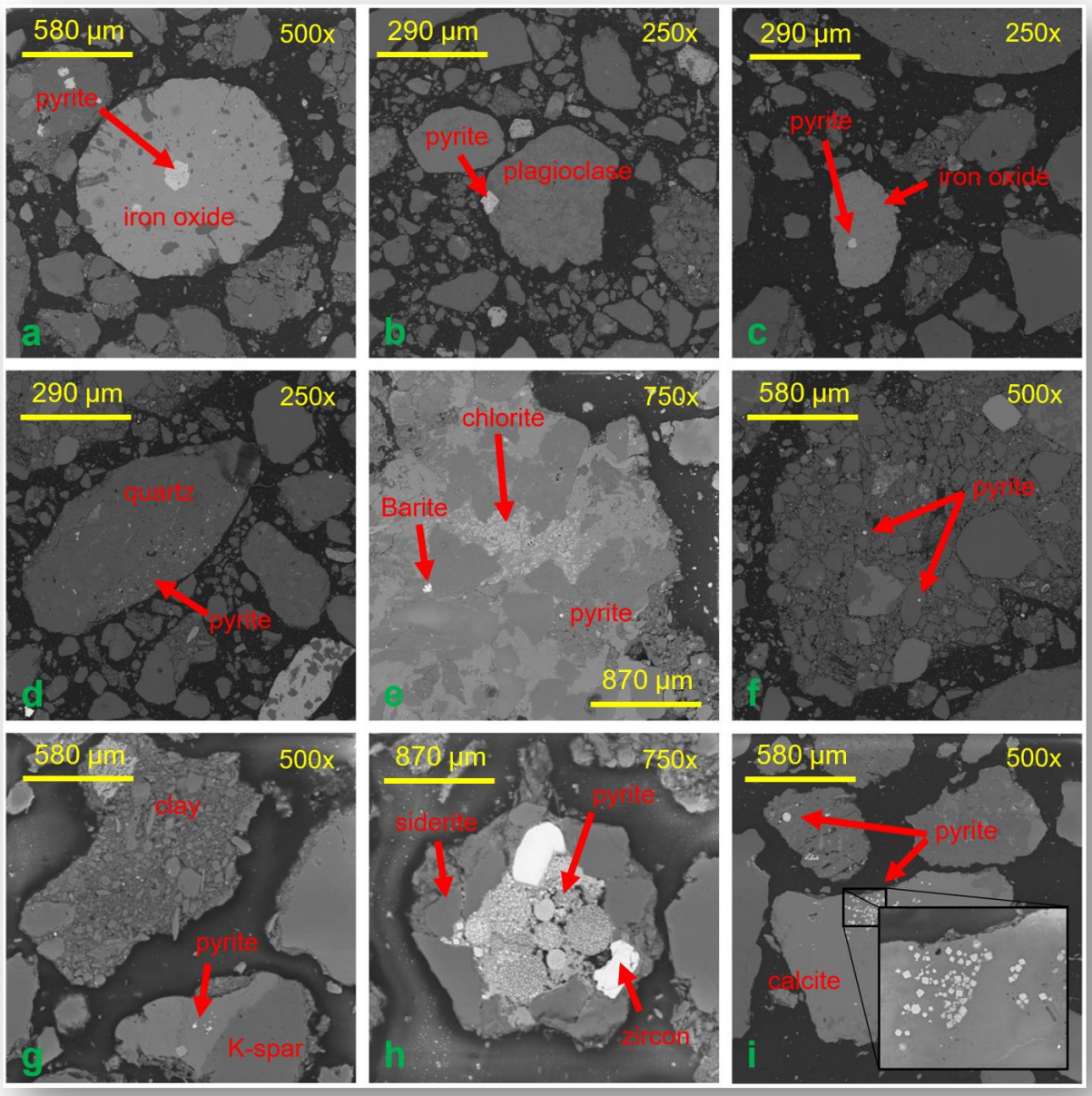

Figure 6. SEM images of pyrite in geological materials recovered from monitoring wells EERI-1 (from 40 m BGS, in sand and gravel) (a,b,c,d,f), EERI-15 (from 75 m BGS, in sandstone and shale) (e), and EERI-2 (from 45 m BGS in shale) (g,h,i).

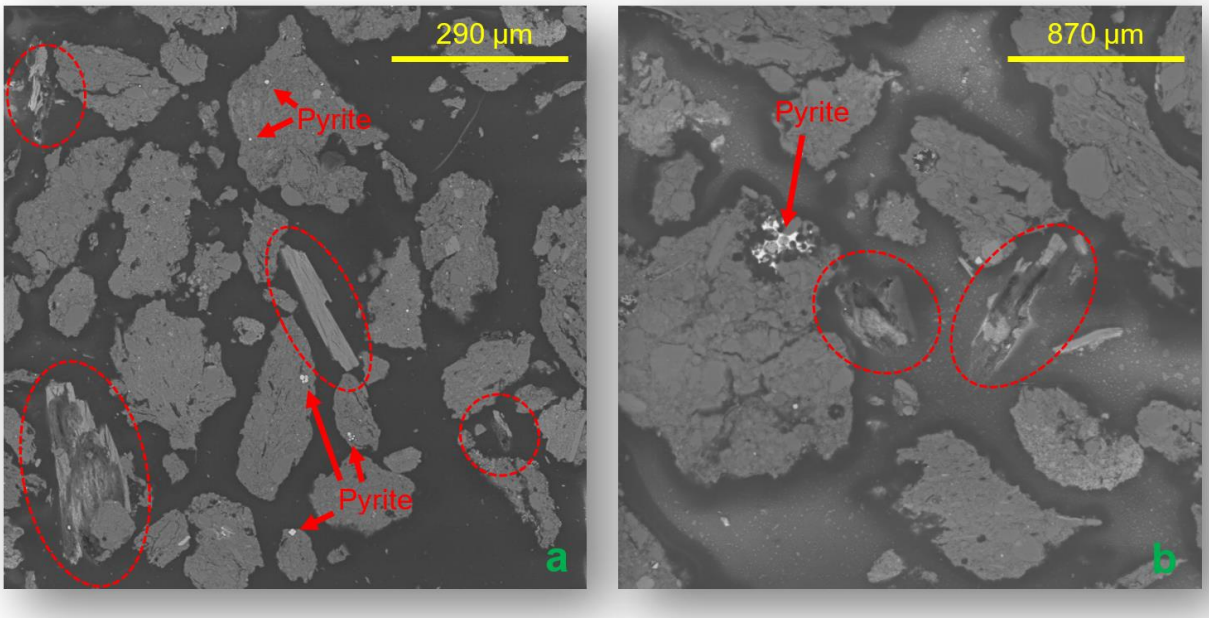

Figure 7 shows two SEM images of gypsum and pyrite crystals. Gypsum was challenging to find among bedrock and sediment samples and was only observed in one rock sample collected near the upper surface of the bedrock (EERI-4 from 195 to 200 ft BGS). In this sample, the gypsum grains occur near pyrite, and most gypsum crystals are weathered.

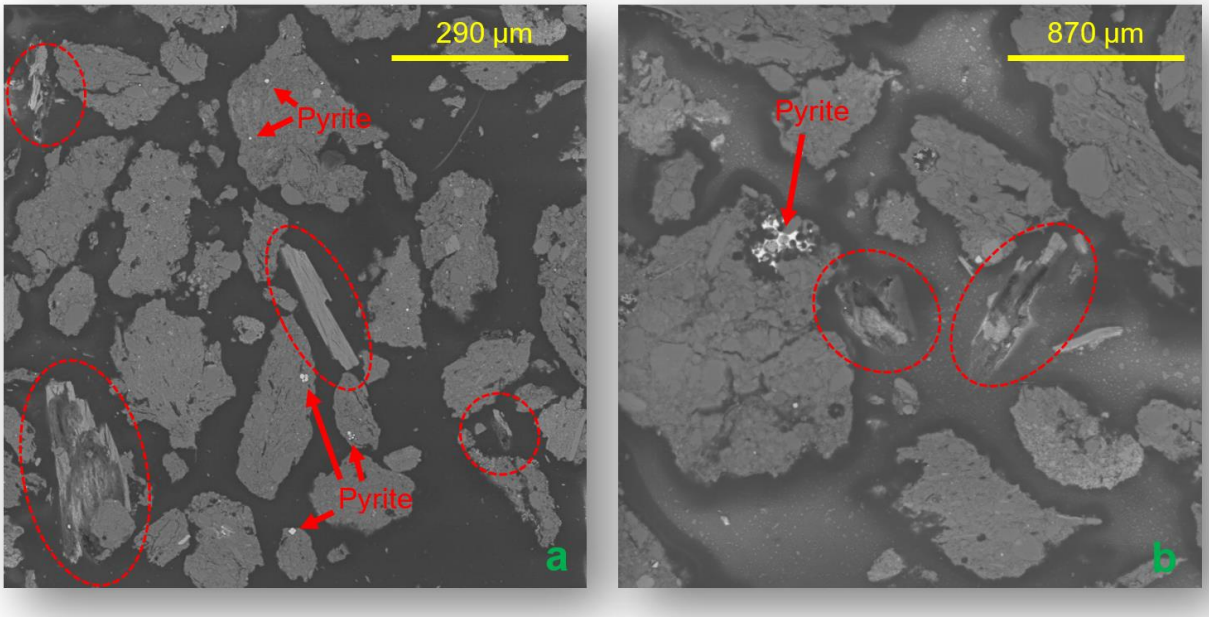

Figure 7. SEM images of gypsum (circled) and pyrite grains at 250x magnification (a) and 750x magnification (b).

6.2. Hydrochemical Baselines and Water Types in the Unconsolidated Groundwater System

Twenty-four CDP/boxplot figures were constructed with hydrochemical data from the sediments. Additionally, box plots were constructed for major ion concentrations in precipitation. The hydrochemical baselines of the unconsolidated groundwater system are summarized in **Table 5**, and Martinolich Plots with all remaining data distributions (i.e., baselines) are shown in **Appendix B**. The Martinolich plots consist of a box plot showing values within the 2.5th to 97.5th percentiles, the interquartile range (IQR), and the median, as well as a CDP showing the full range of data. The hydrochemical baselines can be interpreted as such: the median value represents the regional hydrochemical baseline, the IQR represents "typical" groundwater quality, and values within the 2.5th to 97.5th percentiles represent the full range of values representing natural groundwater quality in the region. Outlying values beyond the 2.5th to 97.5th percentiles reflect atypical groundwater quality. However, it is emphasized that these values may change over time, and an effort should be made to recalculate the baselines over a logical timeframe and as more groundwater quality data is collected in the PR.

Figure 8 is an example of a Martinolich plot that illustrates baseline groundwater temperatures in the unconsolidated groundwater system. The boxplot in **Figure 8** shows temperature values ranging from the 2.5th to 97.5th percentiles, the IQR, and the median temperature. The black trendline describes the data distribution. The p-value (0.13) indicates the goodness-of-fit to a normal distribution. The CDP can be interpreted by considering the change in height between vertical bars, i.e., the difference in height between adjacent bars represents the amount of data in each bin. For example, **Figure 8** shows a relatively large change in height between bars positioned between 5.5 and 6.5 °C, indicating that about 32% of the data plots between 5.5 and 6.5 °C. The median temperature shown in the boxplot is 6.2 °C, which is consistent with the center of the normal trendline and reflects the regional baseline temperature.

Table 5. The hydrochemical baselines of the unconsolidated groundwater system.

Parameter	Unit	2.5th percentile	Inter Quartile Range			97.5th percentile	Distribution
			25th percentile	Median	75th percentile		
EC	µS/cm	261	573	780	1,040	1,643	Normal
ORP	mV	-145	7.8	86	151	338	Normal
pH	-	6.22	6.83	7.06	7.33	8.99	Normal
Temperature	˚C	3.2	5.7	6.2	7.6	12.1	Normal
Arsenic	mg/L	$6.5x10^{-5}$	$1.5x10^{-3}$	$4.0x10^{-3}$	$8.0x10^{-3}$	0.319	Log-normal
Bicarbonate	mg/L	118	364	480	563	738	Normal
Boron	mg/L	0.011	0.03	0.064	0.108	0.443	Log-normal
Calcium	mg/L	0.933	79.3	98.2	121	188	Normal
Chloride	mg/L	0.12	0.36	1.21	4.2	119	Log-normal
Fluoride	mg/L	0.05	0.13	0.219	0.345	1.18	Log-normal

Iron	mg/L	0.001	$1.67x10^{-2}$	0.263	2.09	7.03	Log-normal
Magnesium	mg/L	7.8	24.6	42.5	59.6	93.8	Normal
Manganese	mg/L	$2.54x10^{-5}$	0.004	0.085	0.191	1.2	Log-normal
Potassium	mg/L	0.8	1.74	2.4	3.4	8.1	Log-normal
Silicon	mg/L	2.07	4.23	5.56	7.18	11.4	Normal
Sodium	mg/L	2.873	7.5	17	38.4	109.3	Bimodal
Strontium	mg/L	$8.42x10^{-4}$	0.272	0.43	0.54	1.22	Normal
Sulphate	mg/L	3.4	17.4	43.2	141	378	Power
$\delta^{13}C_{CH4}$	‰ VPDB	-147	-81.2	-69.0	-62.7	-39.0	Normal
$\delta^{13}C_{DIC}$	‰ VPDB	-14.7	-13.8	-12.9	-12.0	-6.21	Normal
Tritium	TU	0	0.12	4.12	7.28	11	Normal
CO_2	mg/L	6.27	33.0	54.0	75.9	152	Log-normal
Methane	mg/L	$1.84x10^{-4}$	$2.19x10^{-3}$	$6.61x10^{-3}$	$2.79x10^{-2}$	1.03	Log-normal

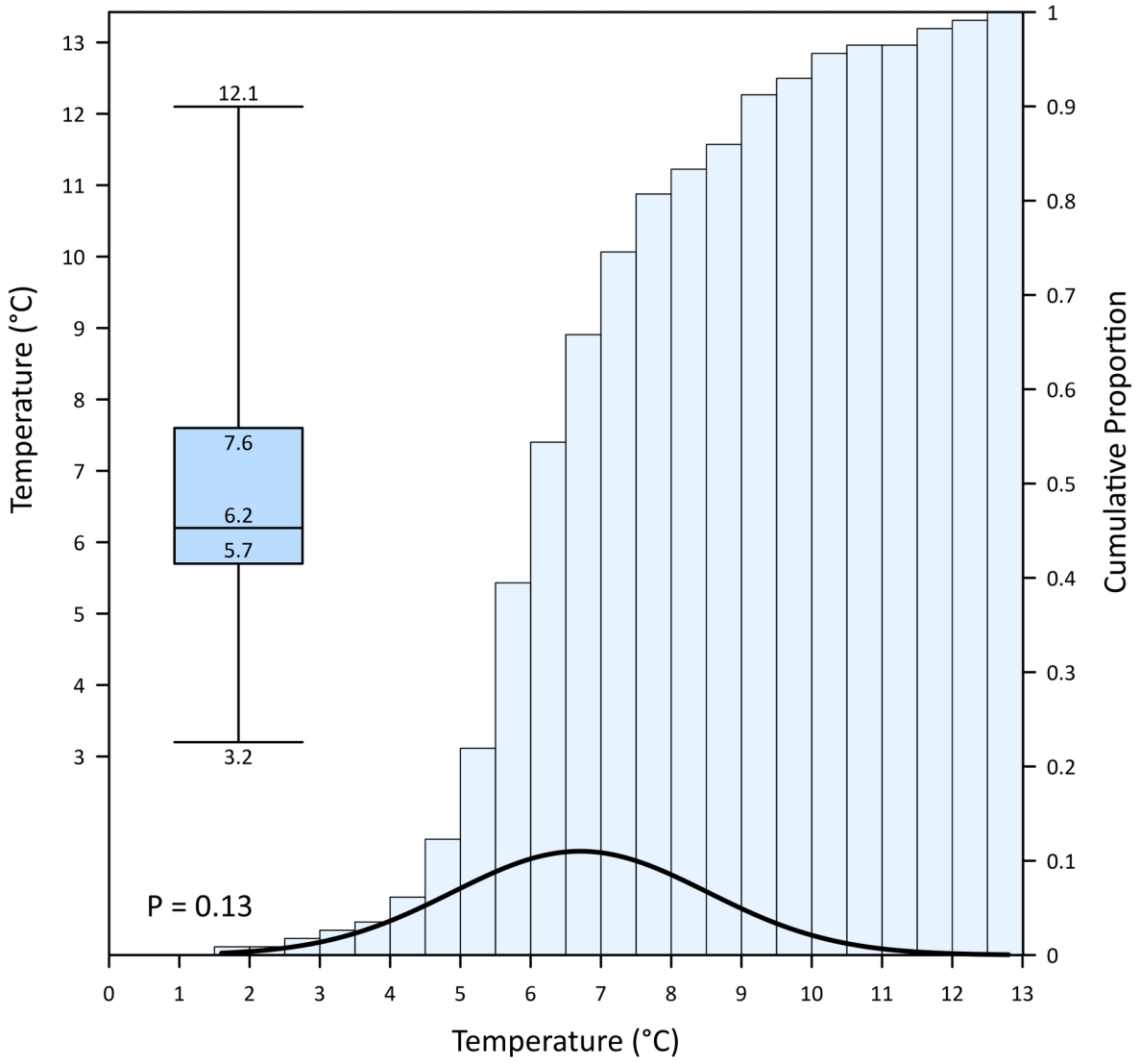

Figure 8. Baseline temperatures in the unconsolidated groundwater system. The median temperature is shown on centerline of the box plot, and box plot whiskers mark the 97.5th and 2.5th percentiles. Temperature values are normally distributed, with a p-value of 0.13.

The KMC analysis was used to identify three primary water types in the unconsolidated groundwater system, and the median major ion concentrations of the three data clusters were used to generate Stiff diagrams (**Figure 9**) and a Piper plot (**Figure 10**). The groundwater ranges from Ca-HCO_3 (C1U) to Ca-Mg-HCO_3-SO_4 type (C3U), with an intermediate Ca-Mg-HCO_3 type (C2U). Groundwater chemistry throughout the unconsolidated groundwater system is relatively consistent, with few groundwater samples exhibiting elevated sulphate and sodium concentrations. The three primary water types are ordered with respect to salinity, indicating the KMC algorithm distinguished the water types mostly on the basis of EC. This interpretation is supported by overlapping data in the Piper plot. It was inferred that the three water types are ordered with respect to a hydrogeochemical evolution, and numerical hydrogeochemical modeling showed that the hydrogeochemical evolution of groundwater in the sediments is controlled primarily by carbonate mineral dissolution driven by carbon dioxide and methane flux, gypsum mineral dissolution, and mixing with groundwater from the bedrock (Martinolich, 2022).

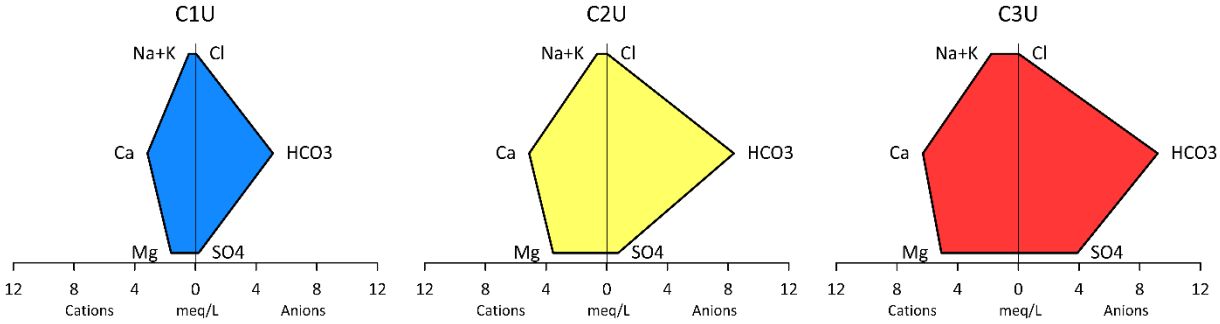

Figure 9. Stiff diagrams constructed with median major ion concentrations of groundwater quality data groups segregated via KMC.

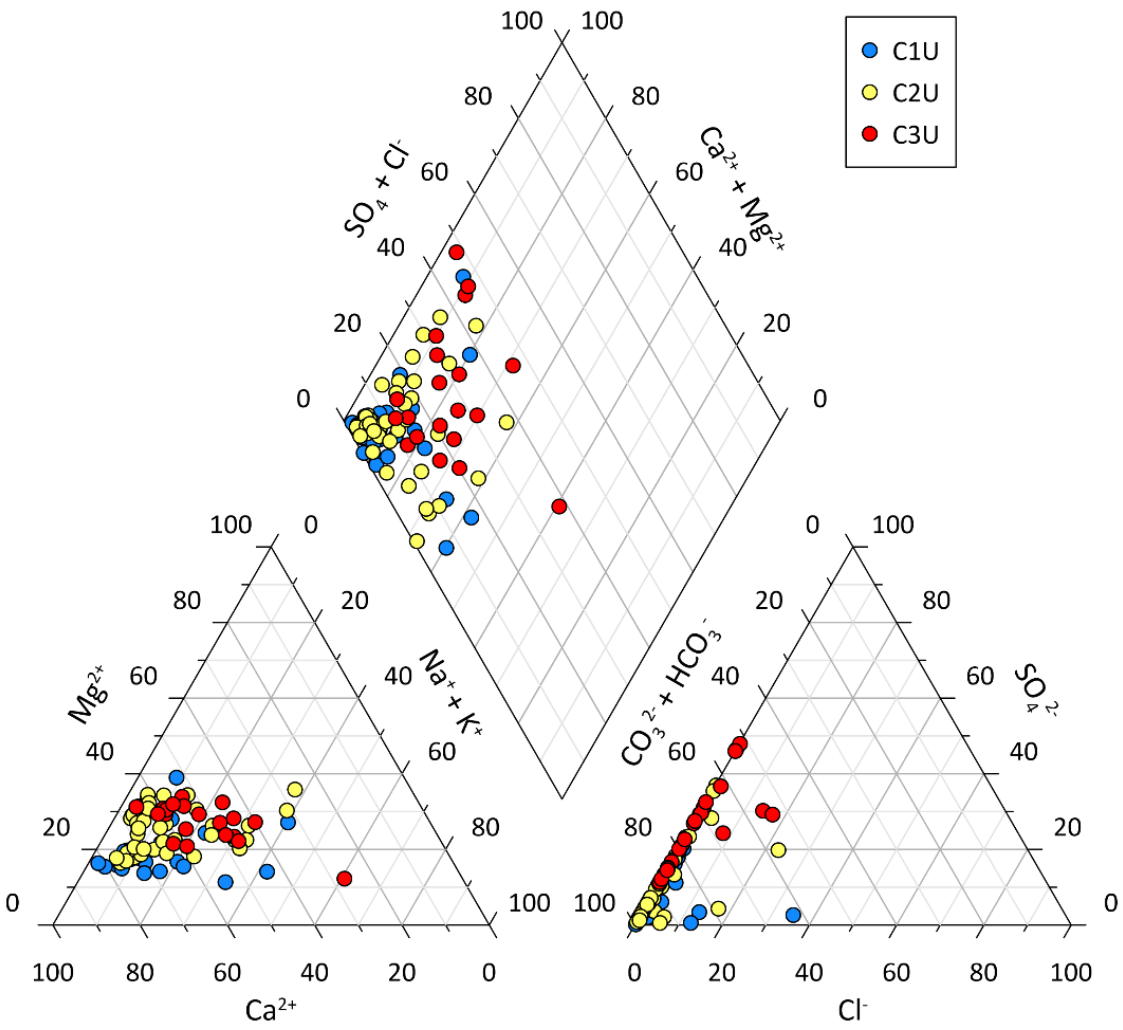

Figure 10. Piper plot with groundwater quality data collected from the unconsolidated groundwater system, grouped via KMC.

6.3. Hydrochemical Map of the Unconsolidated Groundwater System

The hydrochemical map of the unconsolidated groundwater system is shown in **Figure 11**. The map shows the distribution of the three water types defined in the cluster analysis (C1U, C2U and C3U) at their sampling point locations. Polygons were delineated in areas that contain mostly a single water type. Most polygons contain more than one water type.

The following comments are provided based on preliminary insights from the interpretation of **Figure 11**. Interpretations/comments represent regional generalizations and reflect the limitations of the spatial distribution of the sample dataset and the approach described above.

Figure 11 indicates that relatively fresh groundwater (C1U) is located in the southeast area of the PR in the RMFs and east of the Kiskatinaw River. The Kiskatinaw River forms a regional groundwater boundary that separates

relatively evolved groundwater in the west and relatively dilute groundwater in the east. The relatively low salinity of groundwater interpreted in the area east of the Kiskatinaw River may indicate that this is an area of relatively high groundwater flow and discharge rates, allowing less time for water-rock interactions to occur. Alternatively, the lower TDS water may reflect a limited source of carbonate minerals in Laurentide glacial drift deposits, or the limited number of groundwater samples collected in the area may be confounding the current interpretation.

Figure 11 indicates that relatively saline, sulphate-rich groundwater (C3U) is typically found in or near the paleovalleys, particularly in the GP. Groundwater originating from the Rocky Mountain Foothills (RMFs) in the southwest likely discharges from the bedrock into the GP. The red zone surrounding the GP was extended south-southeast along the Kiskatinaw River because a single groundwater sample (EERI-9) with exceptionally high sulphate and sodium concentrations was collected there. The sample was screened as an outlier during the cluster analysis, so it was excluded from the map. Still, the data suggest that relatively saline groundwater from the bedrock may be discharging into the Kiskatinaw River Paleovalley.

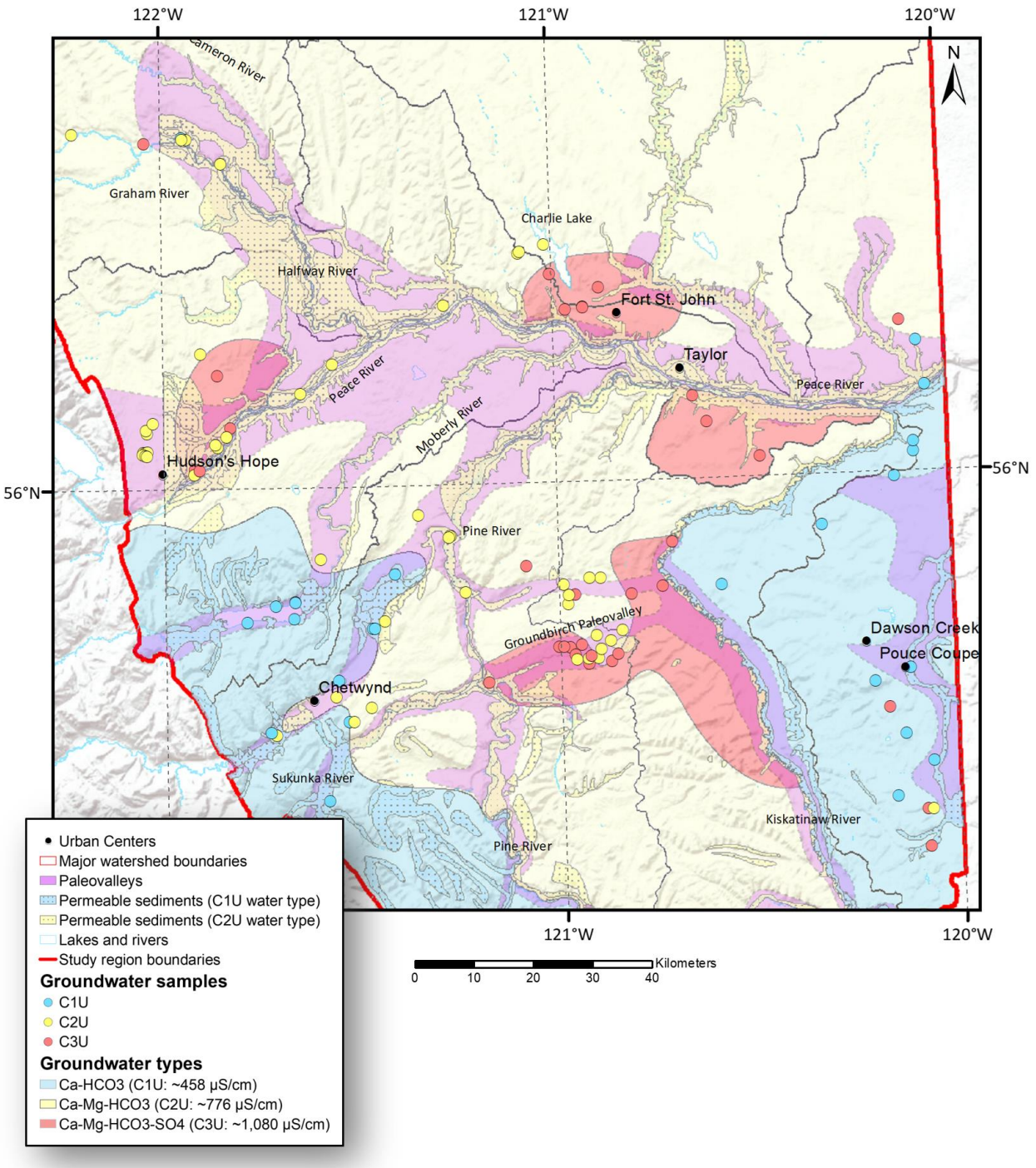

Figure 11: Conceptualized hydrochemical map of the unconsolidated groundwater system showing the interpreted distribution of water types.

6.4. Hydrochemical Baselines and Water Types in the Bedrock Groundwater System

Twenty-four CDP/boxplot figures were constructed with hydrochemical data from the bedrock. The hydrochemical baselines of groundwater in the bedrock are summarized in **Table 6,** and the CDP/boxplot figures are provided in **Appendix C**. The hydrochemical baselines can be interpreted as such: the median value represents the regional hydrochemical baseline, the IQR represents "typical" groundwater quality, and values within the 2.5th to 97.5th percentiles represent the full range of values representing natural groundwater quality in the region. Outlying values beyond the 2.5th to 97.5th percentiles reflect atypical groundwater quality. However, it is emphasized that these values may change over time, and an effort should be made to recalculate the baselines over a logical timeframe and as more groundwater quality data is collected in the PR.

Table 6. The hydrochemical baselines of the bedrock groundwater system.

Parameter	Unit	2.5th percentile	Inter Quartile Range			97.5th percentile	Distribution
			25th percentile	Median	75th percentile		
EC	µS/cm	778	1,480	2,040	3,120	5,340	Power
ORP	mV	-190	-16.6	73.6	137	248	Normal
pH	-	6.3	6.88	7.16	7.61	9.05	Normal
Temperature	˚C	3.6	5.7	6.65	8.4	12.6	Normal
Arsenic	mg/L	$1.08x10^{-4}$	0.002	0.006	$1.48x10^{-2}$	0.902	Log-normal
Bicarbonate	mg/L	304	663	803	1,090	1,950	Log-normal
Boron	mg/L	0.041	0.206	0.331	0.523	1.01	Log-normal
Calcium	mg/L	0.981	12.0	54.1	136	470	Log-normal
Chloride	mg/L	0.2	1.78	4.82	14.4	229	Exponential
Fluoride	mg/L	0	0.2	0.551	1.0	3.0	Log-normal
Iron	mg/L	0.001	0.0259	0.185	1.57	14.1	Normal
Magnesium	mg/L	0.4	9.3	39.1	90	276	Normal
Manganese	mg/L	$5.09x10^{-5}$	0.006	0.048	0.213	2.86	Power
Potassium	mg/L	0.9	2.3	3.51	5.6	13.4	Log-normal
Silicon	mg/L	2.64	3.36	4.13	5.25	7	Normal
Sodium	mg/L	41.7	201	336	552	1,090	Normal
Strontium	mg/L	$1.68x10^{-3}$	0.211	0.509	1.03	2.74	Normal
Sulphate	mg/L	1	98.4	296	986	3,310	Power
$\delta^{13}C_{CH4}$	‰ VPDB	-91.2	-77.9	-72.9	-54.6	-39.6	Normal
$\delta^{13}C_{DIC}$	‰ VPDB	-20.8	-13.1	-9.35	-7.39	5.02	Normal
Tritium	TU	0.01	0.01	0.03	0.57	5.22	Normal[1]
CO_2	mg/L	0.289	12.9	51.1	112	357	Normal
Methane	mg/L	$2.93x10^{-4}$	$4.23x10^{-3}$	$1.28x10^{-2}$	0.211	25.5	Power

[1]The p-value representing the goodness of fit of tritium concentrations to a normal distribution is <0.05.

The KMC analysis was used to identify three primary water types in the bedrock groundwater system, and the median major ion concentrations of the three data clusters were used to generate Stiff diagrams (**Figure 12**) and a Piper plot (**Figure 13**). The groundwater ranges from Na-Ca-Mg-HCO_3-SO_4 type (C1B) to Na-HCO_3 (C2B) and Na-SO_4-HCO_3 types (C3B). Groundwater chemistry throughout the bedrock groundwater system varies considerably reflecting different gas-water-rock interactions. The three primary water types are ordered with respect to salinity, however, C2B exhibits the highest range in salinity, likely reflecting groundwater collected from relatively deep bedrock. It was inferred that the C1B and C2B water types are ordered with respect to a hydrogeochemical evolution, reflecting dilute groundwater from the sediments entering the bedrock and undergoing cation exchange and carbonate mineral dissolution. The C3B water type reflects a C2B water type that has undergone gypsum mineral dissolution. Numerical hydrogeochemical modeling showed that the hydrogeochemical evolution of groundwater is controlled primarily by cation exchange (which implies groundwater mixing), gypsum mineral dissolution, and carbonate dissolution driven by carbon dioxide and methane flux (Martinolich, 2022).

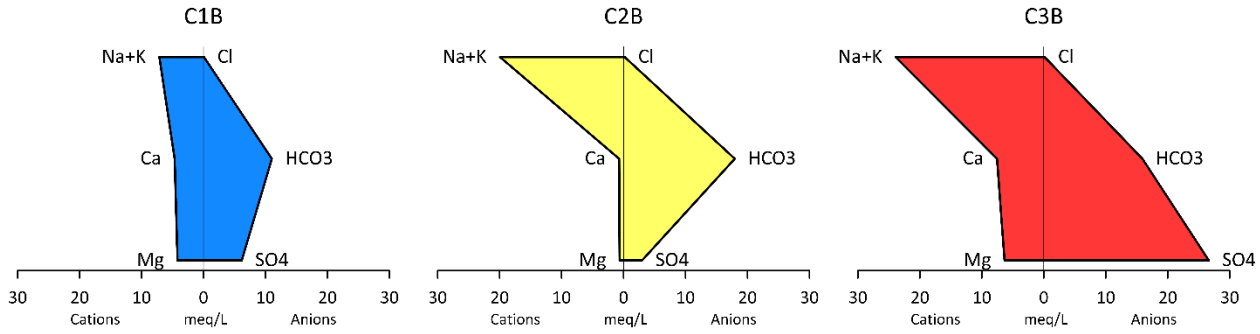

Figure 12. Stiff diagrams constructed with median major ion concentrations of groundwater quality data groups segregated via KMC.

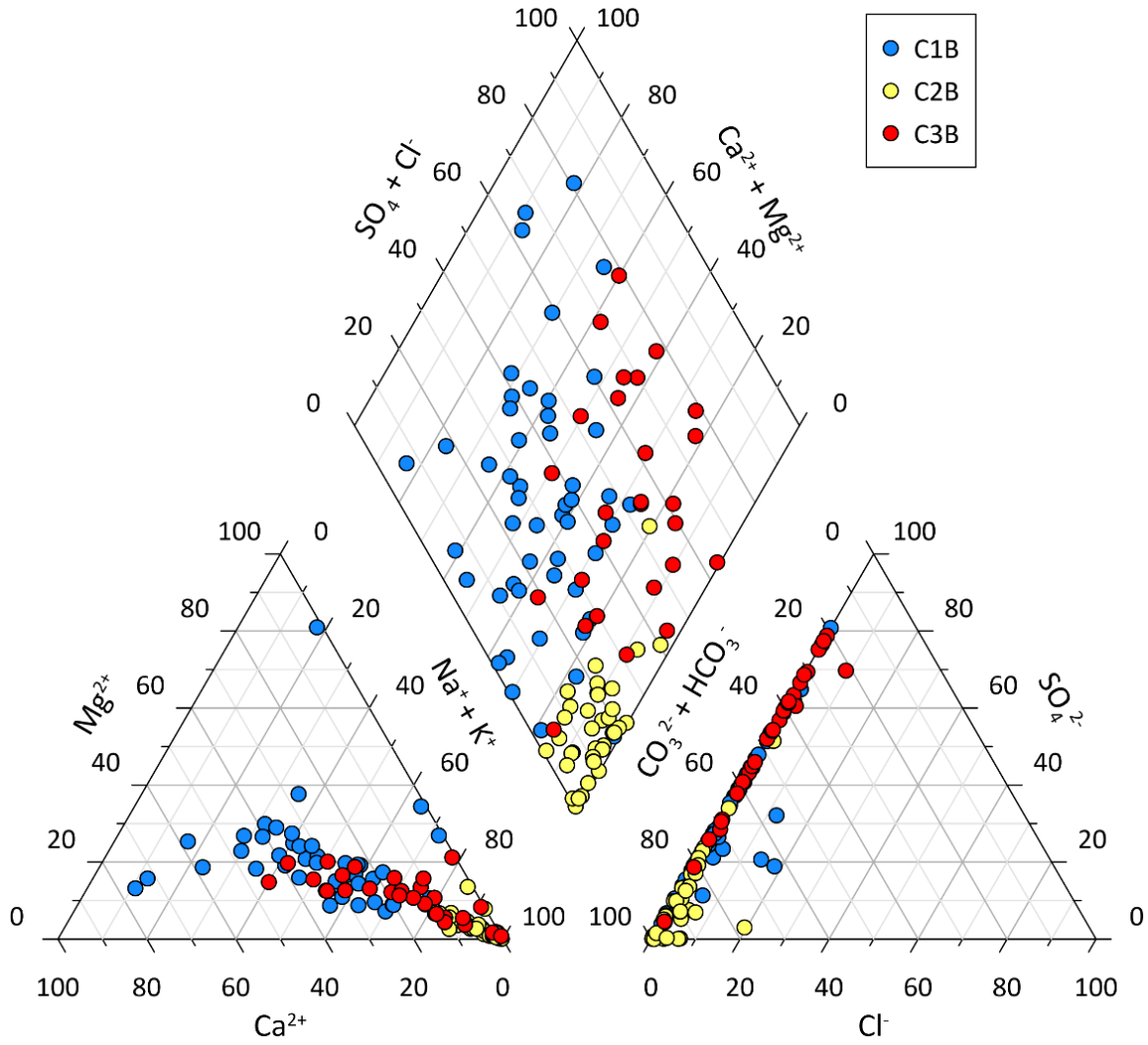

Figure 13. Piper plot with groundwater quality data collected from the bedrock groundwater system, grouped via KMC.

6.5. Hydrochemical Map of the Bedrock Groundwater System

The hydrochemical map of the bedrock groundwater system is shown in **Figure 14**. The map shows the distribution of the three water types defined in the cluster analysis (C1B, C2B and C3B) at their sampling point locations. The Na-HCO3 groundwater type (C2B) was interpolated/extrapolated throughout the entire study area. Polygons were delineated in areas that contain mostly a single water type. Most polygons contain more than one water type.

The following comments are provided based on preliminary insights from the interpretation of **Figure 14**. Interpretations/comments represent regional generalizations and reflect the limitations of the spatial distribution of the sample dataset and the approach described above.

Groundwater in C1B is interpreted to dominate the northwest and southwest regions of the study area, suggesting the groundwater increases in salinity from the west toward the central PR (**Figure 14**). North of the Peace River and northwest of Fort St. John, groundwater in the Dunvegan Fm. is relatively fresh and becomes more saline nearing the Beatton River. Other areas with relatively fresh groundwater, like in the Fort St. John area and south of Taylor (across the Peace River Valley), likely represent areas where the bedrock receives recharge through relatively thin overburden. The regional surficial geology map indicates that a till veneer was deposited at the surface in these areas (Hickin and Fournier, 2011).

Groundwater in C3B is interpreted to dominate the eastern region of the study area, which may indicate gypsum is more prevalent in the eastern PR. There are other areas where the C3B water type occurs, such as around the Charlie Lake area and east of Hudson’s Hope, but C3B groundwater is more prevalent to the east. Like C3U, C3B is sulphate-rich and occurs beneath and around the Groundbirch Paleovalley.

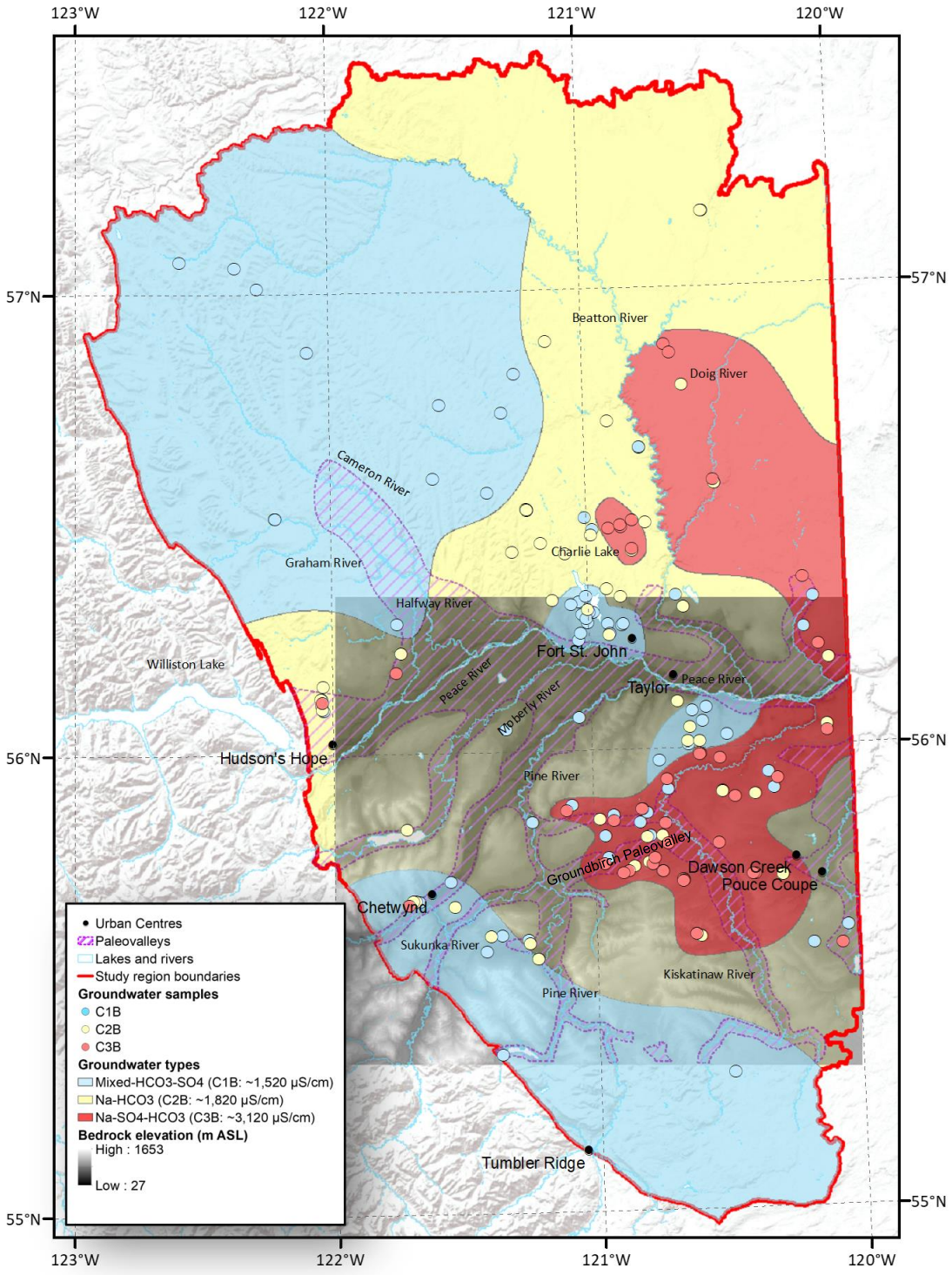

Figure 14: Conceptualized hydrochemical map of the bedrock groundwater system showing the interpreted distribution of water types (C1B, C2B, and C3B). The paleovalleys and bedrock DEM are shown because the bedrock topography and orientation of the paleovalleys impact groundwater flow in the bedrock.

7. Conceptual Hydrogeochemical Model of the Peace Region, Northeast BC.

A hydrogeochemical conceptual model (HCM) of the PR was constructed to illustrate the regional bedrock and surficial geology, aquifers and confining layers, the distribution of groundwater types throughout the shallow groundwater system, and the location of individual minerals (gypsum and pyrite) (**Figure 15**). The HCM shows multiple till layers and buried valley and inter-till aquifers in the central paleovalley. The upper surface of the bedrock is well-fractured. Gypsum is shown near the upper surface of the bedrock, predominantly in the eastern part of the study area, and pyrite is shown in mudstone/shale in the bedrock and in till in the eastern part of the study area. Ion exchange fronts are shown where groundwater originating from the sediments flows into the bedrock, driving cation exchange.

In the HCM, the six water types defined in this research are shown throughout the shallow groundwater system: C1U (Ca-HCO_3) groundwater is found in sediments overlying the bedrock, and C2U (Ca-Mg-HCO_3) groundwater is downgradient of the C1U water type, reflecting the hydrogeochemical evolution groundwater undergoes in the sediments. Hydrochemical mapping showed that C3U (Ca-Mg-HCO_3-SO_4) groundwater typically occurs near or within the paleovalleys (Martinolich, 2022), as illustrated in **Figure 15**. It was inferred that the composition of C3U groundwater reflects carbonate mineral dissolution, potentially gypsum mineral dissolution, and mixing with groundwater from the bedrock, as C3U groundwater exhibits elevated sulphate and sodium concentrations. Hence, C3U is shown within the paleovalley in the HCM. It was inferred that C2U may occur in the paleovalleys, in areas where gypsum is not present in the adjacent/underlying bedrock. Hence, C2U groundwater is shown in the paleovalley in the HCM.

In the HCM, C1B groundwater is shown within the fractured upper surface of the bedrock. It was inferred that the C1B may reflect groundwater within the bedrock fracture network, as C1B groundwater exhibits considerable calcium and magnesium concentrations and moderate sodium concentrations. The composition of C1B groundwater implies that it has undergone only minor cation exchange, which may reflect relatively abundant porosity (hence, relatively low reactive surface area) in the bedrock fractures. Na-HCO_3 groundwater is characteristic of paleomarine aquifers, so C2B groundwater is shown relatively deep in the bedrock in the HCM and can likely be found anywhere in the bedrock if a well is completed deep enough. C3B groundwater is shown where gypsum is present in the bedrock.

The HCM shows groundwater flow paths that reflect groundwater flow modeling results from Goetz et al. (2021). Groundwater flow modeling showed that the paleovalleys receive approximately 99% of their recharge from the underlying and adjacent bedrock, and groundwater may flow relatively rapidly through the fractured upper surface of the bedrock, eventually discharging into the paleovalleys.

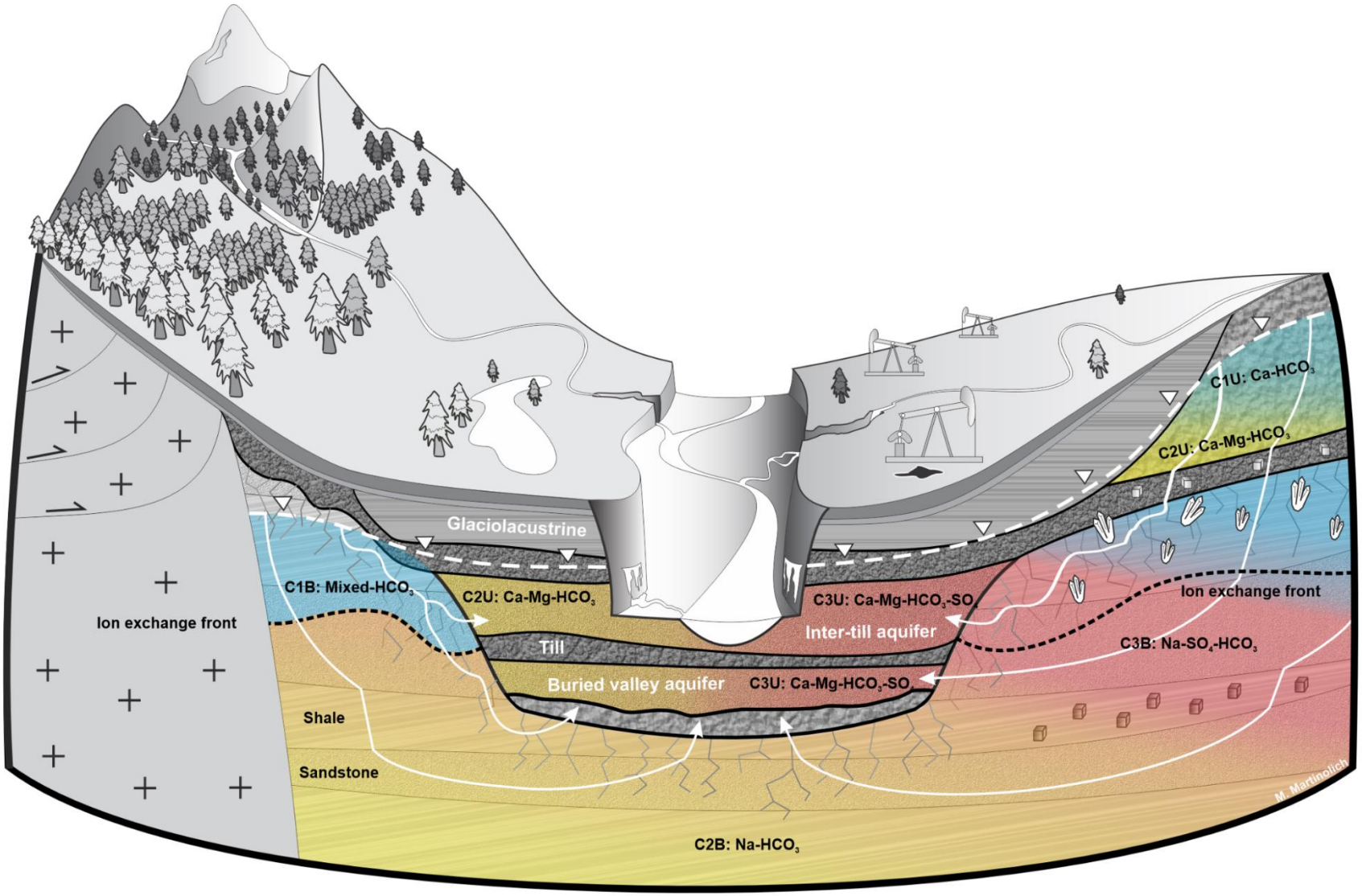

Figure 15: Conceptual hydrogeochemical model of the shallow groundwater system in the Peace Region, northeast BC. All water types defined in the cluster analyses (C1U-C3U, and C1B-C3B) and their inferred locations in the shallow groundwater system are illustrated.

8. Assessment of Groundwater Quality in Lone Prairie, Northeast BC

The purpose of this section is to demonstrate how the baselines characterized in this research can be used as a tool for interpreting groundwater quality data collected in the PR. As discussed, an effort was made to collect groundwater samples in Lone Prairie (LP), located approximately 25 km southeast of Chetwynd. LP is a prime area for collection of “background”, i.e., “ambient” groundwater samples because there are only three oil and gas wells in the area (see **Figure 3**), none of which are active. None of the LP residence were aware that oil and gas wells were drilled in the area, which may imply that they never reached production.

During fieldwork of 2021, 15 groundwater samples were collected in LP. Of the 15 groundwater samples, it was determined that two were collected from sediments and three were collected from bedrock based on the residents’ knowledge of their wells. Furthermore, based on sodium, calcium, and magnesium concentrations, it was interpreted that three were collected from the bedrock, and seven were collected from the sediments. For example, groundwater samples with elevated sodium and relatively low calcium and magnesium concentrations were interpreted to have been collected from bedrock, and groundwater samples with low (i.e., < 30 mg/L) sodium concentrations and elevated calcium and magnesium concentrations were interpreted to have been collected from sediments.

Figures 16 - 18 show groundwater quality data points reflecting individual groundwater samples collected in LP overlying box plots representing the regional hydrochemical baselines of the unconsolidated and bedrock groundwater systems (excluding data collected in LP to prevent statistical bias). **Figure 19** compares the stable isotopic composition of groundwater in LP to other groundwater samples collected throughout the PR. Comparing the groundwater quality observed in LP to the regional hydrochemical baselines shows that the groundwater quality in LP is typical for the PR, with few anomalous groundwater quality parameters. Some anomalous data among groundwater samples collected from the bedrock, such as anomalously low calcium and magnesium concentrations (**Figure 16**), may reflect extensive cation exchange and/or fresh recharge entering the bedrock. Other anomalous concentrations, such as fluoride, nitrate, and chloride concentrations, may reflect road salting, the presence of organic acids, or fluoride-bearing minerals. Exceptionally high manganese concentrations and elevated iron concentrations likely reflect reducing redox conditions in the subsurface promoting reduction of manganese- and iron-bearing oxides/oxyhydroxides. Ultimately, additional groundwater sampling should be performed on wells exhibiting anomalous/non-compliant solute concentrations, and the residents at such locations have been informed.

Groundwater collected from the sediments tends to have relatively high fluoride concentrations (**Figure 17**), which may reflect the presence of fluorite, apatite, or hornblende in glacial drift/sediments brought into the study area from the Rocky Mountains. It is unclear if any of these minerals are present in LP, as no geological samples were collected in the area. However, such minerals were not reported in the XRD results. Three groundwater samples collected from the bedrock (LP10a. LP9a, and LP1; see **Figure 3**) and one sample collected from the sediments

(LP10b) exceed the BC Maximum Allowable Concentration (BC-MAC) guideline for fluoride concentration in drinking water (1.5 mg/L) (British Columbia Ministry of Environment and Climate Change Strategy, 2020). However, fluoride concentrations observed in bedrock throughout the PR often exceed this guideline. Other anion concentration data fall within the regional baseline ranges, but nitrate concentrations are relatively high, with one groundwater sample from the sediments (LPX5) and four groundwater samples collected from the bedrock (LP-X6, LP10a, LP10c, and LP1) exceeding the BC-MAC for nitrate concentration in drinking water (3.0 mg/L) (**Figure 17**). Similar to baseline fluoride concentrations, the range of nitrate concentrations observed in the shallow groundwater system throughout the PR often exceeds the BC-MAC. In the case of nitrate, the elevated and non-compliant nitrate concentrations likely reflect fertilizer used for farming or nitrogenous organic acids. However, there is commonly interference in ion chromatography between naturally occurring low molecular weight organic acids and fluoride and nitrate, and this could be a result of elevated concentrations

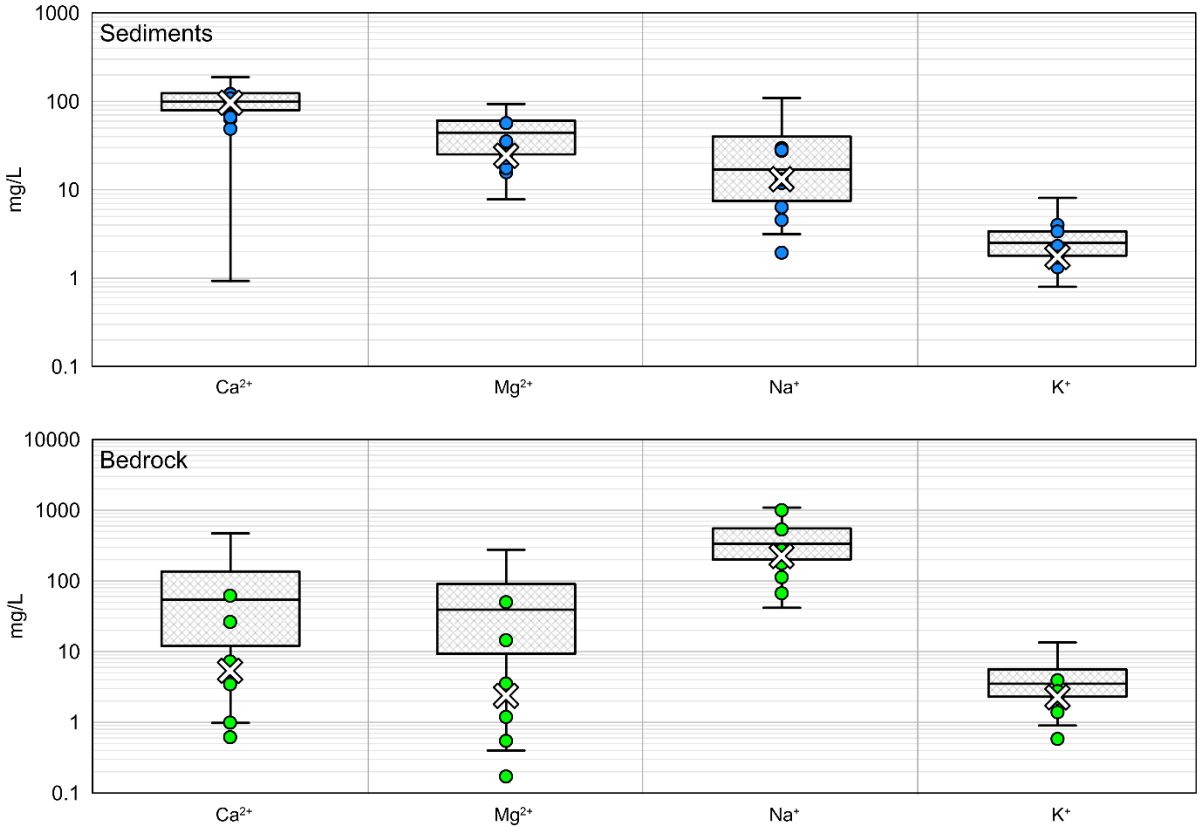

Figure 16. Assessment of cation concentrations in groundwater collected in Lone Prairie (LP), northeast BC. The data points represent individual groundwater quality data collected in LP. The underlying box plots show the baseline cation concentrations of the unconsolidated (upper plots) and bedrock groundwater systems (lower plots) in the Peace Region (excluding samples collected in LP to prevent statistical bias).

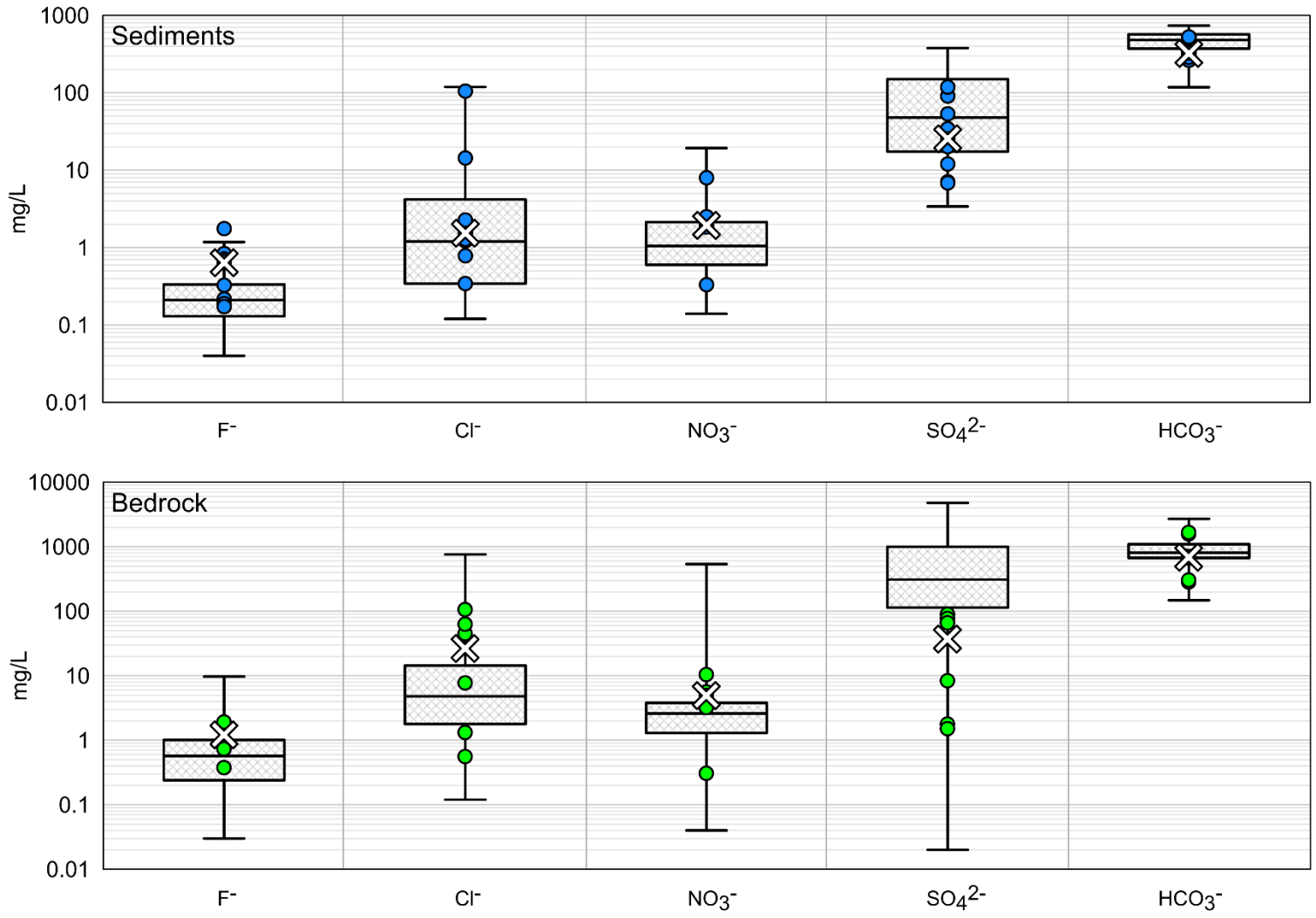

Figure 17. Assessment of anion concentrations in groundwater collected in Lone Prairie (LP), northeast BC. The data points represent individual groundwater quality data collected in LP. The underlying box plots show the baseline anions concentrations of the unconsolidated (upper plots) and bedrock groundwater systems (lower plots) in the Peace Region (excluding samples collected in LP to prevent statistical bias).

Comparing groundwater samples collected in LP to the baseline trace/minor metal concentrations of the entire PR indicates that there was one anomalously high manganese concentration observed in groundwater collected from the sediments in LP (**Figure 18**). The anomalous manganese concentration may reflect the presence of manganous minerals such as pyrolusite and relatively reducing ORP conditions, promoting mineral reduction in the sediments. Although the baseline box plots indicate that only one groundwater sample exhibited an anomalously high manganese concentration, two groundwater samples collected from the sediments (LP-X3 and LP7b) exceeded the BC-MAC for manganese concentration in drinking water (0.12 mg/L). Fortunately, relatively low arsenic concentrations were observed in LP (**Figure 18**), with no groundwater samples exceeding the BC-MAC for arsenic concentrations in drinking water (0.01 mg/L).

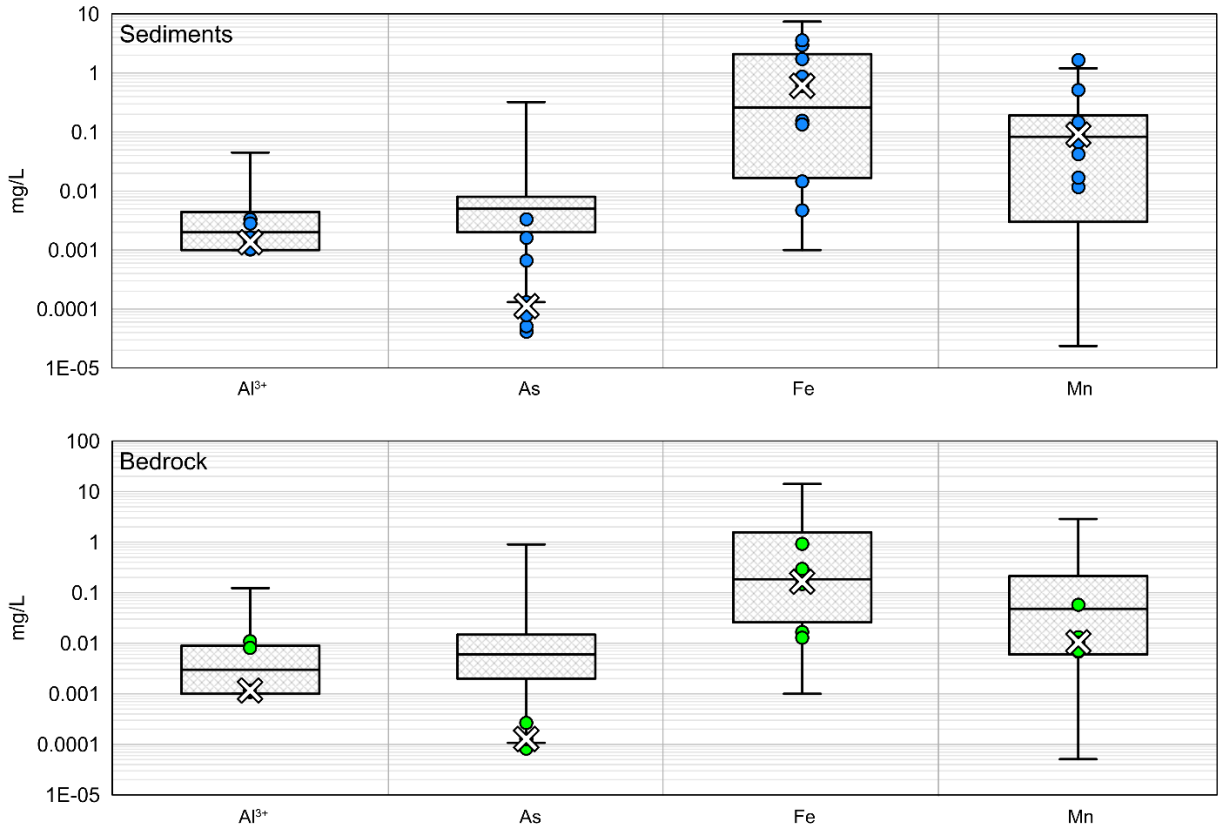

Figure 18. Assessment of minor metal concentrations in groundwater collected in Lone Prairie (LP), northeast BC. The data points represent individual groundwater quality data collected in LP. The underlying box plots show the baseline minor metal concentrations of the unconsolidated (upper plots) and bedrock groundwater systems (lower plots) in the Peace Region (excluding samples collected in LP to prevent statistical bias).

Comparing the stable isotopic composition of groundwater samples collected in LP to the stable isotopic composition of all groundwater samples collected in the PR indicates that the stable isotopic signature of groundwater in LP is typical for the region, with all groundwater samples falling within the range of modern $\delta^{18}O$-$\delta^{2}H$ values (**Figure 19**)

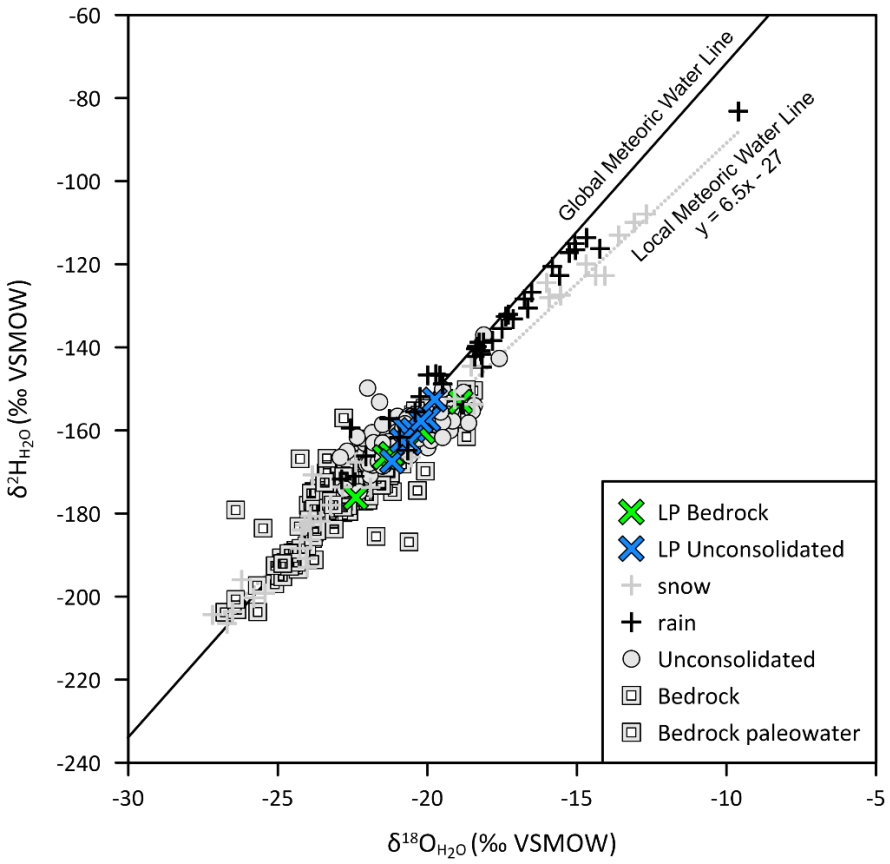

Figure 19. Assessment of the stable isotopic composition of groundwater collected in Lone Prairie (LP), northeast BC. The coloured data points represent individual groundwater quality data collected in LP. The grey datapoints show the stable isotopic composition of groundwater samples collected throughout the Peace Region.

9. Conclusions

9.1. Regional Hydrochemical Baselines

The hydrochemical baselines of the unconsolidated and bedrock groundwater systems in the PR were defined independently using descriptive statistics and a large hydrochemical dataset. The purpose of defining the hydrochemical baselines was to provide the BC Provincial Government with a tool to assess/interpret the groundwater quality. The baselines were defined in terms of concentration and chemical property ranges, with values outside the 2.5th and 97.5th percentiles excluded as outliers. This approach has been utilized throughout

Europe by Edmunds and Shand (2008). Ultimately, the baseline solute concentration, isotopic, and chemical property ranges defined in this research are likely to change over time, as more groundwater quality data is collected throughout the PR, but the baselines are supported by the size of the dataset and the extent of the sampling area. It is difficult to validate the hydrochemical baselines quantitatively, but the baseline solute concentration ranges are consistent with reactive transport modeling results presented in the full Thesis document (Martinolich, 2022). Still, as more hydrochemical data is collected in the PR and added to the SFU-EERI-FLNRORD dataset, the baseline values may shift slightly, so an effort should be made to revaluate the hydrochemical baselines over a logical timeframe.

9.2. Hydrochemical Mapping

Separate hydrochemical maps showing the distribution of groundwater types in the unconsolidated and bedrock groundwater systems were constructed based on the results of a K-means cluster analysis. Groundwater samples from each groundwater system (bedrock and unconsolidated) were segregated into groups based on major ion concentrations (Na^+ Mg^{2+}, Ca^{2+}, K^+, SO_4^{2-}, HCO_3^-) and EC. Mapping the distribution of chemically distinct groundwater in the PR proved challenging, due mostly to the complexity of the regional hydrogeology/geology and groundwater flow regime. The distribution of water types does not seem to correspond to any obvious topographic trends, except more evolved groundwater tends to occur within and around the paleovalleys.

Interpretations of the hydrochemical map are limited in their complexity due to the lack of well depth information. The goal of the hydrochemical maps was to delineate areas with chemically distinct groundwater, but many areas contain several groundwater types. Drawing polygons that contain individual water types would result in several polygon “islands”, which likely reflects the chemical variability of the groundwater with depth. For example, wells drilled near each other may be screened by tens of metres apart vertically, and what appears as a lateral hydrochemical facies change related to groundwater flow (in 2D) is realistically two separate flow systems.

The delineated polygons cover relatively large areas and show regions that generally contain the same water type. When predicting the groundwater type in an unsampled area of the PR, the geochemist/hydrogeologist should consider the glacial history of the area (Laurentide vs Cordilleran drift), regional geological features such as paleovalleys, confining layers of glaciolacustrine and till, and the mineralogy of the bedrock and sediments, The outcome of the hydrochemical mapping suggests it is an approach more suitable for smaller regions with higher data density and a better understanding of the well infrastructure. However, the cluster analysis provided a powerful tool for segregating the hydrochemical data.

10. Limitations

10.1. The SFU-EERI-FLNRORD Dataset

The main limitation in this research was a lack of groundwater well infrastructure data. The depths of the sampled wells are predominantly unknown, so groundwater samples collected from the sediments and bedrock were differentiated geochemically based on their sodium concentrations and any well records available in the BC GWELLS database. Groundwater samples with elevated sodium concentration (i.e., > 50 mg/L) were assumed to be collected from the bedrock, however drill log information confirmed that some samples with elevated sodium concentration were collected from the sediments. Ultimately, the groundwater analytical data was given a bedrock or sediments designation, and the two groups of samples were analyzed independently. Distinguishing the sampled depths or aquifer types based on the groundwater chemistry is problematic due to the variability in the groundwater chemistry and the evidence of mixing among most of the groundwater analytical data. Uncertainty in the sample classification impacts the validity of the hydrochemical baselines. However, the water quality assessment in LP demonstrated that the baselines are robust, and the hydrochemical data were screened for outliers to limit the uncertainty in the results.

Another critical limitation that mostly impacts the hydrochemical mapping results is the distribution of groundwater sample sites; there are considerably more groundwater sample sites in the eastern PR, and the bedrock hydrochemical map shows the groundwater EC and sulphate concentration generally increase to the east. This result may be influenced by the abundance of groundwater samples collected around the Dawson Creek-Groundbirch area. However, the results/interpretation is consistent with the glacial history of the region, considering the mineralogy of Laurentide glacial drift deposits.

10.2. K-Means Cluster analysis and Hydrochemical Mapping

Cluster analysis is a powerful tool for grouping groundwater analytical results, but it is difficult to determine the optimal number of clusters. For this research, groundwater samples collected from the sediments and bedrock were segregated into three groups based on their major ion concentrations (except chloride) and EC. However, including different chemical parameters such as ORP and minor/trace element concentrations in the analysis or increasing the number of clusters may reveal different water types and change the hydrochemical maps substantially. Ultimately, the resolution of the hydrochemical map varies with the number of clusters. For this research, three clusters were utilized because delineating areas with distinct groundwater chemistry was challenging with four clusters. Of course, a polygon could be constructed around each data point, but often four samples near each other would have varying chemistry, and sometimes the groundwater EC appears to increase with elevation. These trends are hard to interpret without knowledge of well-depths, and the sparse data distribution amplifies the problem. Another reason three clusters were utilized is that adding a fourth group in either analysis resulted in two groups with very similar chemistry. More chemical variables should be included in the analysis to use four groups. Overall, the maps are relatively simple and can be refined as more groundwater samples are collected throughout the PR.

11. Recommendations

The hydrochemical baselines presented in this research are “living” data and should be updated over a logical timeframe (perhaps over five-year terms) and as more groundwater quality data is collected throughout the PR. However, the assessment of groundwater quality in Lone Prairie demonstrated that the baselines are likely to undergo only minor changes as more data is added to the analysis. It is unclear if adding more data to the analysis is necessary. It is recommended that future research funding be directed mostly to developing hydrochemical baselines in other areas of BC.

If a need arises to better characterize groundwater quality in the Peace Region, drilling additional EERI groundwater monitoring wells would be beneficial. Installing additional EERI wells adjacent to existing EERI wells to observe spatial changes in groundwater quality along flow paths directly would be ideal.

Groundwater quality impacts related to oil and gas activities are the main concern for shallow groundwater quality in the Peace Region, so future research should investigate groundwater quality near leaky oil and gas wells to characterize the chemical signature of impacted groundwater.

12. References

Allen, D.M. & Morgan, S. (2018). *Geoscience BC Peace Project: Final Report.* Geoscience BC.

Appelo, C.A. and Postma (2005). *Geochemistry, Groundwater, and Pollution.* Amsterdam, Netherlands: Balkema Publishers.

Back, W. (1961). *Techniques for mapping of hydrochemical facies.* Short papers in the geological and hydrogeological sciences: US Geological Survey.

Baye, A., Rathfelder, K., Wei, M, Yin, J. (2016). *Hydrostratigraphic, Hydraulic, and Hydrogeochemical Descriptions of Dawson Creek-Groundbirch Areas, Northeast BC.* Victoria, Prov of BC: Water Science Series.

British Columbia Ministry of Environment and Climate Change Strategy. 2020. B.C. Source Drinking Water Quality Guidelines: Guideline Summary. Water Quality Guideline Series, WQG-01. Prov. B.C., Victoria B.C.

Bhattacharya, J. & Walker, R.G. (1991). Allostratigraphic subdivision of the Upper Cretaceous Dunvegan, Shaftsbury, and Kaskapau formations in the northwestern Alberta subsurface. *Bulletin of Canadian Petroleum Geology*, 145-164.

Catto, N.R. (1991). *Quaternary Landforms of the Eastern Peace River Region, British Columbia.* Victoria, BC, Canada: Ministry of Energy, Mines, and Petroleum Resources.

Clague, J. & Hartman, G.M.D. (2008). Quaternary stratigraphy and glacial history of the Peace River valley, northeast British Columbia. *Canadian Journal of Earth Sciences*, 549-564.

Cloutier, V., Lefebvre, R., Savard, M.M., Borque, E., Therrien, R. (2006). Hydrogeochemistry and Groundwater Origin of the Basses-Laurentides Sedimentary Rock Aquifer System, St. Lawrence Lowlands, Quebec, Canada. *Hydrogeology Journal*. vol 14. p 573-590.

Cloutier, V., Lefebvre, R., Savard, M.M., Borque, E., Therrien, R. (2008). Multivariate statistical analysis of geochemical data as indicative of the hydrogeochemical evolution of groundwater in a sedimentary rock aquifer system. Journal of Hydrogeology, 294-313.

Cowen, A. (1998). *BC Peace Region groundwater initiative interm report.* Agriculture and Agri-Food Canada, Prairie Farm Rehabilitation Administration.

Cummings, D.R. (2012). Buried-valley aquifer in the Canadian Praries: geology, hydrogeology, and origin. *Canadian Journal of Earth Sciences*, 987-1004.

Davis, J.C. (1985). *Statistical and Data Analysis in Geology.* Kansas, USA: Wiley.

Edmunds, W.M. & Shand, P. (2008). *Natural Groundwater Quality.* Malden, MA: Blackwell Publishing.

Goetz, M., Beckie, R.D., Cahill, A.G. (2021). Groundwater Recharge in a Confined Paleovalley Setting, Northeast British Columbia, Canada. *Hydrogeology Journal*, vol. 29, no. 5, pp. 1797-1812.

Guler, C. (2004). Delineation of hydrochemical facies distribution in a regional groundwater system by means of fuzzy c-means clustering. *Water Resources Research*.

Guler, C.T. (2002). Evaluation of graphical and multivariate statistical methods for classification of water chemistry data. *Journal of Hydrogeology*, 455-474.

Hamilton, S., Matheson, E.J., Freckelton, C.N., Burke, H.E. (2011). Ambient Groundwater Geochemistry Program: the 2011 Aurora-Orillia Study area and Selected Results for the Bruce and Niagra Peninsulas. Ontario Geological Survey, Open File Report 6270.

Hem, J.D. (1989). *Study and Interpretation of the Chemical Characteristics of Natural Water.* Alexandria, VA: US Geological Survey.

Hickin, A.S. & Best, M.E. (2016). *Geometry and valley-fill stratigraphic framework for aquifers in the Groundbirch paleovalley assessed through shallow seismic and ground-based field-Based Hydrogeological Research.* Malden, US. Blackwell Publishing Ltd. *Groundwater 2013-07, Vol.51(4), p. 488-510.electromagnetic surveys.* BC Ministry of Energy and Mines, British Columbia Geological Survey.

Holding, S. and Allen, D.M. . (2015). *Shallow Groundwater Intrinsic Vulnerability Mapping in Northeast British Columbia.* Burnaby, BC: Simon Fraser University.

Holland, H.D., Turekian K. K., (2004). *Treatise in Geochemistry: Surface and Ground Water, Weathering, and Soils.* Wyoming, USA: Elsevier Pergamon.

Jackson, R.E., Gorody, A.W., Mayer, B., Roy, J.W., Ryan, M.C., Van Stempvoort, D.R. (2013). *Groundwater Protection and Unconventional Gas Extraction: The Critical Need for*

Jones, J.F. (1966). *Geology and groundwater resources of the Peace River district, Northwestern Alberta.* Edmonton, Alberta: Research Council of Alberta.

Levson, V. (2015). *Interpretation of Quaternary sediments and depth to bedrock through data compilation and correction of gamma logs.* Geoscience BC.

Lowen, D. (2011). *Aquifer classification mapping in the Peace River region for the Montney Water Project.* Lowen Hydrogeological Consulting.

Martinolich, M. (2022). *Characterizing the baseline hydrogeochemistry of a shallow groundwater system in the Peace Region, Northeast BC.* Simon Fraser University, 2022.

Mathews, W.H. (1978). *Quaternary stratigraphy and geomorphology of Charlie Lake (94A) Map-Area, British Columbia.* Energy, Mines, and Resources Canada.

McMechan, M. (1994). *Geology and structure cross section, Dawson Creek, British Columbia.* Ottawa, ON: Geological Survey of Canada.

Morgan, S.E. (2018). *Investigating the role of buried valley aquifer systems in the regional hydrogeology of the Central Peace Region in Northeast British Columbia (M.Sc. Thesis).* Burnaby, Canada: Simon Fraser University.

Piper, A. (1944). A graphical procedure in the geochemical interpretation of water analyses. *Transactions of the American Geophysical Union*, 914-923.

Plint, A. (2003). Clastic Sediment Partitioning in a Cretaceous Delta System, Western Canada: Response to Tectonic and Sea-Level Controls. *Geologia Croatica*, 39-68.

Rutherford, R. (1930). *Geology and water resources in parts of the Peace River and Grand Prarie Districts, Alberta.* Alberta Research Council, Report 21.

Sharma, P. (2019). *The Most Comprehensive Guide to K-Means Clustering You Will Ever need. url: https://www.analyticsvidhya.com/blog/2019/08/comprehensive-guide-k-means-clustering/#:~:text=In%20K%2DMeans%2C%20each%20cluster,and%20their%20respective%20cluster%20centroid.*

Steinhorst, K. &. Williams, J. (1985). Discrimination of Groundwater Sources Using Cluster Analysis, MANOVA, Canonical Analysis and Discriminant Analysis. *Water Resources Research*, 1149-1156.

Stelck, C.R. & Wall, J.H. (1955). *Foraminifera of the Cenomanian Dunveganoceras zone from the Peace River area of western Canada.* Alberta Research Council, Report no. 75.

Stiff, H. J. (1951). The interpretation of chemical water analysis by means of patterns. *Journal of Petroleum Technology*.

Stott, D.F. (1982). Lower Cretaceous Fort St. John Group and Upper Cretaceous Dunvegan Formation of the Foothills and Plains of Alberta, British Columbia, District of Mackenzie and Yukon Territory. Geological Survey of Canada.

Toth, J. (1963). A Theoretical Analysis of Groundwater Flow in Small Drainage Basins. Journal of Geophysical Research, 4795.

Vengosh, A., Jackson, Robert B., Warner, N., Darrah, Thomas H, Kondash, A. (2014) A Critical Review of the RIsks to Water Resources from Unconventional Shale Gas Development and Hydraulic Fracturing in the United States. American Chemical Society, Environmental Science and Technology, 2014-08-05, Vol.48 (15), p.8334-8348.

13. Appendix A – XRD Mineralogy Results

Table A-1. XRD Mineralogy data from sediment samples

	Actinolite	Anatase	Barite	Calcite-Mg-Calcite	Clinochlore	Dolomite-Ankerite	Dravite	Goethite	Gypsum	Halite	Illite-Muscovite 1M	Illite-Muscovite 2M1	Iron-alpha	Jarosite	Kaolinite	K-feldspar	Kutnohorite	Lepidocrocite	Palygorskite	Plagioclase	Pyrite	Quartz	Rhodochrosite	Rutile	Siderite	Titanite
clay/silt	0.0	0.5	0.0	9.3	4.7	4.7	0.0	0.0	0.0	0.0	0.0	39.6	0.0	0.0	4.6	2.5	0.0	0.0	0.0	2.7	0.0	30.9	0.0	0.6	0.0	0.0
clay/silt	0.0	0.3	0.0	0.0	1.8	0.0	0.6	0.0	0.2	0.0	0.0	13.1	0.1	0.6	3.3	1.9	0.0	0.0	0.0	3.0	0.0	74.7	0.0	0.5	0.0	0.0
clay/silt	0.0	0.4	0.0	0.0	2.3	0.0	0.0	0.0	0.0	0.0	0.0	18.5	0.0	0.0	5.3	4.0	0.0	0.0	0.0	6.3	0.0	62.4	0.0	0.7	0.0	0.0
clay/silt	0.7	0.1	0.0	11.0	1.4	20.5	0.0	0.0	0.0	0.0	0.0	4.5	0.0	0.0	0.5	3.0	0.0	0.0	0.0	7.6	0.0	50.1	0.0	0.4	0.2	0.0
clay/silt	0.9	0.2	0.0	15.0	4.7	13.9	0.0	0.0	0.0	0.0	0.0	17.4	0.0	0.0	2.0	3.7	0.0	0.0	0.0	7.3	0.0	34.9	0.0	0.0	0.0	0.0
clay/silt	0.0	0.5	0.0	11.0	4.4	9.1	0.0	0.0	0.0	0.0	0.0	30.1	0.0	0.0	4.8	2.5	0.0	0.0	0.0	3.1	0.6	33.5	0.0	0.4	0.0	0.0
clay/silt	0.0	0.7	0.0	2.1	4.3	2.7	0.0	0.0	0.0	0.0	2.5	38.9	0.0	0.0	8.6	1.8	0.0	0.0	0.0	3.5	0.6	33.6	0.0	0.7	0.0	0.0
clay/silt	0.0	0.0	0.0	13.0	3.8	8.9	0.0	0.0	0.0	0.0	0.0	22.9	0.0	0.0	2.2	2.2	0.0	0.0	0.0	3.0	0.5	43.4	0.0	0.0	0.1	0.0
clay/silt	0.0	0.0	0.0	11.8	4.8	7.2	0.0	0.0	0.0	0.0	0.0	27.4	0.0	0.0	3.0	0.9	0.0	0.0	0.0	2.7	0.8	40.9	0.0	0.5	0.0	0.0
clay/silt	0.0	0.7	0.0	0.0	3.1	0.4	0.0	0.0	0.0	0.0	0.0	24.5	0.0	0.0	4.6	0.5	0.0	0.0	0.0	3.4	0.2	62.1	0.0	0.5	0.0	0.0
Average	0.2	0.4	0.0	7.3	3.5	6.7	0.1	0.0	0.0	0.0	0.3	23.7	0.0	0.1	3.9	2.3	0.0	0.0	0.0	4.3	0.3	46.6	0.0	0.4	0.0	0.0
diamict-mud	0.0	0.1	0.0	4.6	0.8	2.3	0.0	0.8	0.0	0.0	0.0	4.4	0.1	0.0	1.5	1.0	0.0	0.0	0.0	2.6	0.1	80.9	0.0	0.3	0.1	0.4
diamict-mud	0.0	0.4	0.0	1.1	2.2	1.2	0.0	0.0	0.0	0.0	0.0	12.0	0.1	0.0	4.6	3.6	0.0	0.0	0.0	6.7	0.4	66.4	0.0	0.5	0.7	0.0
diamict-mud	0.0	0.5	0.0	1.5	2.3	1.6	0.0	0.0	3.9	0.0	0.0	16.1	0.0	0.0	4.3	2.8	0.0	0.0	0.0	5.6	0.0	60.6	0.0	0.8	0.0	0.0
diamict-mud	0.0	0.6	0.4	0.0	1.6	0.0	0.0	0.0	0.0	0.0	0.0	16.8	0.0	0.0	7.0	3.3	0.0	0.0	0.0	5.8	0.0	63.8	0.0	0.6	0.2	0.0
diamict-mud	0.0	0.5	0.0	0.3	1.9	0.9	0.0	0.0	0.0	0.0	0.0	25.3	0.0	0.0	4.9	2.4	0.0	0.0	0.0	2.8	0.7	57.3	0.0	0.0	3.0	0.0
Average	0.0	0.4	0.1	1.5	1.7	1.2	0.0	0.2	0.8	0.0	0.0	14.9	0.0	0.0	4.5	2.6	0.0	0.0	0.0	4.7	0.2	65.8	0.0	0.4	0.8	0.1
diamict-sand	0.0	0.0	0.0	9.5	2.5	4.2	0.0	0.0	0.0	0.0	0.0	4.1	0.0	0.0	1.7	2.0	0.0	0.0	0.0	3.3	0.4	71.7	0.0	0.0	0.4	0.0
diamict-sand	0.0	0.5	0.0	3.0	1.2	3.2	0.0	0.6	0.0	0.0	0.0	14.8	0.0	0.0	4.0	0.0	0.0	0.0	0.0	3.0	0.3	68.3	0.0	0.9	0.0	0.0
diamict-sand	0.0	0.7	0.0	0.0	0.8	0.0	0.0	0.0	0.0	0.0	0.0	17.6	0.0	3.5	4.5	1.7	0.0	0.0	0.0	4.7	0.0	65.8	0.0	0.9	0.0	0.0
diamict-sand	0.0	0.3	0.4	0.5	1.5	0.0	0.0	5.4	0.0	0.0	0.0	11.2	0.0	0.0	3.7	3.4	0.0	0.0	0.0	6.5	0.0	66.2	0.0	0.6	0.3	0.0
Average	0.0	0.4	0.1	3.3	1.5	1.9	0.0	1.5	0.0	0.0	0.0	11.9	0.0	0.9	3.4	1.8	0.0	0.0	0.0	4.4	0.2	68.0	0.0	0.6	0.2	0.0
sandy gravel	0.0	0.3	0.0	9.2	1.6	4.7	0.0	2.8	0.0	0.0	0.0	6.6	0.0	0.0	2.9	0.0	1.2	0.0	0.0	2.1	0.2	64.5	0.0	0.3	2.7	1.0
sandy gravel	0.0	0.2	0.0	7.5	0.9	4.8	0.0	4.3	0.0	0.0	0.0	7.3	0.0	0.0	2.3	0.0	0.0	0.0	0.0	2.3	0.2	69.5	0.0	0.6	0.0	0.0
sandy gravel	0.0	0.5	0.0	0.0	0.0	0.0	0.0	0.0	0.0	0.0	0.0	22.8	0.0	1.1	3.5	1.2	0.0	0.0	0.0	3.8	0.0	66.6	0.0	0.4	0.0	0.0
sandy gravel	0.0	0.3	0.0	7.0	1.7	3.5	0.5	0.7	0.0	0.0	0.0	8.0	0.0	0.0	2.4	1.3	0.0	0.0	0.0	3.0	0.0	70.3	0.0	0.4	0.4	0.6
sandy gravel	0.0	0.2	0.0	7.0	1.3	4.3	0.0	0.6	0.0	0.0	0.0	6.1	0.0	0.0	2.0	1.1	0.0	0.0	0.0	2.9	0.3	72.2	0.0	0.4	0.9	0.7
sandy gravel	0.0	0.0	0.0	0.0	0.0	0.0	0.0	11.9	0.0	0.0	1.3	6.0	0.0	0.0	3.1	0.9	0.0	0.4	0.0	1.0	0.0	74.7	0.0	0.7	0.0	0.0
sandy gravel	0.0	0.2	0.0	0.0	0.0	0.0	0.0	7.5	0.0	0.0	0.0	6.6	0.0	0.0	2.1	1.2	0.0	0.0	0.0	1.2	0.0	80.9	0.0	0.3	0.0	0.0
sandy gravel	0.0	0.1	0.0	10.0	0.0	2.5	0.0	0.6	0.0	0.0	0.0	2.9	0.0	0.0	0.7	0.0	0.0	0.0	0.3	1.8	0.0	80.6	0.0	0.4	0.1	0.0
sandy gravel	0.0	0.0	0.0	9.5	0.9	2.6	0.0	0.0	0.0	0.0	0.0	3.5	0.0	0.0	1.4	1.6	0.0	0.0	0.0	2.2	0.2	77.7	0.0	0.0	0.3	0.0
sandy gravel	0.0	0.6	0.0	6.8	2.6	5.6	0.0	0.0	0.4	0.0	0.0	17.0	0.0	0.0	4.0	3.4	0.0	0.0	0.0	2.9	0.6	55.6	0.0	0.0	0.4	0.0
sandy gravel	0.0	0.2	0.0	2.3	1.2	1.3	0.0	0.7	0.0	0.0	0.0	4.5	0.0	0.0	1.9	1.0	0.0	0.0	0.0	2.1	0.2	83.8	0.0	0.4	0.2	0.3
sandy gravel	0.0	0.1	0.0	2.7	1.0	0.0	0.0	5.6	0.0	0.0	0.0	4.7	0.0	0.0	3.3	4.0	0.0	0.0	0.0	8.0	0.0	70.0	0.0	0.6	0.0	0.0
Average	0.0	0.2	0.0	5.2	0.9	2.4	0.0	2.9	0.0	0.0	0.1	8.0	0.0	0.1	2.5	1.3	0.1	0.0	0.0	2.8	0.1	72.2	0.0	0.4	0.4	0.2
silt/sand	0.0	0.2	0.0	8.7	1.0	3.3	0.0	1.9	0.0	0.0	0.0	6.6	0.0	0.0	2.2	0.0	0.0	0.0	0.0	2.3	0.2	72.9	0.0	0.6	0.2	0.0
silt/sand	0.0	0.3	0.0	11.1	0.9	2.9	0.8	1.7	0.0	0.0	0.0	7.4	0.0	0.0	2.8	0.0	0.0	0.0	0.0	2.5	0.1	68.0	0.0	0.4	0.2	0.8
silt/sand	0.0	0.2	0.0	0.1	0.8	0.0	0.0	0.0	0.4	0.0	0.0	7.5	0.1	0.0	2.2	2.1	0.0	0.0	0.0	2.8	0.3	83.0	0.0	0.5	0.0	0.0
silt/sand	0.8	0.1	0.0	11.1	1.8	10.0	0.0	0.0	0.0	0.0	0.0	5.5	0.0	0.0	0.5	3.4	0.0	0.0	0.0	9.2	0.0	57.1	0.0	0.4	0.1	0.0
silt/sand	0.0	0.0	0.0	7.4	1.5	6.7	0.0	0.0	0.0	0.0	0.0	4.9	0.0	0.0	1.2	1.4	0.0	0.0	0.0	3.0	0.3	73.4	0.0	0.0	0.2	0.0
silt/sand	0.0	0.0	0.0	9.8	1.1	3.5	0.0	0.0	0.0	0.0	0.0	4.2	0.0	0.0	0.9	1.6	0.0	0.0	0.0	2.5	0.2	76.0	0.0	0.2	0.2	0.0
silt/sand	0.0	0.4	0.0	0.0	1.6	0.0	0.0	0.0	0.0	1.9	0.0	20.2	0.0	0.0	3.5	1.3	0.0	0.0	0.0	2.2	0.3	68.2	0.0	0.3	0.3	0.0
silt/sand	0.0	0.2	0.0	2.7	0.7	2.9	0.0	0.0	0.0	0.0	0.0	7.7	0.0	0.0	1.9	2.2	0.0	0.0	0.0	2.3	0.5	77.9	0.0	0.0	1.0	0.0
silt/sand	0.0	0.4	0.0	7.2	1.3	4.4	0.0	0.8	0.0	0.0	0.0	9.7	0.0	0.0	2.5	1.5	0.0	0.0	0.0	3.4	0.6	66.6	0.0	0.5	0.6	0.6
silt/sand	0.0	0.1	0.0	1.8	1.0	1.7	0.0	0.0	0.0	0.0	0.0	3.2	0.0	0.0	1.6	0.6	0.0	0.0	0.0	1.7	0.2	87.4	0.0	0.3	0.2	0.3
silt/sand	0.0	0.2	0.0	0.8	1.1	0.4	0.0	1.7	0.0	0.0	1.3	6.8	0.0	0.0	2.9	3.7	0.0	0.0	0.0	7.2	0.0	73.1	0.0	0.7	0.1	0.0
Average	0.1	0.2	0.0	5.5	1.2	3.2	0.1	0.6	0.0	0.2	0.1	7.6	0.0	0.0	2.0	1.6	0.0	0.0	0.0	3.6	0.2	73.0	0.0	0.4	0.3	0.2

Table A-2. XRD Mineralogy data from bedrock samples

	Actinolite	Anatase	Barite	Calcite-Mg-Calcite	Clinochlore	Dolomite-Ankerite	Dravite	Goethite	Gypsum	Halite	Illite-Muscovite 1M	Illite-Muscovite 2M1	Iron-alpha	Jarosite	Kaolinite	K-feldspar	Kutnohorite	Lepidocrocite	Palygorskite	Plagioclase	Pyrite	Quartz	Rhodochrosite	Rutile	Siderite	Titanite
mudstone	0.0	1.0	0.0	0.2	3.2	0.0	0.0	0.0	0.7	0.0	0.0	25.5	0.0	0.0	5.0	2.5	0.0	0.0	0.0	5.3	0.9	53.5	0.0	0.8	1.4	0.0
mudstone	0.0	0.9	0.0	0.0	2.7	0.0	0.0	1.0	0.0	0.0	0.8	23.1	0.2	0.0	6.0	4.4	0.0	0.0	0.0	6.1	0.0	53.8	0.0	0.9	0.0	0.0
mudstone	0.0	0.4	0.2	0.1	0.0	0.8	0.0	0.0	0.8	0.0	0.0	10.5	0.1	0.0	2.0	0.0	0.9	0.0	0.0	2.7	5.1	75.1	0.0	0.5	0.1	0.7
mudstone	0.0	0.3	0.0	0.2	1.2	0.5	0.0	0.0	0.0	0.0	0.0	18.7	0.1	0.0	2.7	1.9	0.0	0.0	0.0	3.4	1.2	68.3	0.3	0.3	0.7	0.0
mudstone	0.0	0.4	0.0	0.3	0.8	0.5	0.0	0.0	0.6	0.0	0.0	14.1	0.1	0.0	2.0	1.1	0.0	0.0	0.0	3.1	1.9	74.6	0.0	0.2	0.2	0.0
mudstone	0.0	0.7	0.0	0.0	0.0	0.0	0.0	0.0	1.0	0.0	0.0	26.8	0.0	2.1	5.6	0.0	0.0	0.0	0.0	2.0	0.0	61.1	0.0	0.7	0.0	0.0
mudstone	0.0	0.8	0.0	0.3	4.5	0.0	0.0	0.0	0.0	0.0	0.0	20.9	0.0	0.0	8.9	5.6	0.0	0.0	0.0	8.3	0.0	49.8	0.0	0.9	0.0	0.0
mudstone	0.0	1.0	0.0	0.4	2.5	0.0	0.0	0.0	0.6	0.7	2.2	20.7	0.1	0.0	4.2	1.9	0.0	0.0	0.0	3.0	2.6	59.0	0.0	0.9	0.4	0.0
mudstone	0.0	1.0	0.0	0.3	2.4	0.0	0.0	0.0	0.6	0.0	2.2	27.2	0.0	0.0	5.1	4.1	0.0	0.0	0.0	5.3	0.0	50.2	0.0	0.8	0.9	0.0
mudstone	0.0	1.0	0.0	0.2	1.1	0.0	0.0	0.0	0.4	0.0	2.8	22.9	0.2	0.0	6.2	1.9	0.0	0.0	0.0	3.4	2.8	56.0	0.0	0.8	0.3	0.0
mudstone	0.0	0.6	0.0	0.0	3.2	0.4	0.0	0.0	0.0	0.0	0.0	34.4	0.0	0.0	7.8	0.0	0.0	0.0	0.0	0.8	1.3	50.2	0.0	0.5	0.7	0.0
mudstone	0.0	0.5	0.0	0.0	3.2	0.4	0.0	0.0	0.0	0.0	0.0	32.1	0.0	0.0	5.9	0.8	0.0	0.0	0.0	1.0	1.4	47.6	0.0	0.3	6.7	0.0
mudstone	0.0	0.5	0.0	0.0	3.5	1.3	0.0	0.0	0.6	0.0	0.0	32.6	0.0	0.0	6.2	1.2	0.0	0.0	0.0	0.9	2.8	50.0	0.0	0.3	0.0	0.0
Average	0.0	0.7	0.0	0.1	2.2	0.3	0.0	0.1	0.4	0.1	0.6	23.8	0.1	0.2	5.2	2.0	0.1	0.0	0.0	3.5	1.5	57.6	0.0	0.6	0.9	0.1
sandstone	0.0	0.1	0.0	0.0	1.0	0.0	0.0	0.0	0.0	0.0	0.0	3.2	0.0	0.0	3.9	7.5	0.0	0.0	0.0	11.4	0.0	72.5	0.0	0.4	0.0	0.0
sandstone	0.0	1.0	0.5	0.4	3.7	0.0	0.0	1.9	0.0	0.0	2.4	21.9	0.0	0.0	7.9	5.0	0.0	0.0	0.0	8.2	0.0	45.2	0.0	1.0	1.0	0.0
sandstone	0.0	0.0	0.0	0.0	0.0	0.0	0.0	0.0	0.0	0.0	0.6	1.2	0.0	0.0	1.6	1.5	0.0	0.0	0.0	1.0	0.0	94.1	0.0	0.0	0.0	0.0
sandstone	0.0	0.5	0.0	0.0	2.3	0.0	0.0	0.0	0.0	0.0	1.2	5.8	0.0	0.0	11.2	2.0	0.0	0.0	0.0	10.6	0.0	64.5	0.0	0.4	1.5	0.0
sandstone	0.0	0.3	0.0	0.0	0.0	0.0	0.0	0.0	0.0	0.0	0.0	20.8	0.1	0.0	2.1	2.3	0.0	0.0	0.0	1.8	0.0	72.1	0.0	0.5	0.0	0.0
sandstone	0.0	0.5	0.0	0.0	2.8	0.0	0.6	0.0	0.0	0.0	0.0	11.7	0.1	0.0	8.1	4.0	0.0	0.0	0.0	9.2	0.2	59.4	0.0	0.5	3.0	0.0
sandstone	0.0	0.5	0.0	2.8	3.2	0.0	0.0	0.0	0.0	0.0	0.0	11.0	0.0	0.0	5.0	4.9	0.0	0.0	0.0	8.8	0.0	60.4	0.0	0.7	2.8	0.0
sandstone	0.0	0.4	0.0	0.0	2.4	0.4	0.0	0.0	0.0	0.0	0.0	15.1	0.0	0.0	6.1	4.6	0.0	0.0	0.0	10.4	0.0	60.0	0.0	0.6	0.0	0.0
Average	0.0	0.4	0.1	0.4	1.9	0.0	0.1	0.2	0.0	0.0	0.5	11.3	0.0	0.0	5.7	4.0	0.0	0.0	0.0	7.7	0.0	66.0	0.0	0.5	1.0	0.0

14. Appendix B – The Hydrochemical Baselines of the Unconsolidated Groundwater System

14.1. Chemical Properties

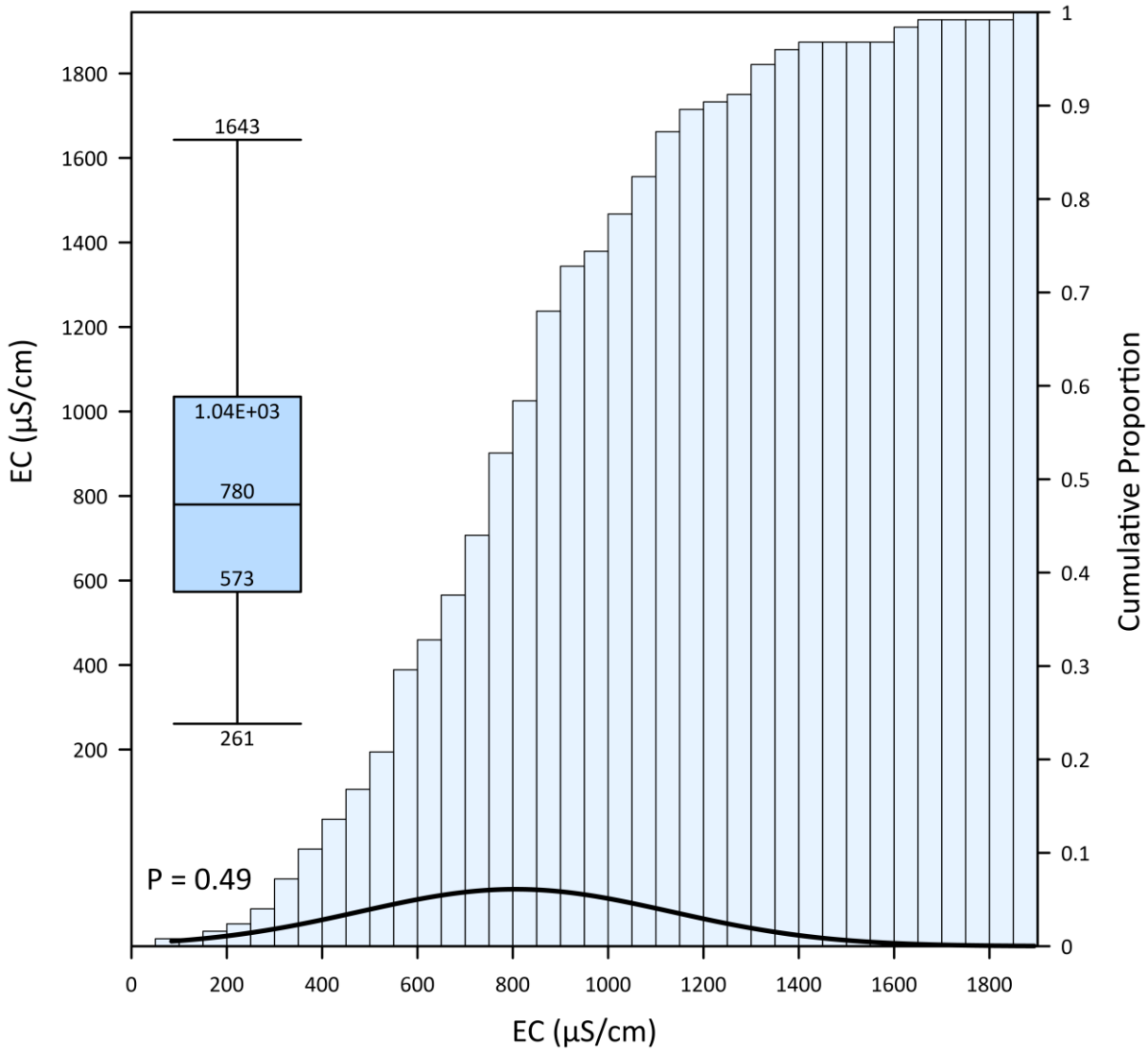

Figure B-1 The baseline EC of groundwater the sediments. The boxplot shows the median value on the centerline. Whiskers mark the 97.5th and 2.5th percentiles. EC values are normally distributed, with a p-value of 0.49.

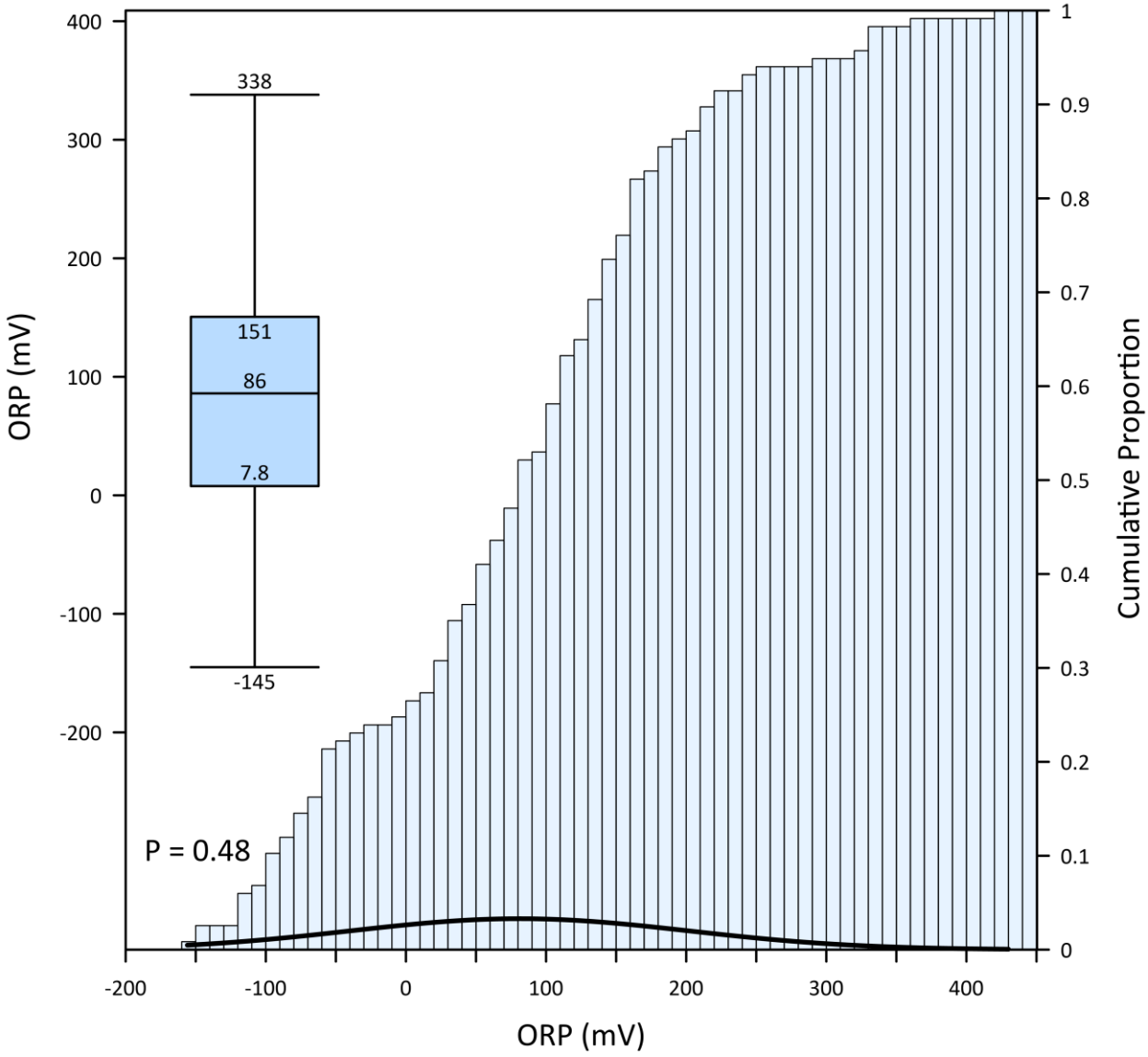

Figure B-2: The baseline ORP of groundwater in the sediments. The boxplot shows the median value on the centerline. Whiskers mark the 97.5th and 2.5th percentiles. ORP values are normally distributed, with a p-value of 0.48.

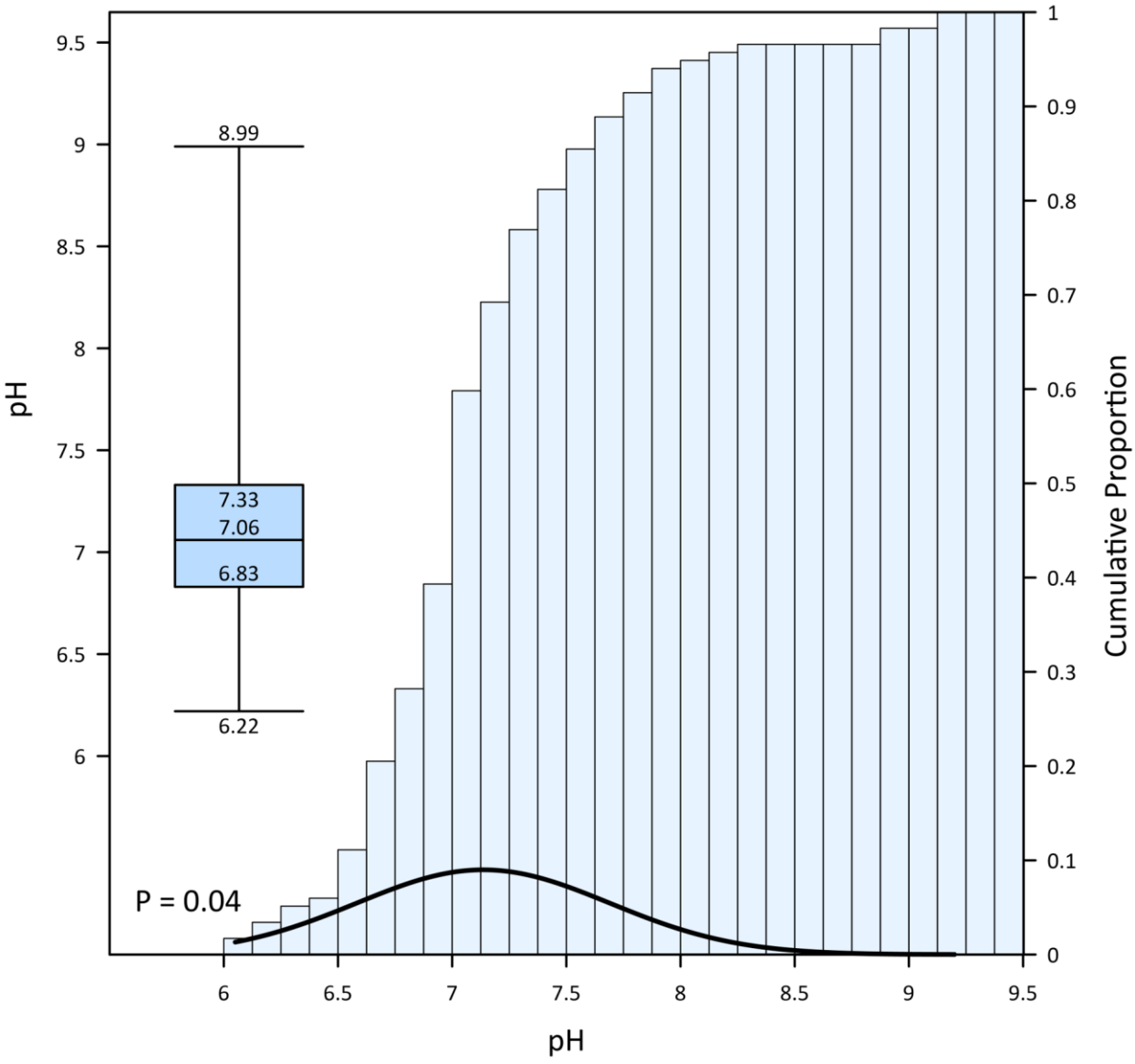

Figure B-3: The baseline pH of groundwater in the sediments. The boxplot shows the median value on the centerline. Whiskers mark the 97.5th and 2.5th percentiles. pH values do not follow a specified distribution. The pH values are normally distributed, with a p-value of 0.04.

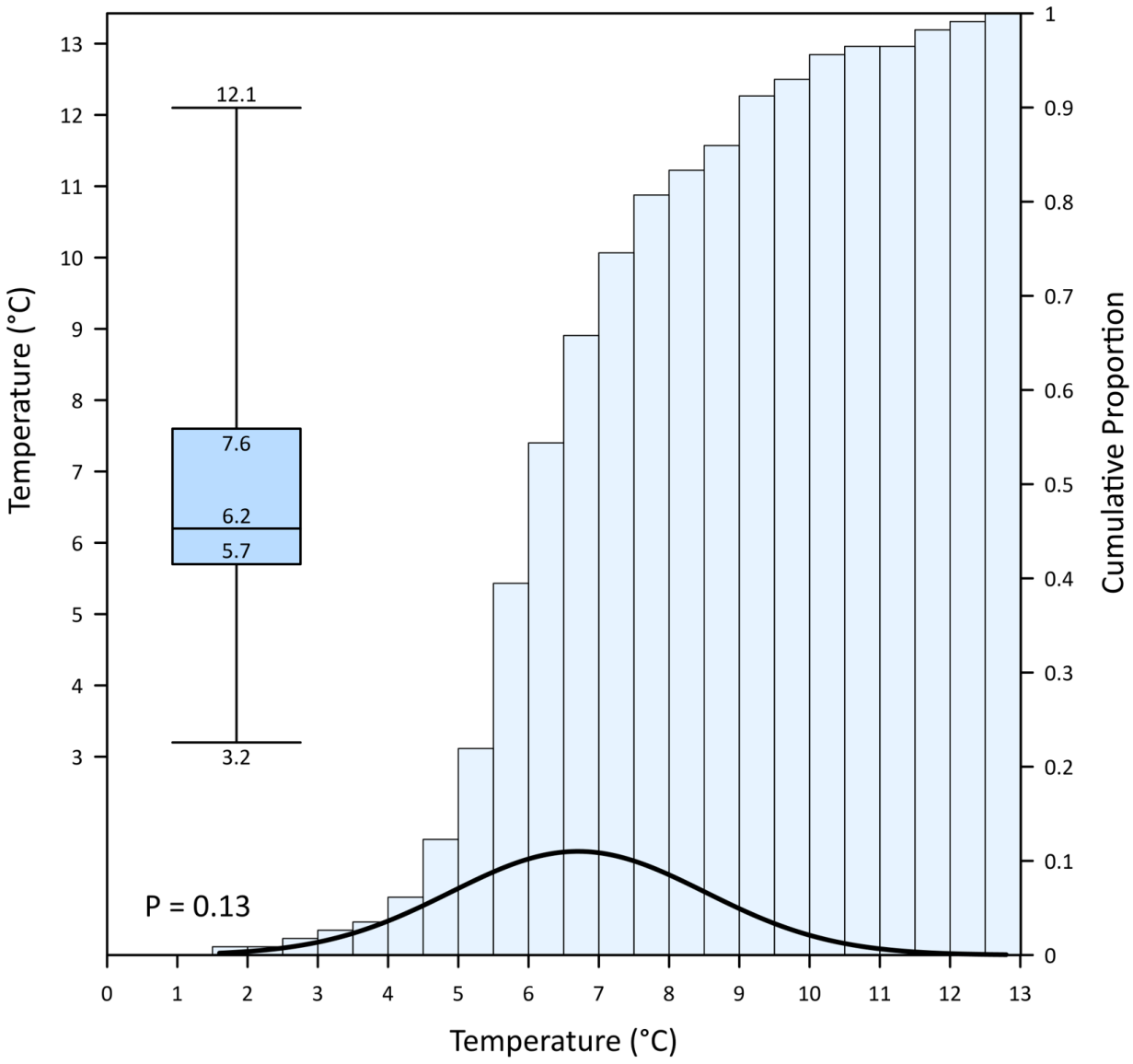

Figure B-4: Baseline temperatures of groundwater in the sediments. The boxplot shows median temperature on the centerline. Whiskers mark the 97.5th and 2.5th percentiles. Temperature values are normally distributed, with a p-value of 0.13.

14.2. Major and Minor Ion Concentrations

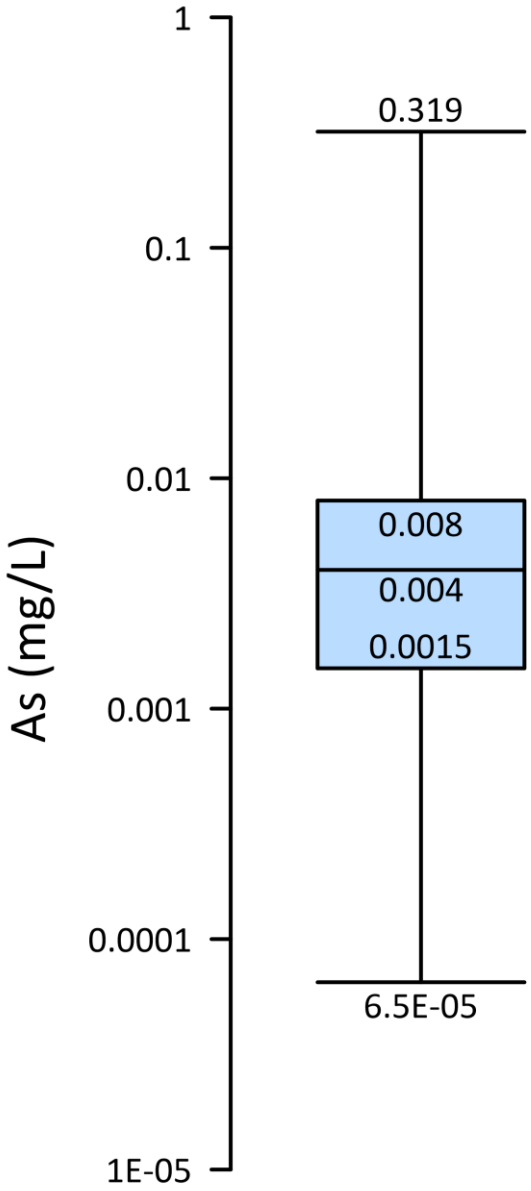

Figure B-5: Baseline arsenic concentrations in groundwater in the sediments. The boxplot shows the median concentration on the centerline. Whiskers mark the 97.5th and 2.5th percentiles. The range of arsenic concentrations is too large to show on a cumulative distribution plot.

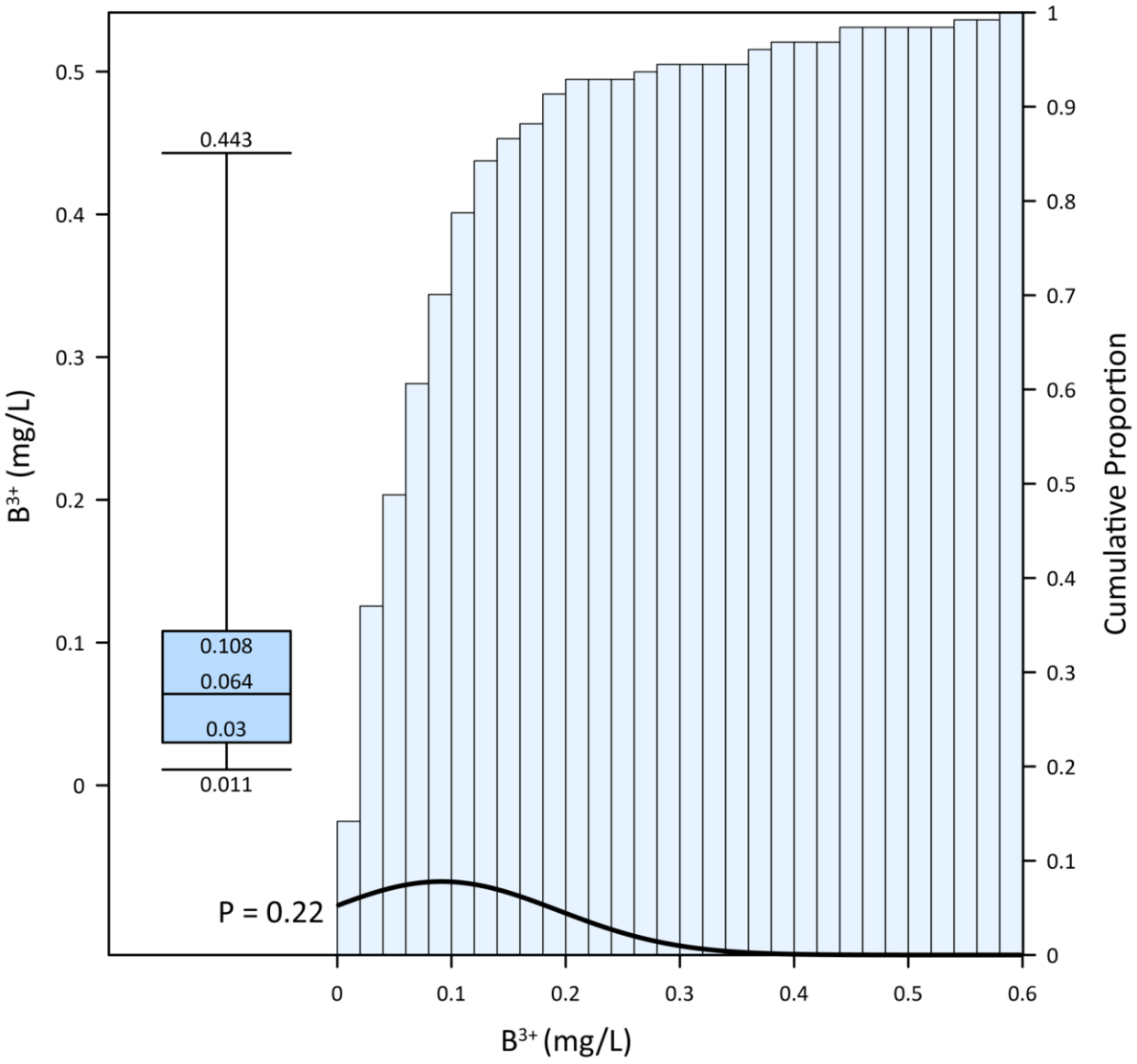

Figure B-6: Baseline boron concentrations in groundwater in the sediments. The boxplot shows the median concentration on the centerline. Whiskers mark the 97.5th and 2.5th percentiles. Boron concentrations are log-normally distributed, with a p-value of 0.22

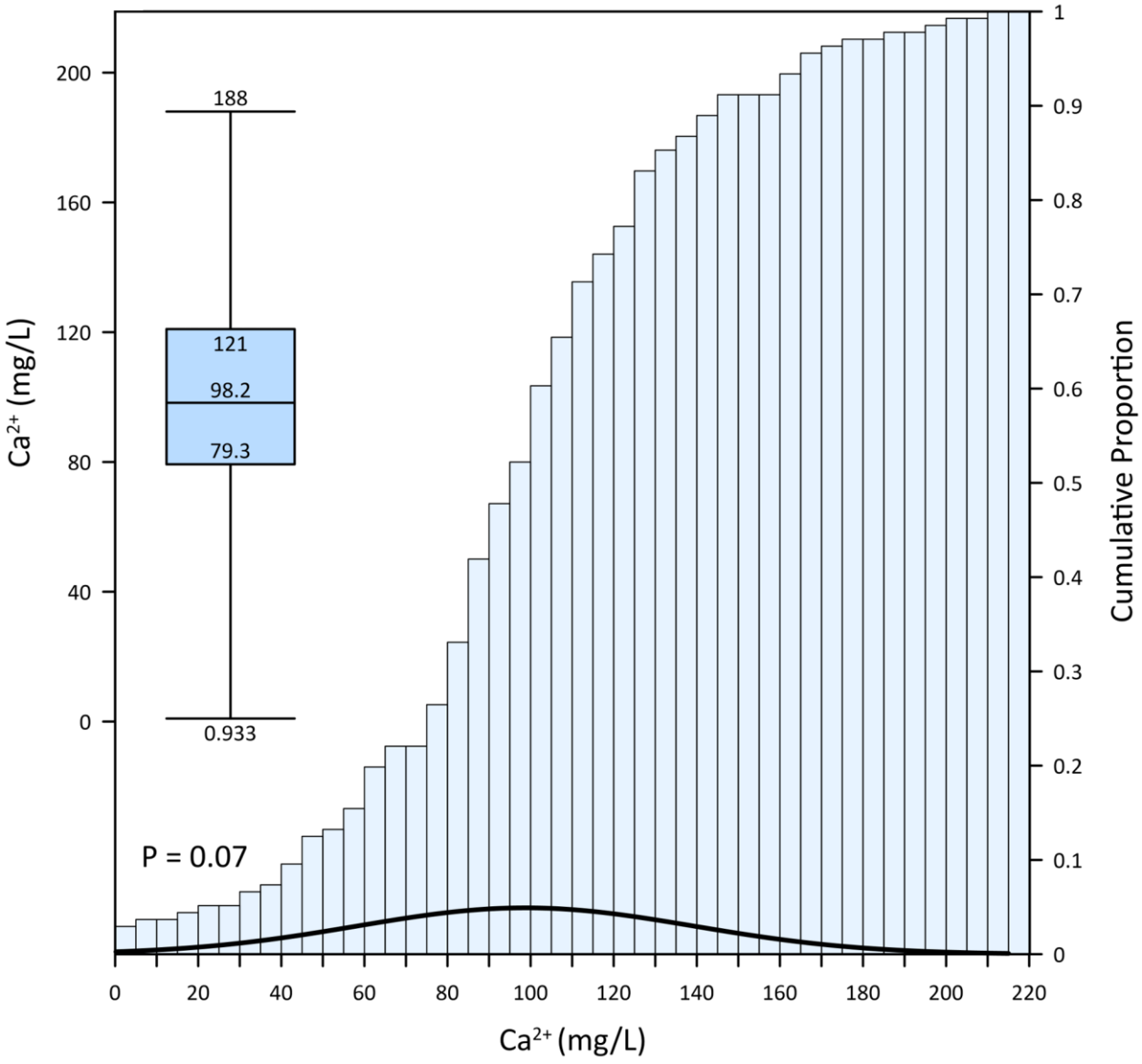

Figure B-7: Baseline calcium concentrations in groundwater in the sediments. The boxplot shows the median concentration on the centerline. Whiskers mark the 97.5th and 2.5th percentiles. Calcium concentrations are poorly normally distributed, with a p-value of 0.07.

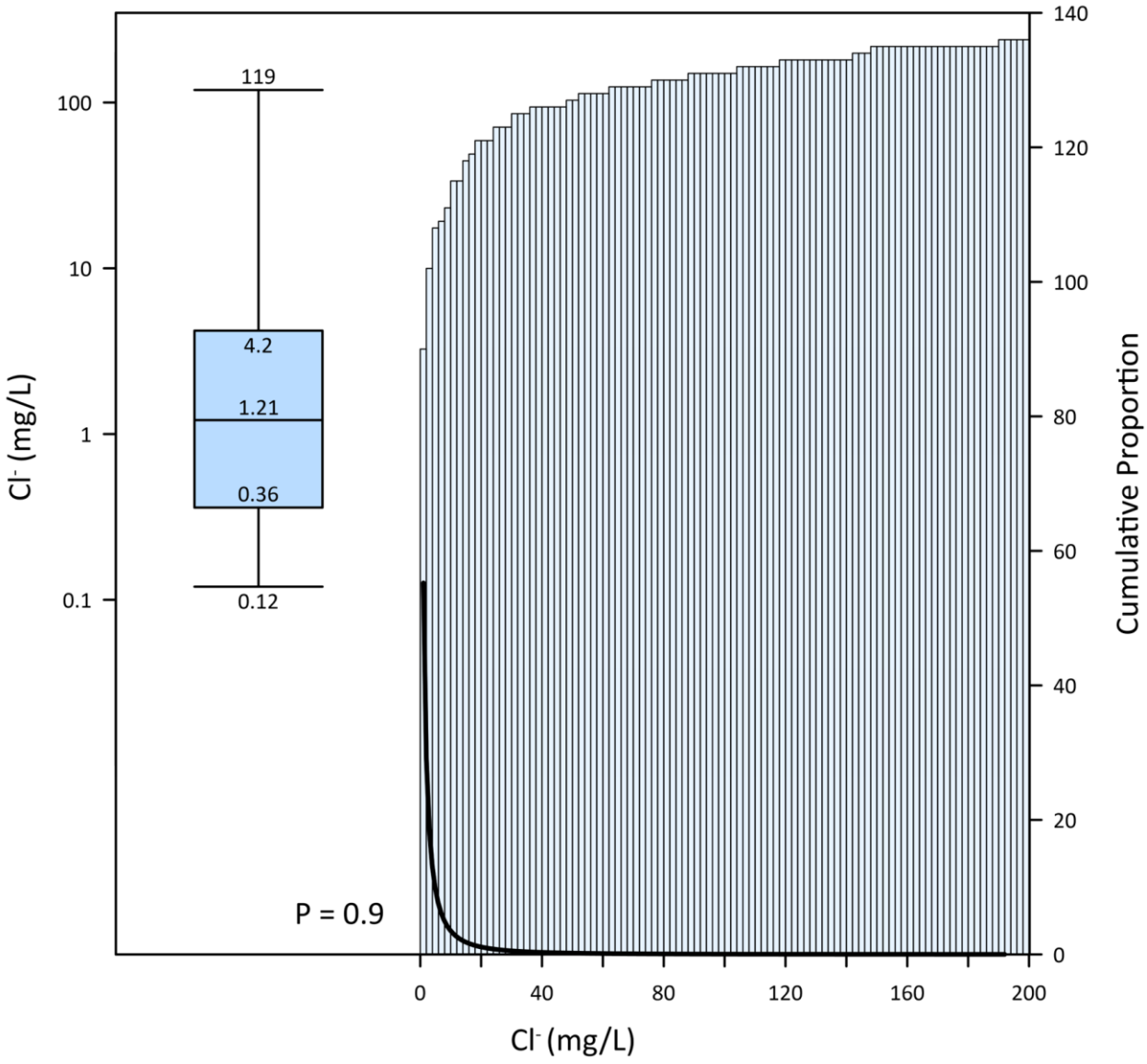

Figure B-8: Baseline chloride concentrations in groundwater in the sediments. The boxplot shows the median concentration on the centerline. Whiskers mark the 97.5th and 2.5th percentiles. Chloride concentrations are log-normally distributed, with a p-value of 0.9.

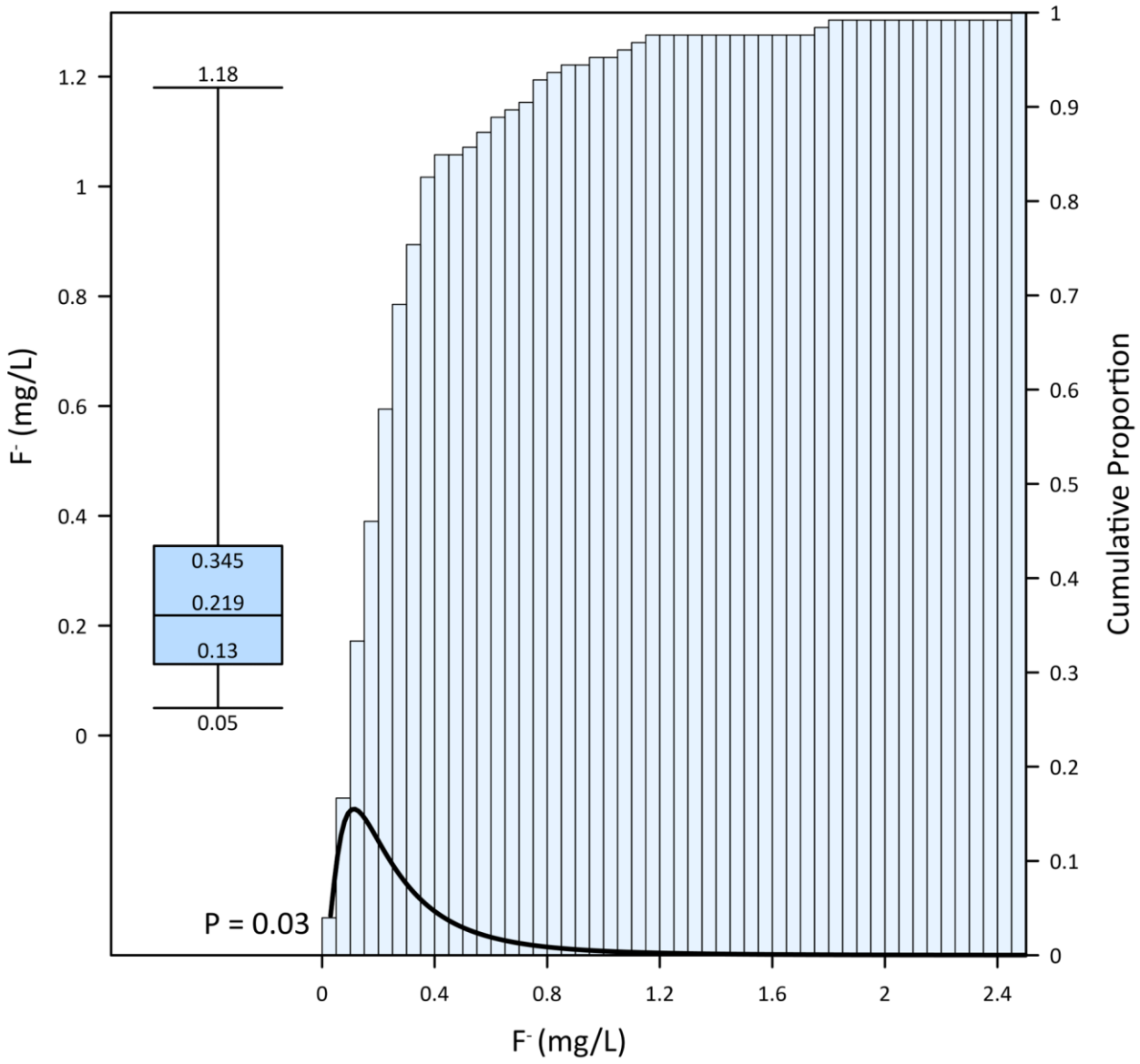

Figure B-9: Baseline fluoride concentrations in groundwater in the sediments. The boxplot shows the median concentration on the centerline. Whiskers mark the 97.5th and 2.5th percentiles. Fluoride concentrations are poorly log-normally distributed, with a p-value of 0.03.

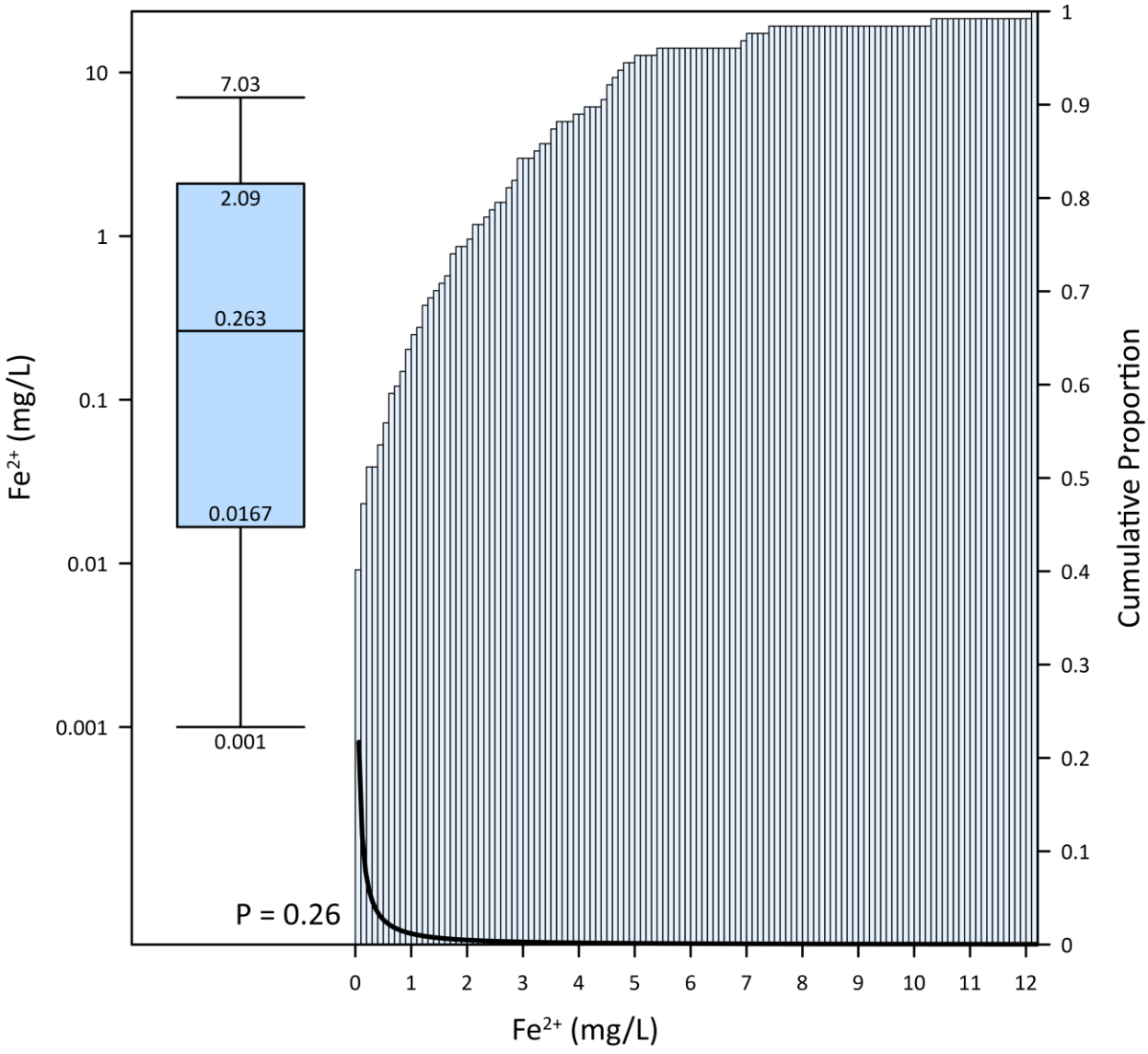

Figure B-10: Baseline ferrous iron concentrations in groundwater in the sediments. The boxplot shows the median concentration on the centerline. Whiskers mark the 97.5th and 2.5th percentiles. Iron concentrations are log-normally distributed, with a p-value of 0.26.

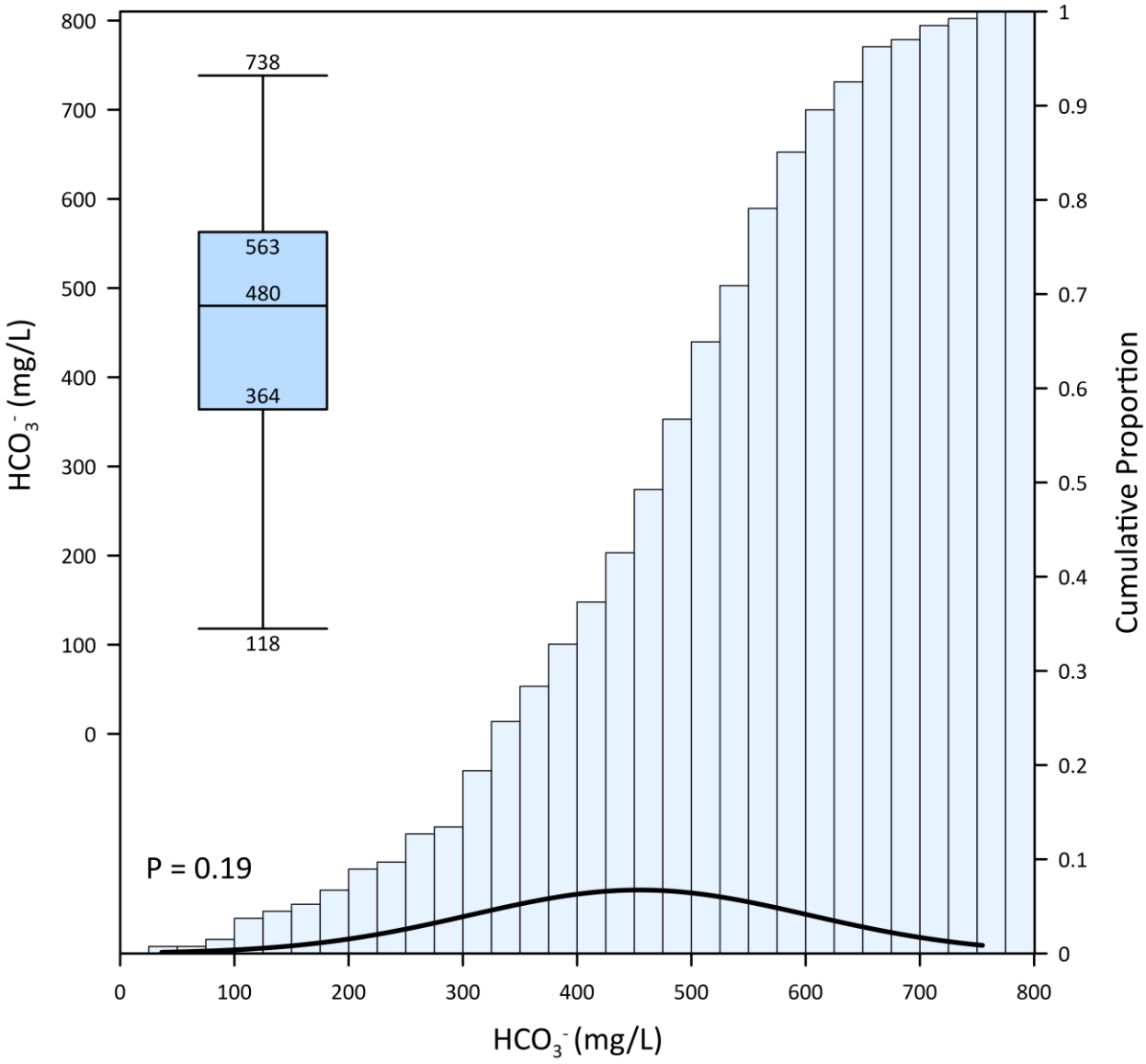

Figure B-11: Baseline bicarbonate concentrations in groundwater in the sediments. The boxplot shows the median concentration on the centerlines. Whiskers mark the 97.5th and 2.5th percentiles. Bicarbonate concentrations are normally distributed, with a p-value of 0.19.

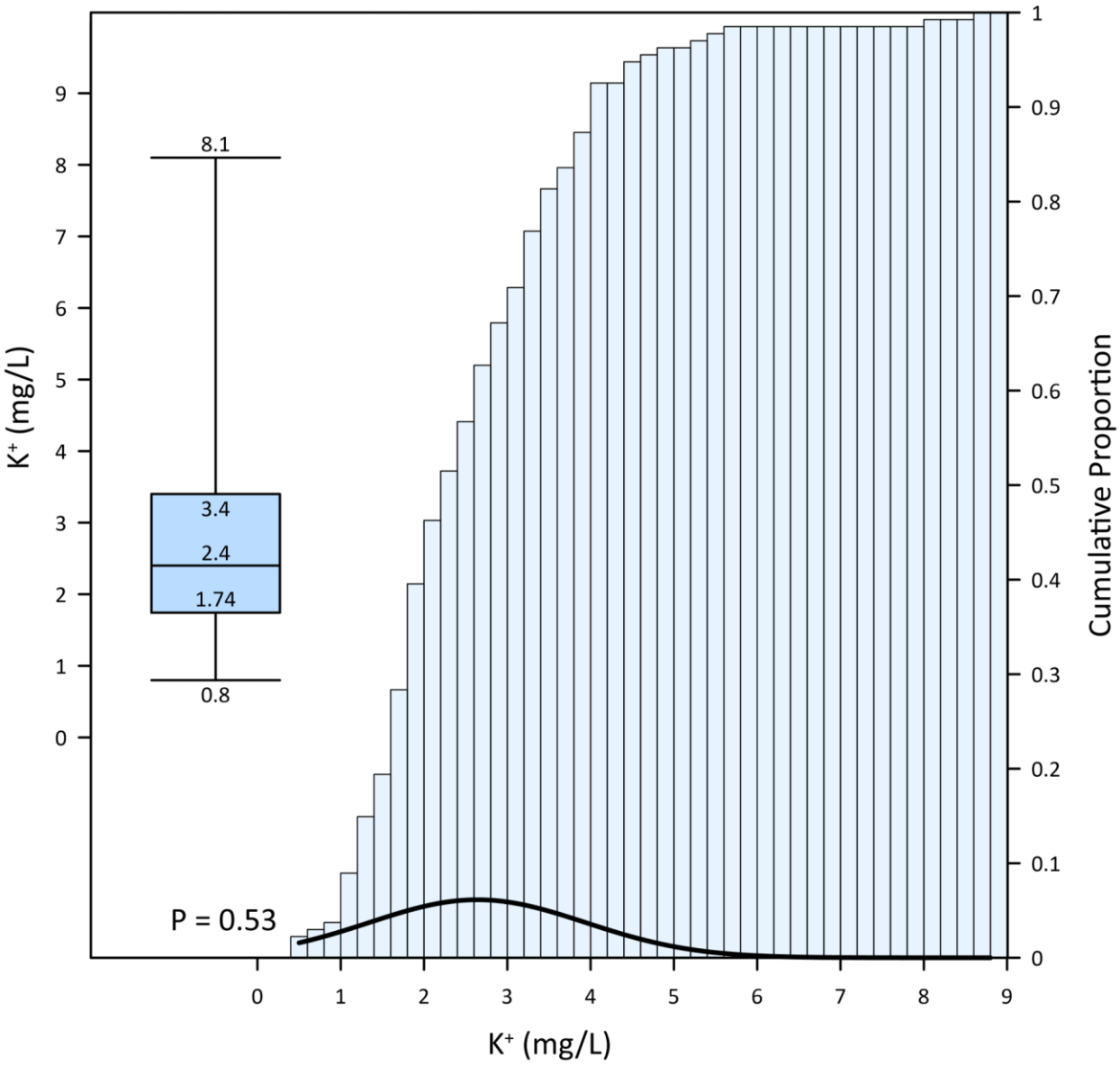

Figure B-12: Baseline potassium concentrations in groundwater in the sediments. The boxplot shows the median concentration on the centerline. Whiskers mark the 97.5th and 2.5th percentiles. Potassium concentrations are log-normally distributed, with a p-value of 0.53.

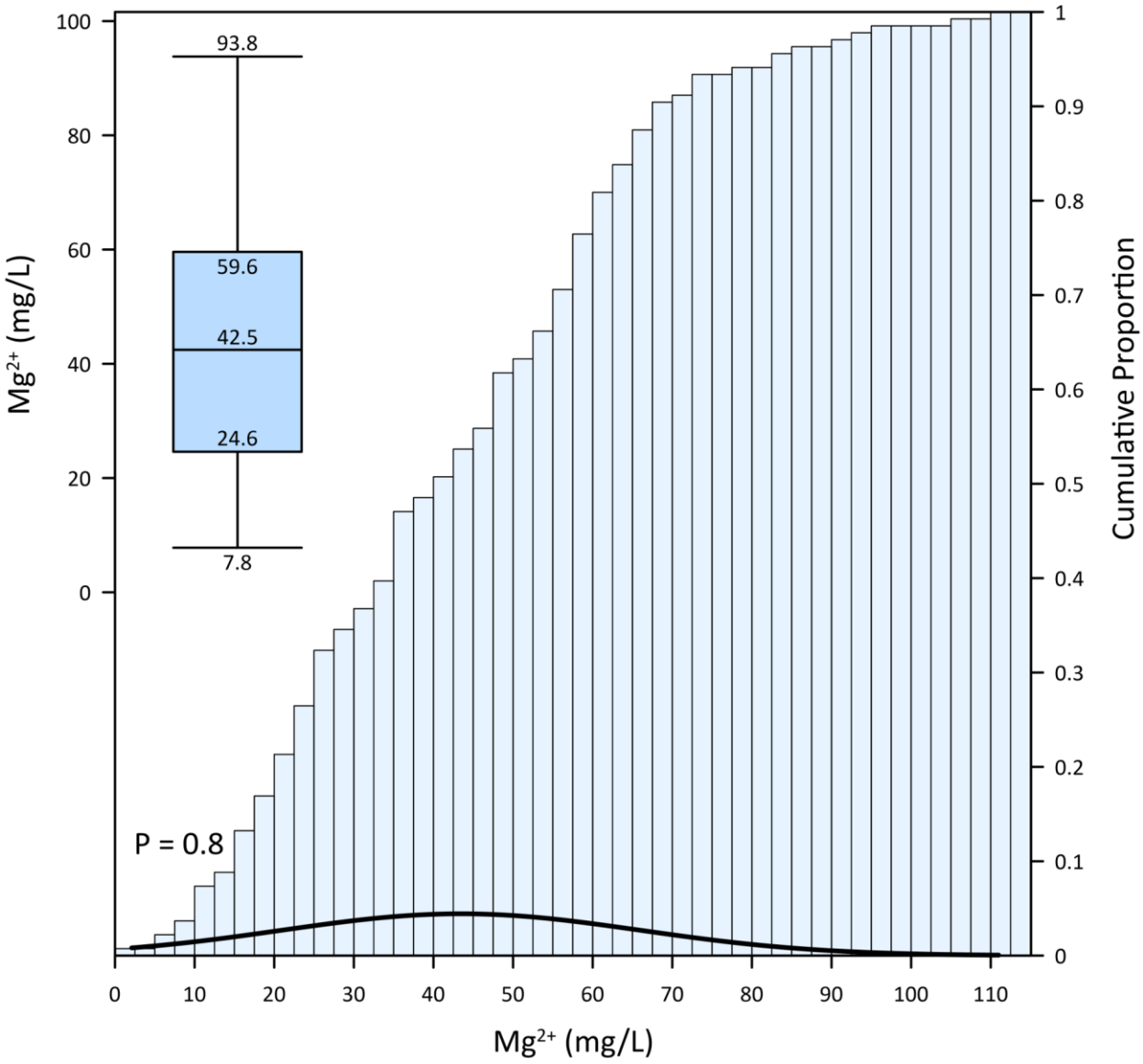

Figure B-13: Baseline magnesium concentrations in groundwater in the sediments. The boxplot shows the median concentration on the centerline. Whiskers mark the 97.5th and 2.5th percentiles. Magnesium concentrations are normally distributed, with a p-value of 0.8.

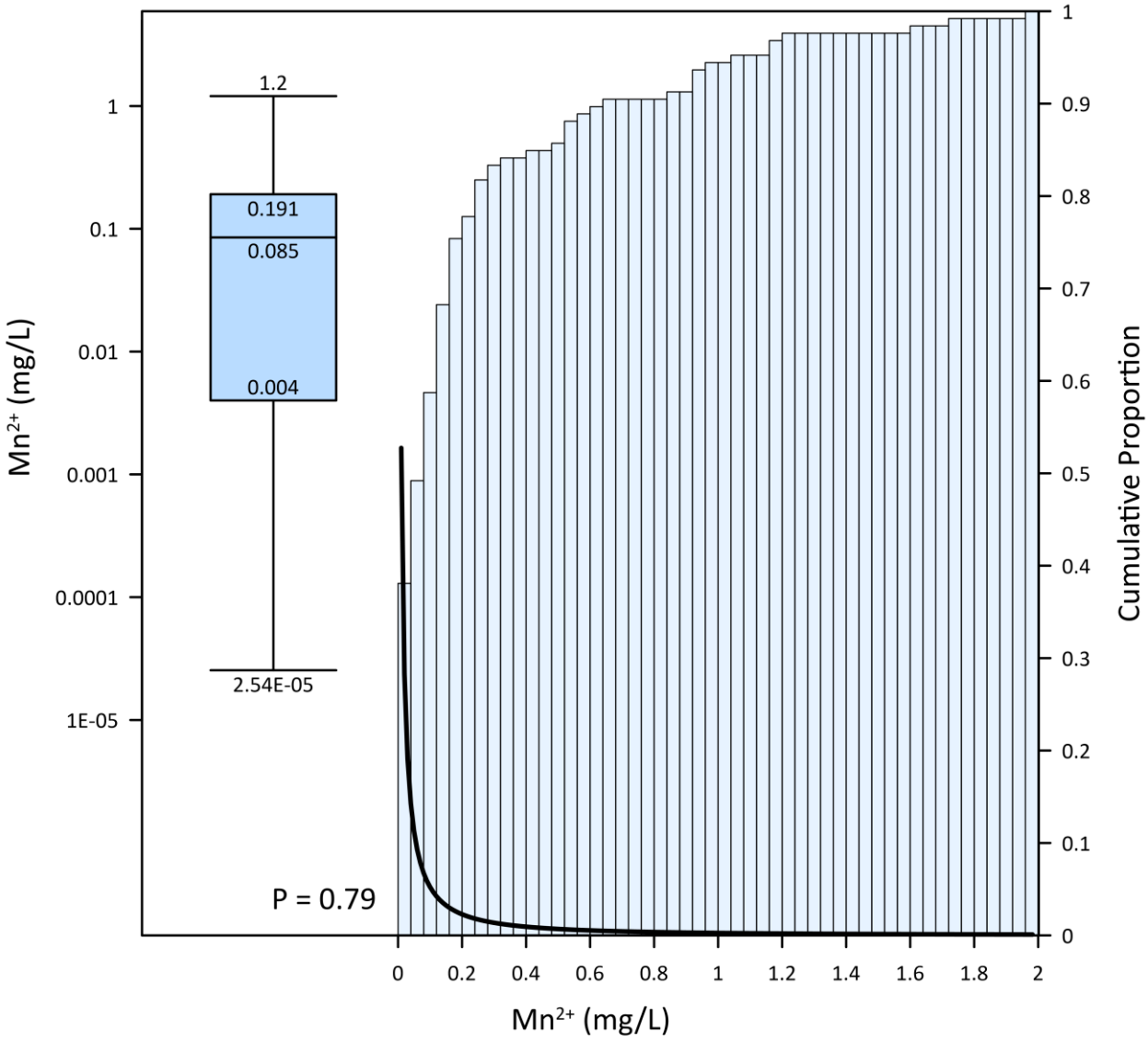

Figure B-14: Baseline total manganese(2+) concentrations in groundwater in the sediments. The boxplot shows the median concentration on the centerline. Whiskers mark the 97.5th and 2.5th percentiles. Manganese concentrations are log-normally distributed, with a p-value of 0.79.

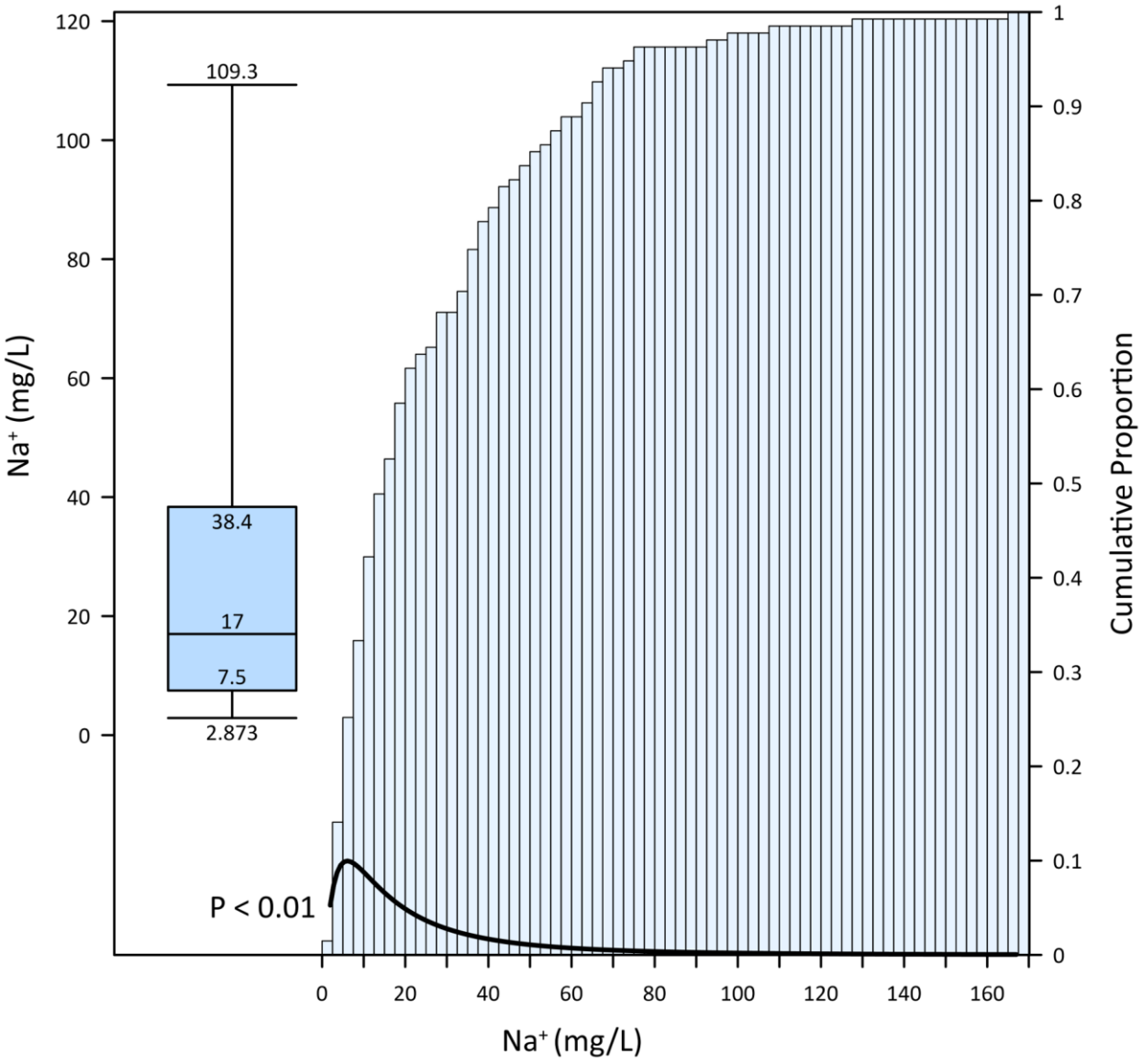

Figure B-15: Baseline sodium concentrations in groundwater in the sediments. The boxplot shows the median concentration on the centerline. Whiskers mark the 97.5th and 2.5th percentiles. Sodium concentrations are poorly log-normally distributed with a p-value of less than 0.01. The distribution appears to be bimodal.

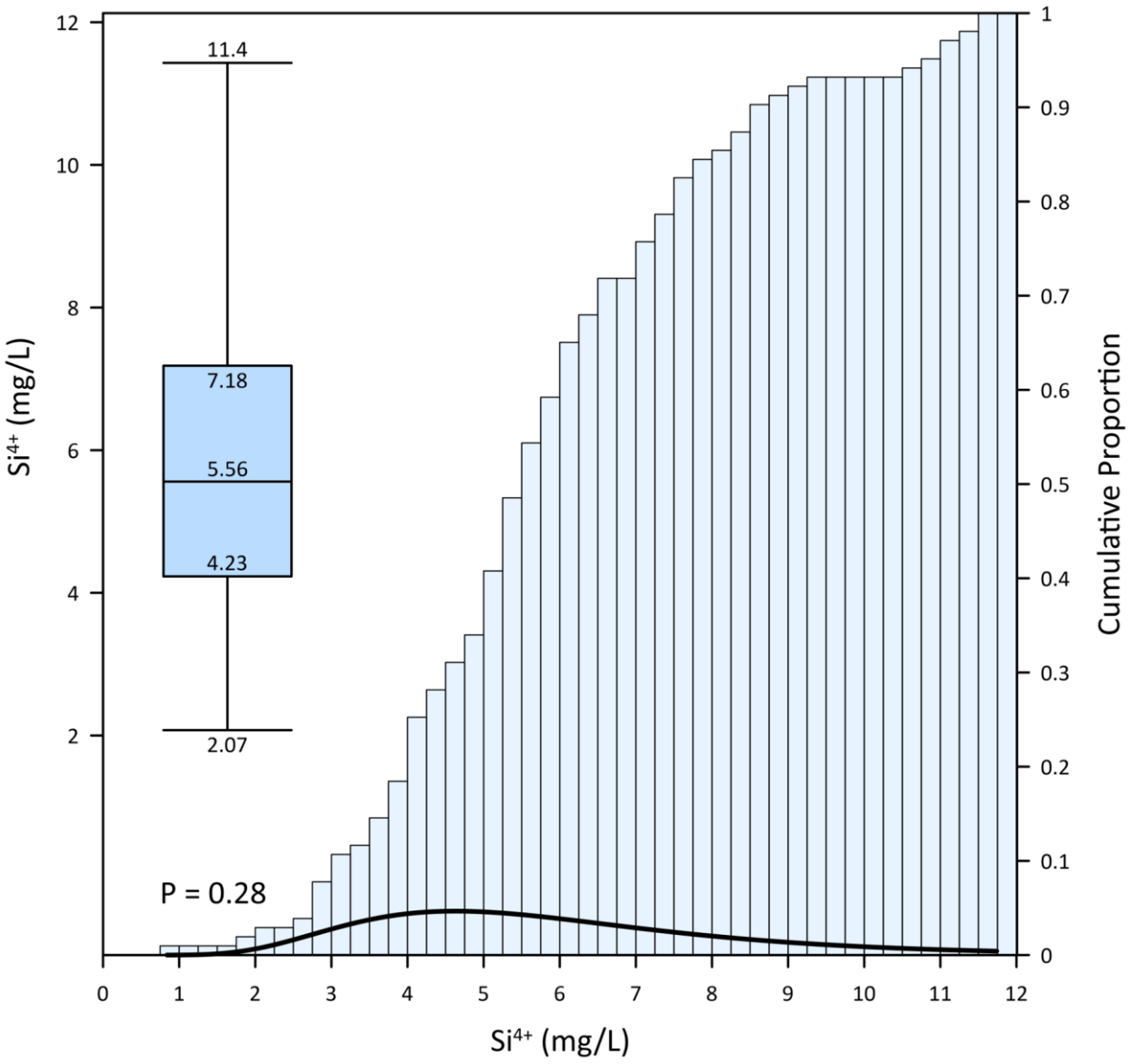

Figure B-16: Baseline silica concentrations in groundwater in the sediments. The boxplot shows the median concentration on the centerline. Whiskers mark the 97.5th and 2.5th percentiles. Silicon concentrations are normally distributed with a p-value of 0.28.

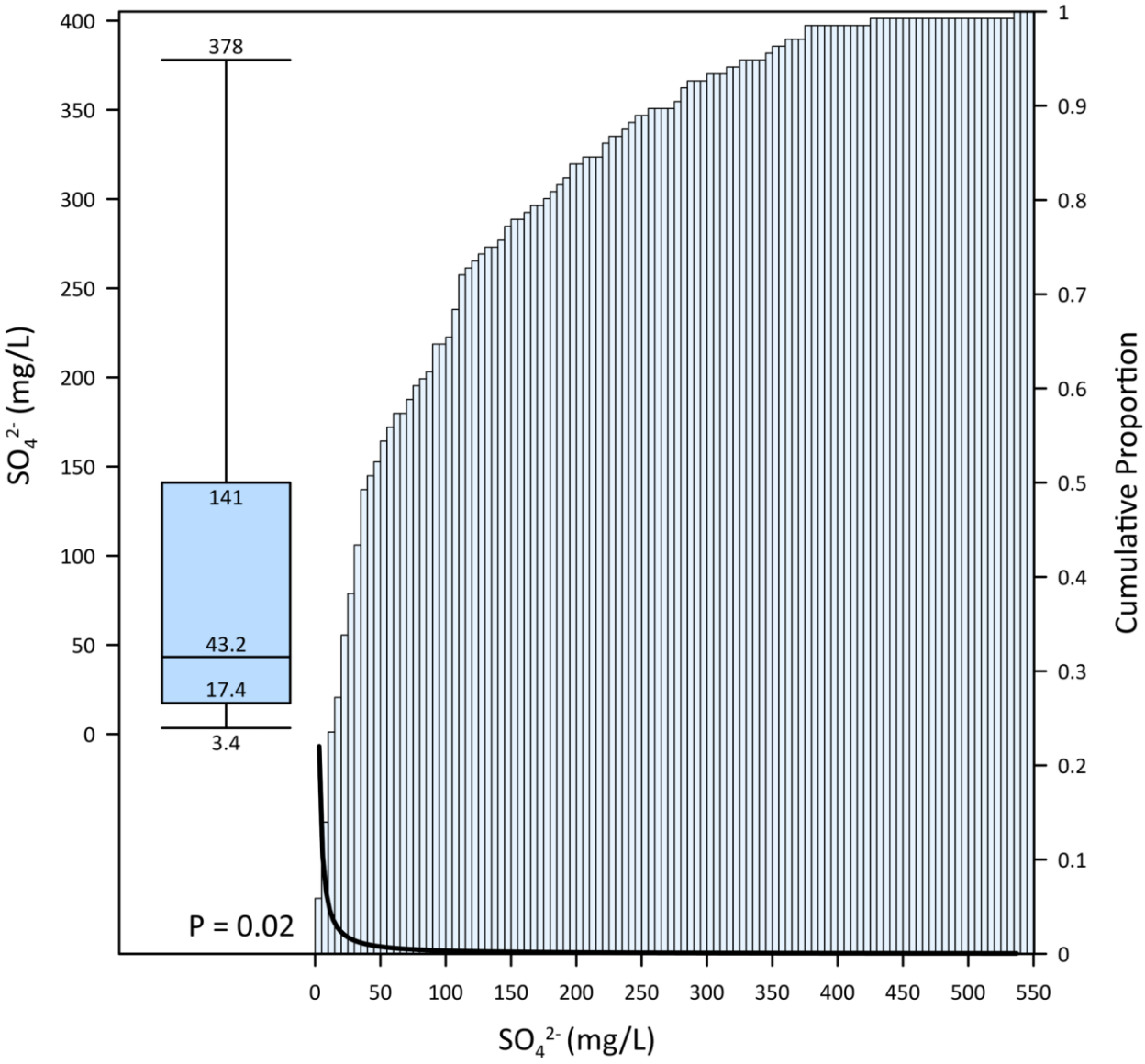

Figure B-17: Baseline sulphate concentrations in groundwater in the sediments. The boxplot shows the median concentration on the centerline. Whiskers mark the 97.5th and 2.5th percentiles. The distribution of sulphate concentrations follows a power function, with a p-value of 0.02

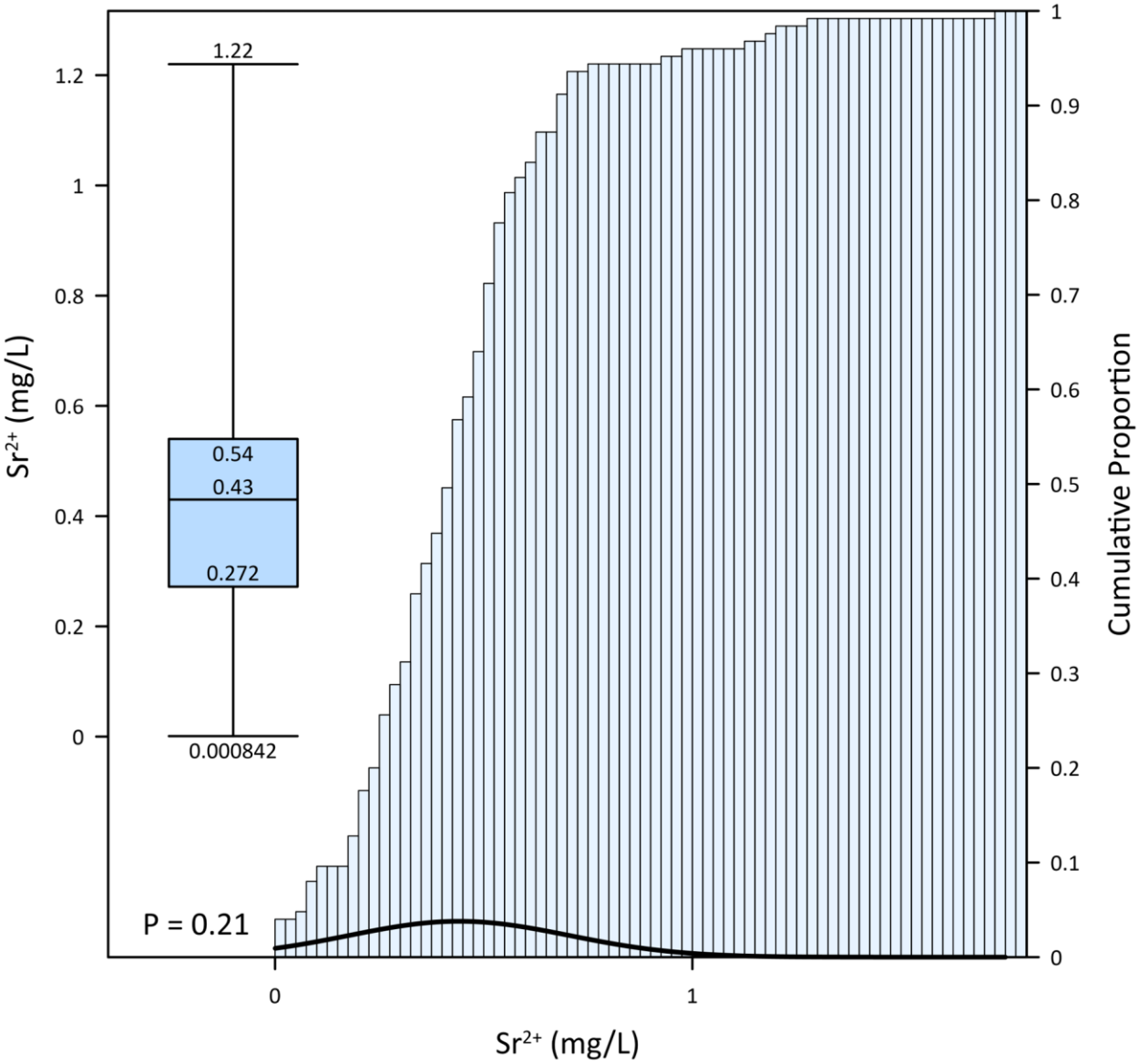

Figure B-18: Baseline strontium concentrations in groundwater in the sediments. The boxplot shows the median concentration on the centerline. Whiskers mark the 97.5th and 2.5th percentiles. Strontium concentrations are normally distributed, with a p-value of 0.21.

14.3. Isotopic Composition

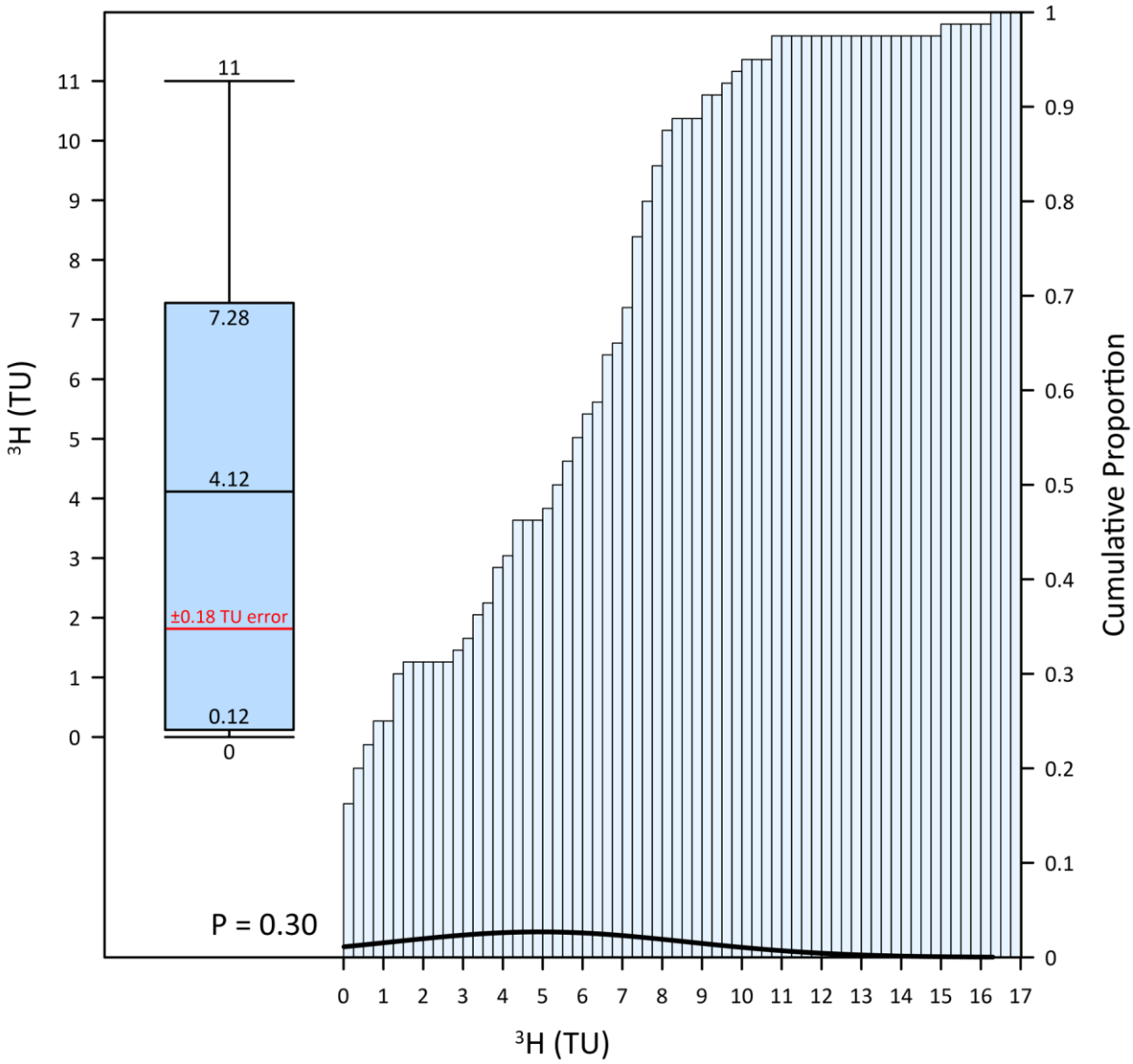

Figure B-19: Baseline tritium concentrations in groundwater in the sediments. The boxplot shows the median concentration on the centerline. Whiskers mark the 97.5th and 2.5th percentiles. Tritium concentrations are normally distributed, with a p-value of 0.3. The red line marks the median error in tritium concentrations.

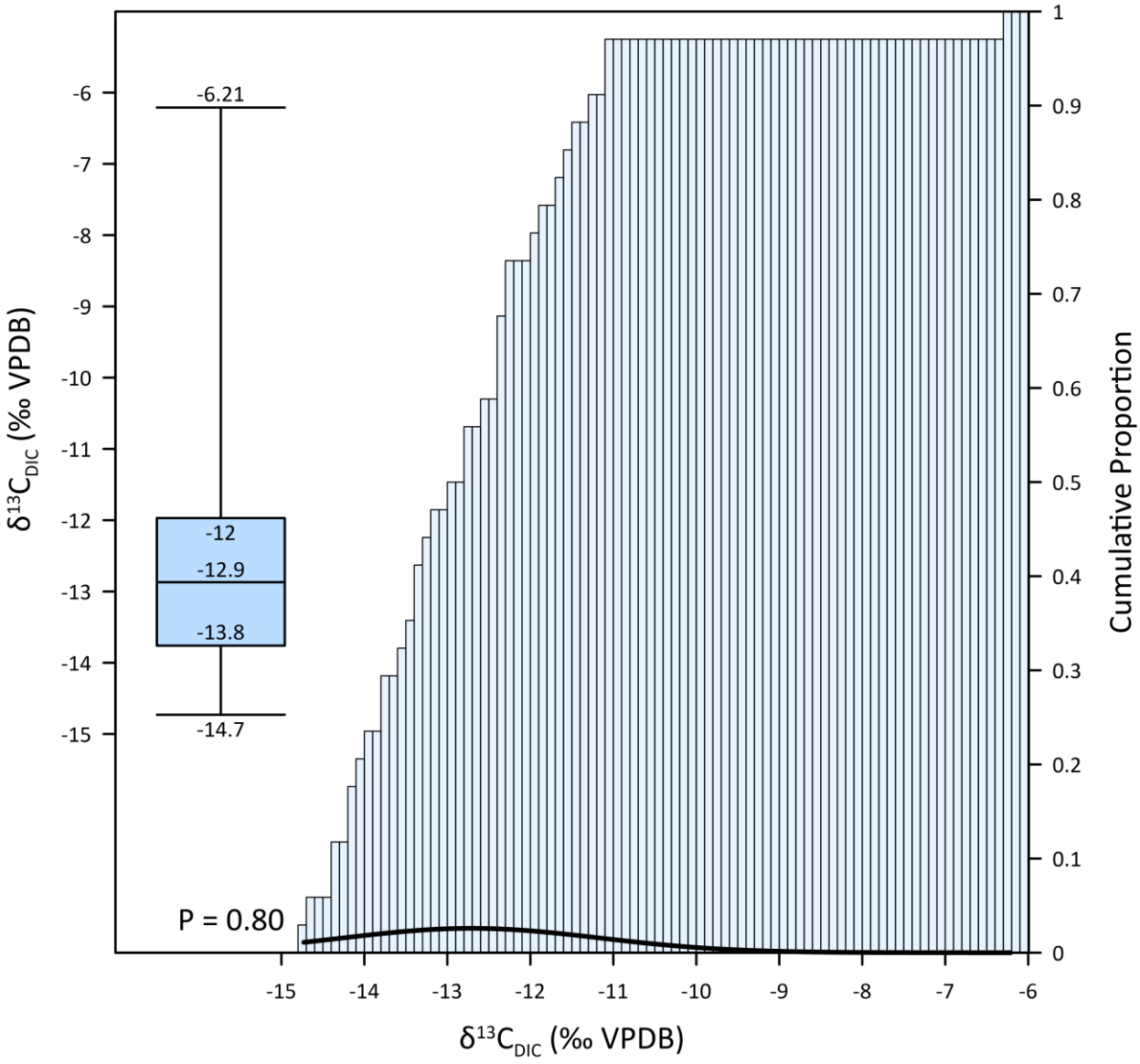

Figure B-20: The baseline $\delta^{13}C_{DIC}$ composition of groundwater in the sediments. The boxplot shows the median value on the centerline. Whiskers mark the 97.5th and 2.5th percentiles. $\delta^{13}C_{DIC}$ values are normally distributed with a p-value of 0.8.

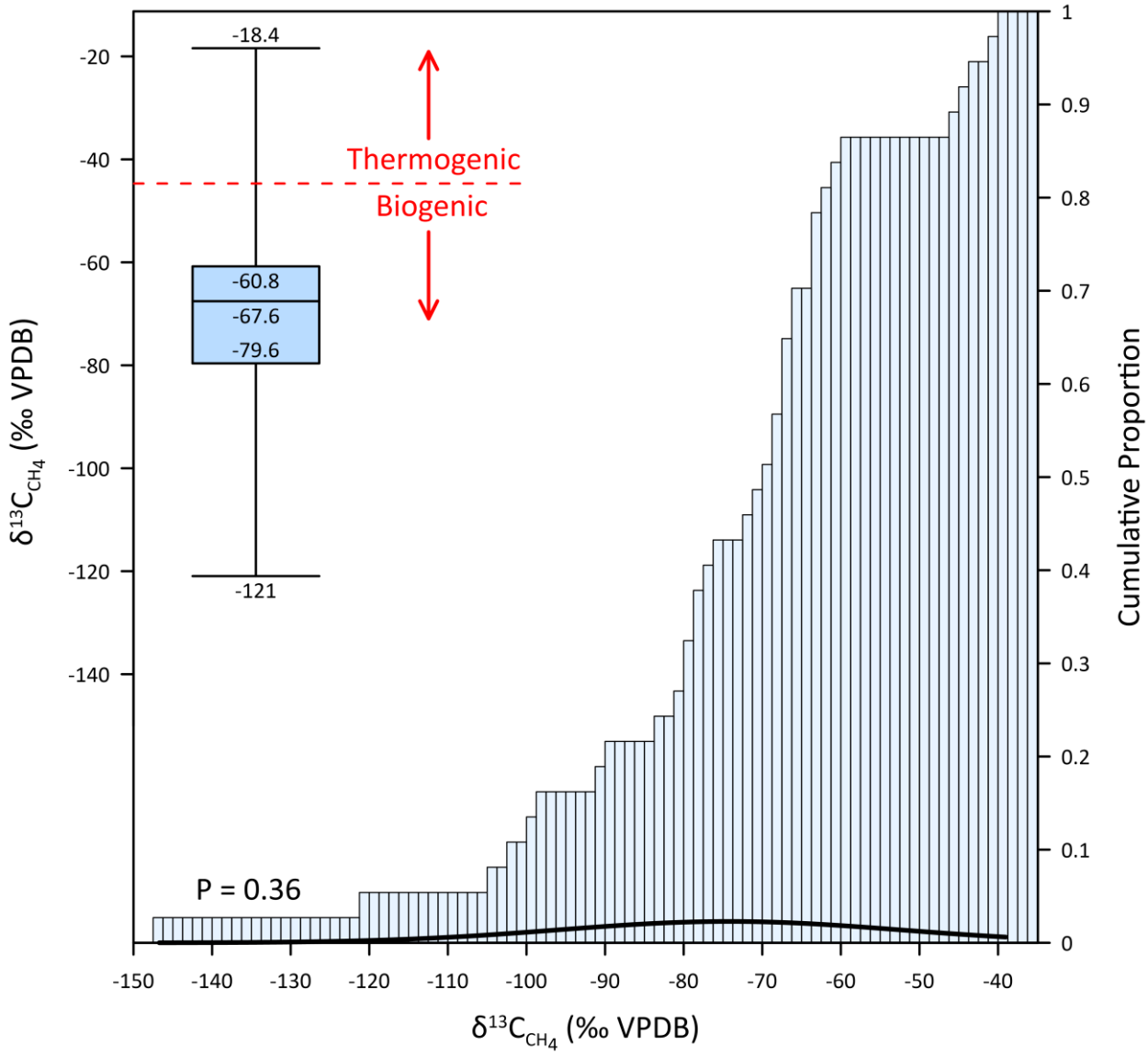

Figure B-21: The baseline $\delta^{13}C_{CH4}$ composition of groundwater in the sediments. The boxplot shows the median value on the centerline. Whiskers mark the 97.5th and 2.5th percentiles. $\delta^{13}C_{CH4}$ values are normally distributed, with a p-value of 0.9. The red dashed line marks the boundary of thermogenic and biogenic $\delta^{13}C_{CH4}$ methane values. However, there is cross-over between the values, so the boundary is approximate.

14.4. Gas Concentrations

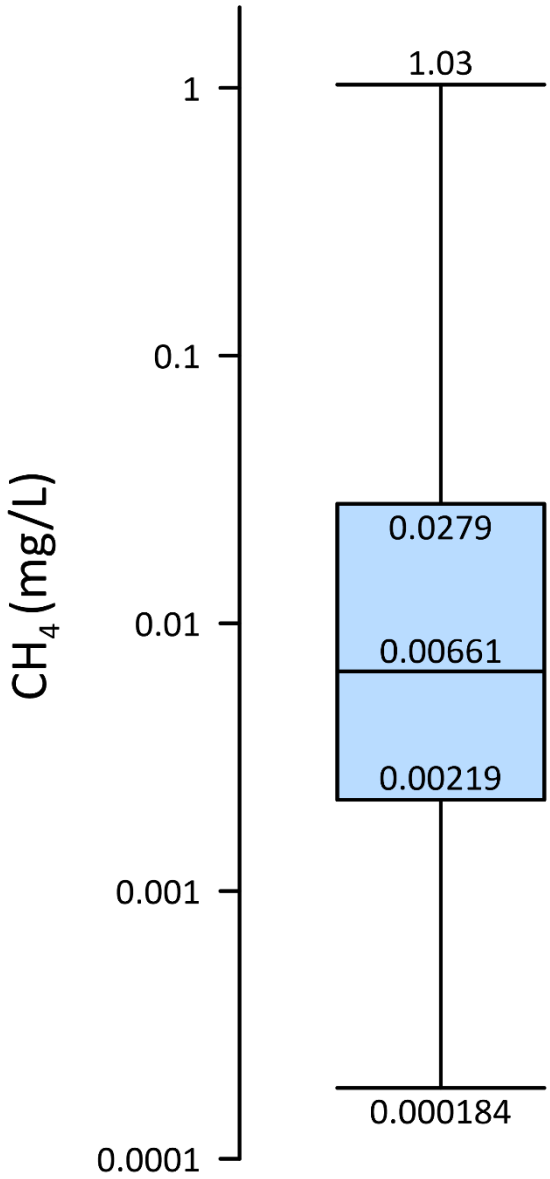

Figure B-22: Baseline methane concentrations in groundwater in the sediments. The boxplot shows the median concentration on the centerline. Whiskers mark the 97.5th and 2.5th percentiles. The range of methane concentrations is too large to create a cumulative distribution plot.

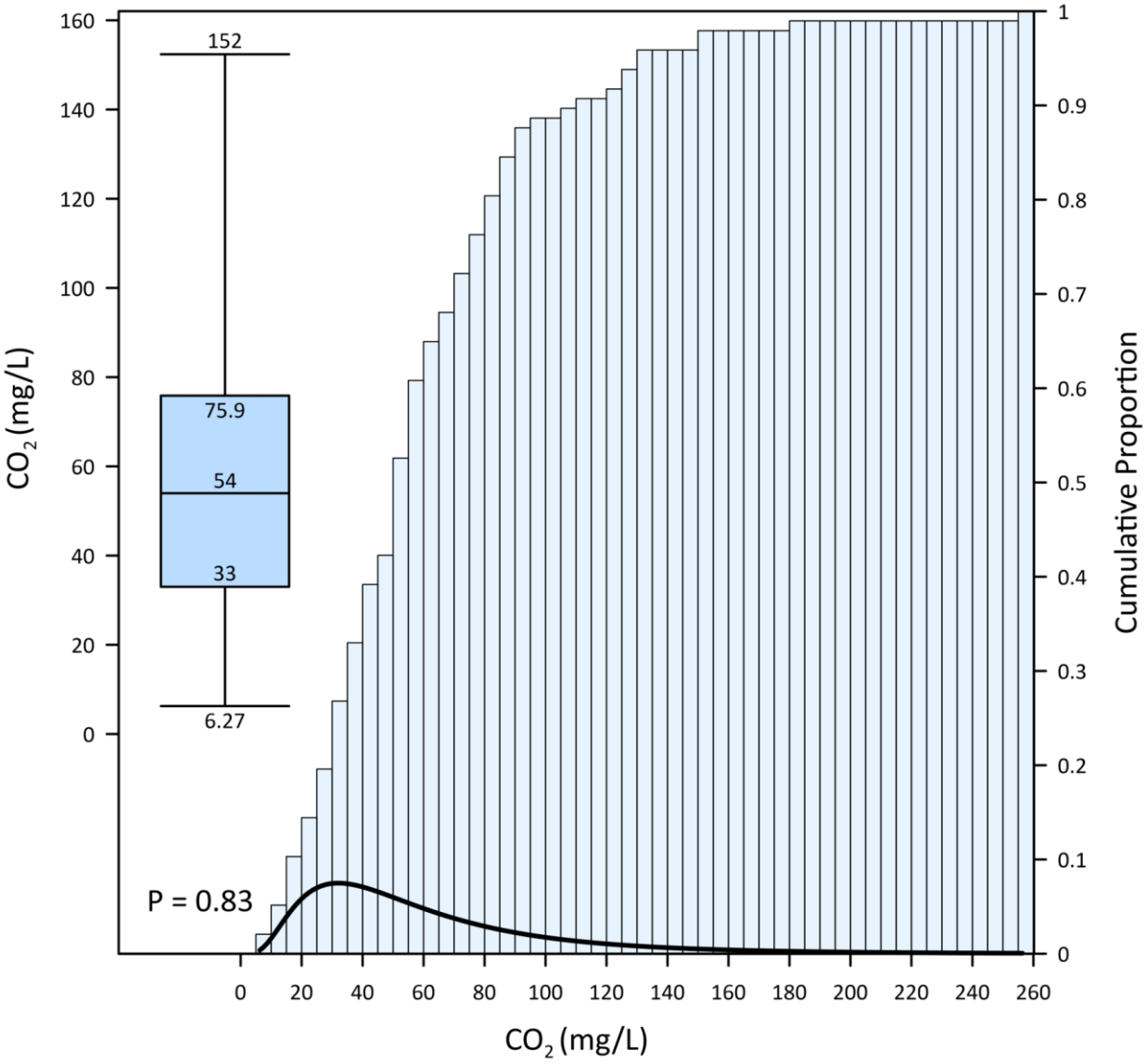

Figure B-23: Baseline carbon dioxide concentrations in groundwater in the sediments. The boxplot shows the median concentration on the centerline. Whiskers mark the 97.5th and 2.5th percentiles. Carbon dioxide concentrations are log-normally distributed, with a p-value of 0.83.

15. Appendix C – The Hydrochemical Baselines of the Bedrock Groundwater System

15.1. Chemical Properties

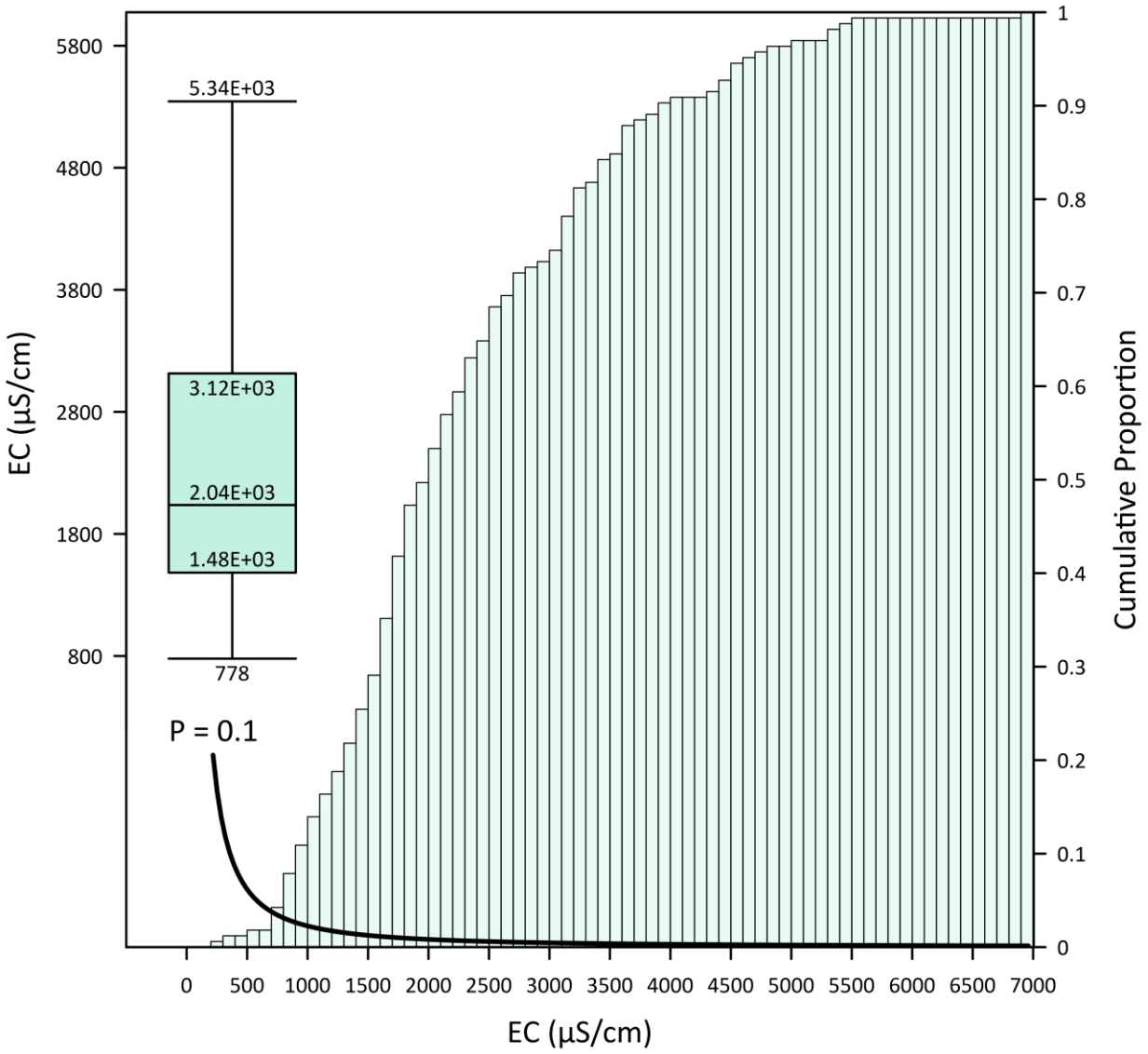

Figure C-1: The baseline EC of groundwater in the bedrock. The boxplot shows the median value on the centerline. Whiskers mark the 97.5th and 2.5th percentiles. The distribution of EC follows a power function, with a p-value of 0.1.

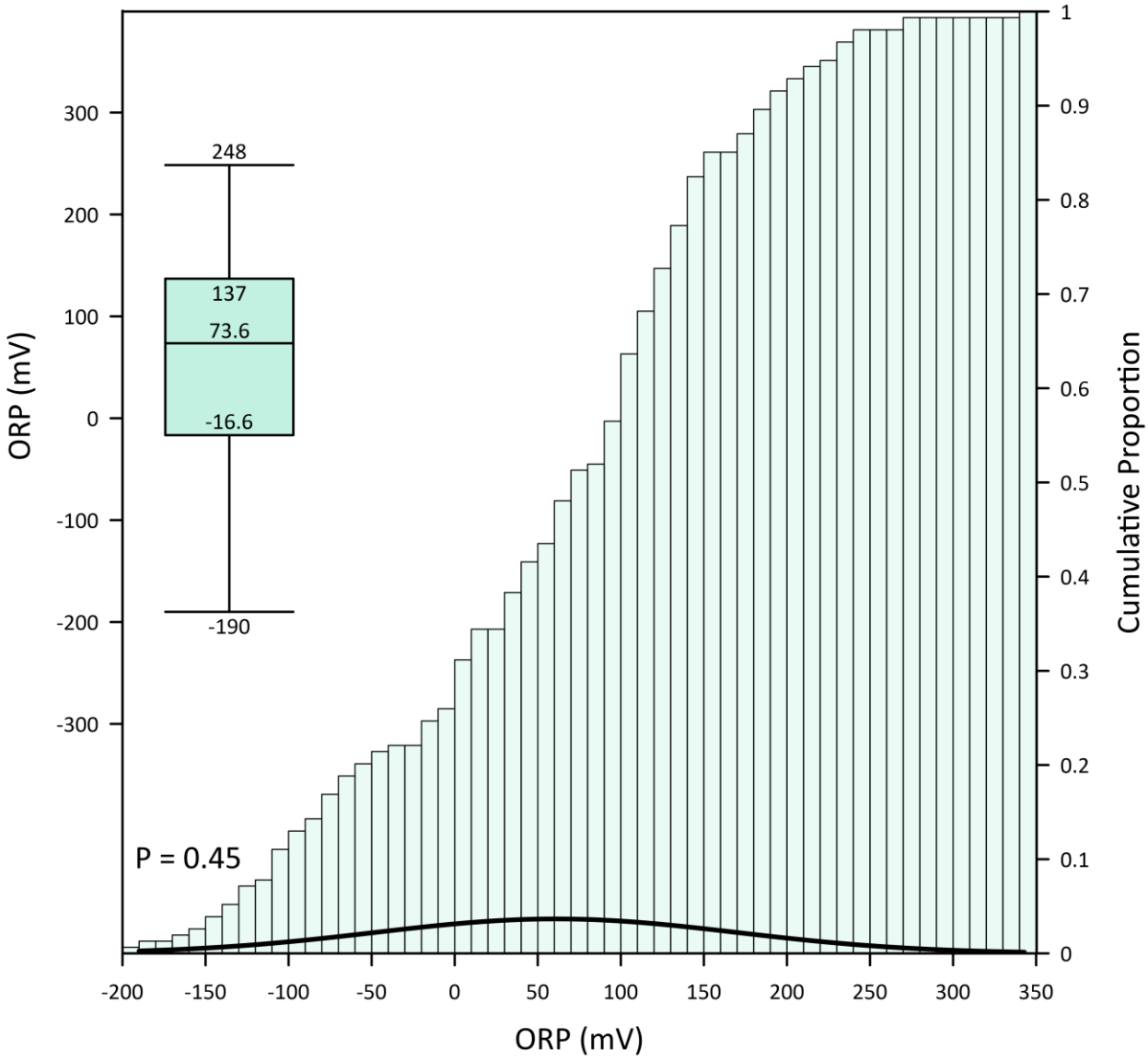

Figure C-2: The baseline ORP of groundwater in the bedrock. The boxplot shows the median value on the centerline. Whiskers mark the 97.5th and 2.5th percentiles. ORP values are normally distributed, with a p-value of 0.45.

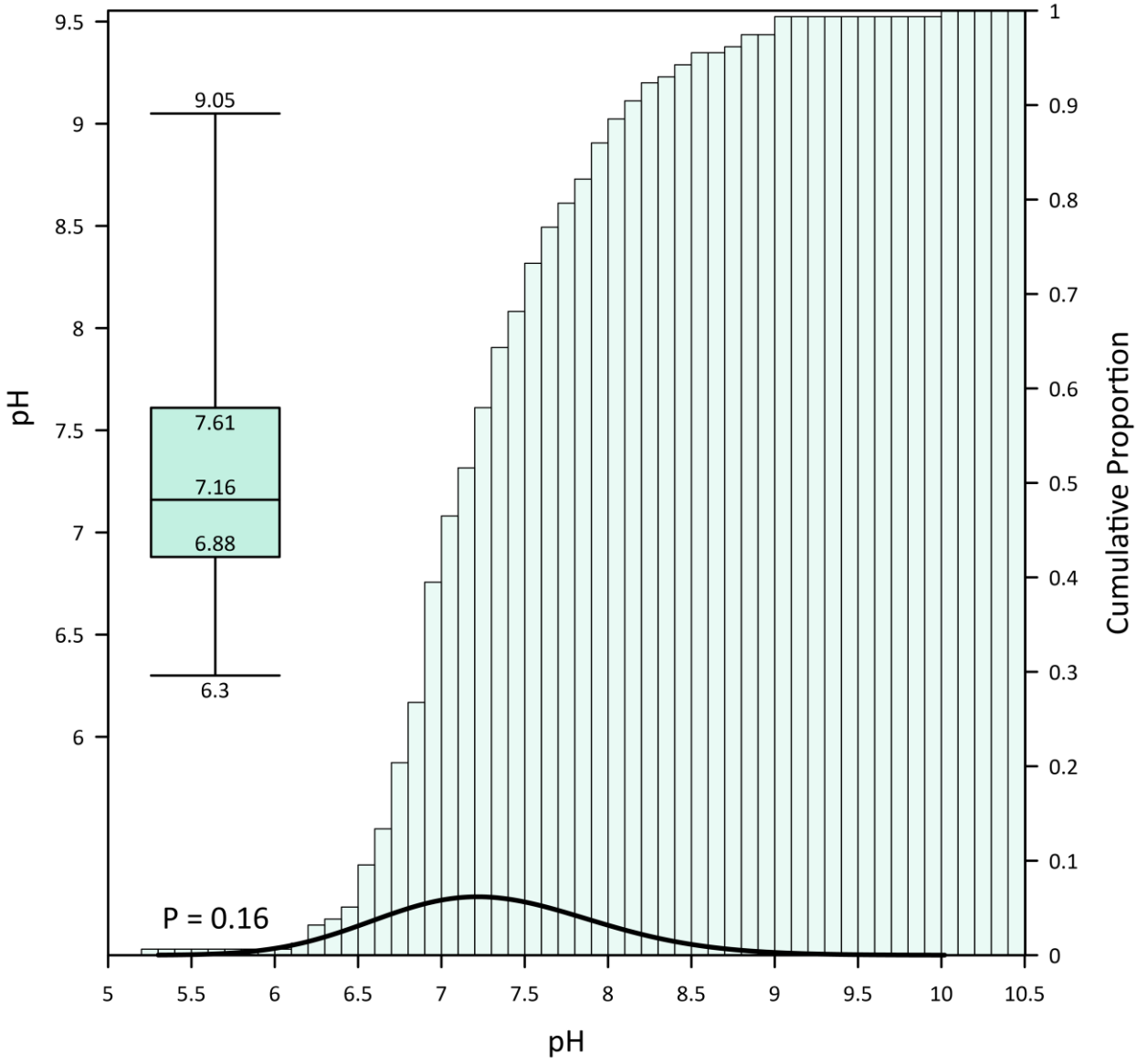

Figure C-3: The baseline pH of groundwater in the bedrock. The boxplot shows the median value on the centerline. Whiskers mark the 97.5th and 2.5th percentiles. The pH values are normally distributed, with a p-value of 0.16.

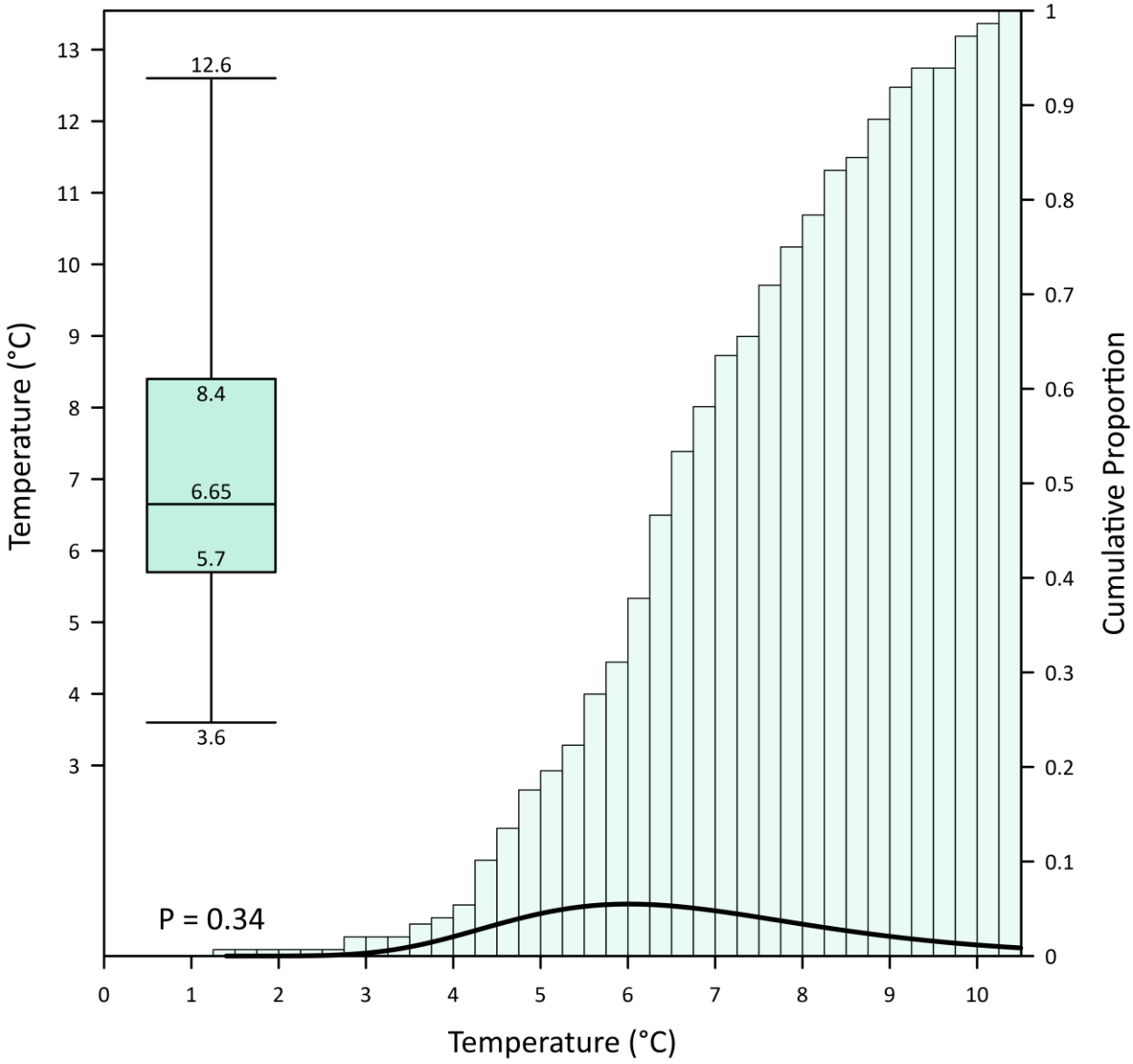

Figure C-4: The baseline temperatures of groundwater in the bedrock. The boxplot shows the median value on the centerline. Whiskers mark the 97.5th and 2.5th percentiles. Temperature values are normally distributed, with a p-value of 0.34.

15.2. Major and Minor Ion Concentrations

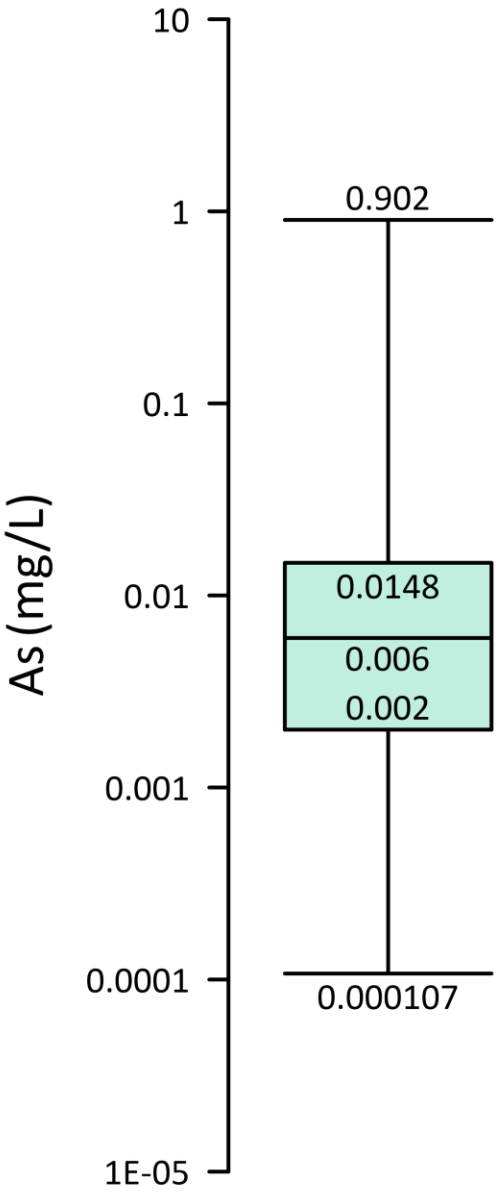

Figure C-5: Baseline arsenic concentrations in groundwater in the bedrock. The boxplot shows the median concentration on the centerline. Whiskers mark the 97.5th and 2.5th percentiles.

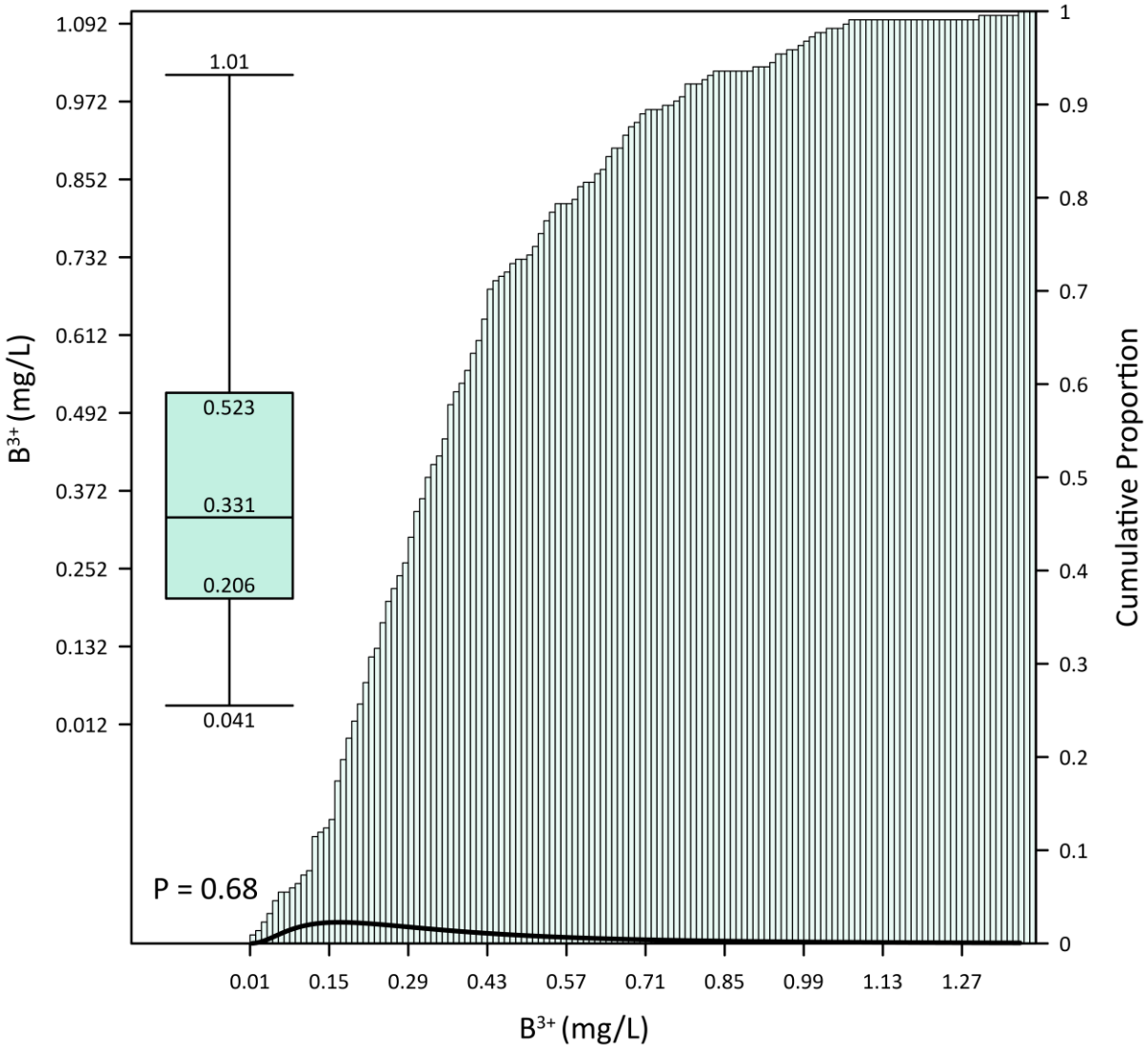

Figure C-6: Baseline boron concentrations in groundwater in the bedrock. The boxplot shows the median concentration on the centerline. Whiskers mark the 97.5th and 2.5th percentiles. Boron concentrations are log-normally distributed, with a p-value of 0.68.

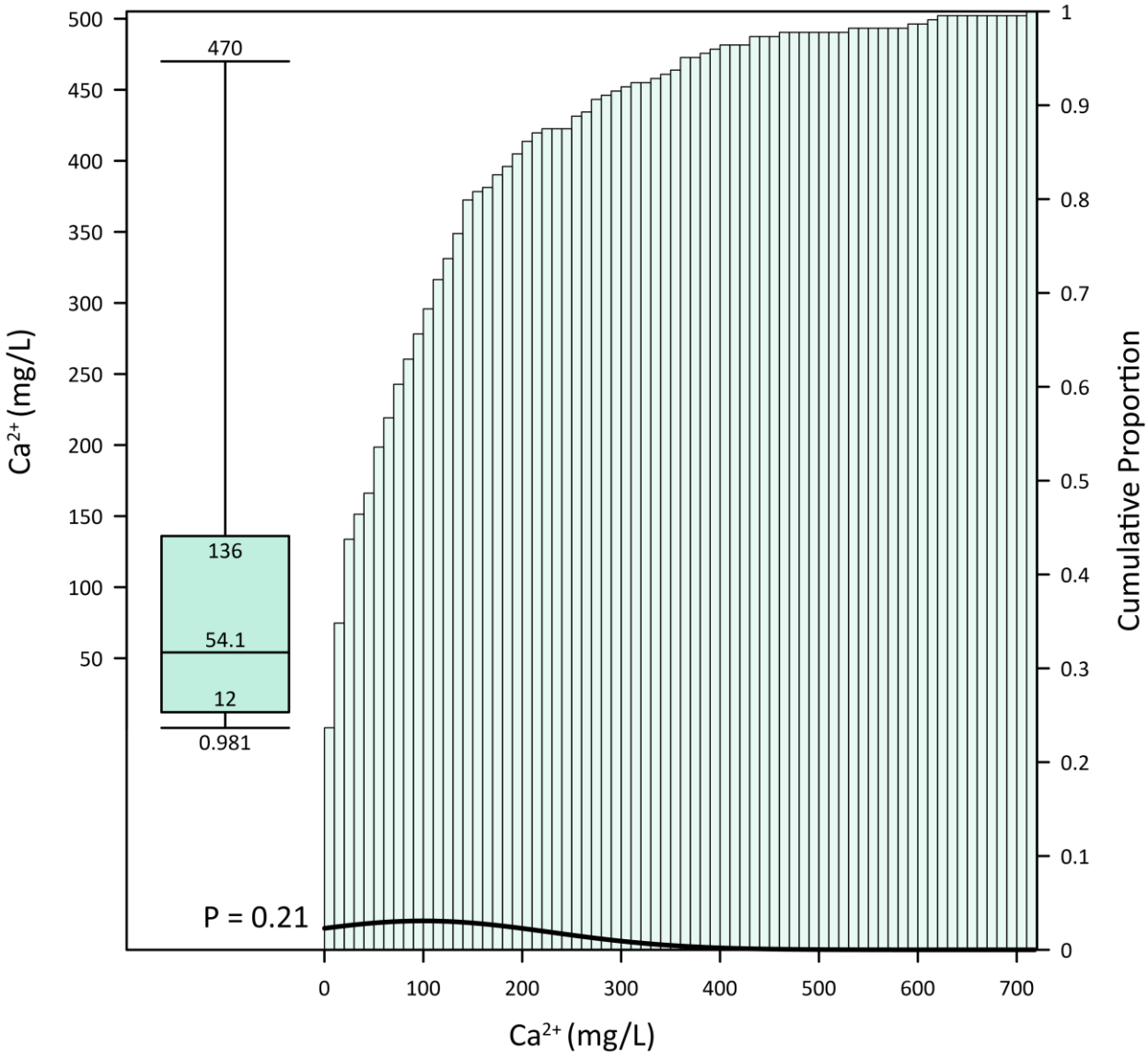

Figure C-7: Baseline calcium concentrations in groundwater in the bedrock. The boxplot shows the median concentration on the centerline. Whiskers mark the 97.5th and 2.5th percentiles. Calcium concentrations are log-normally distributed, with a p-value of 0.21.

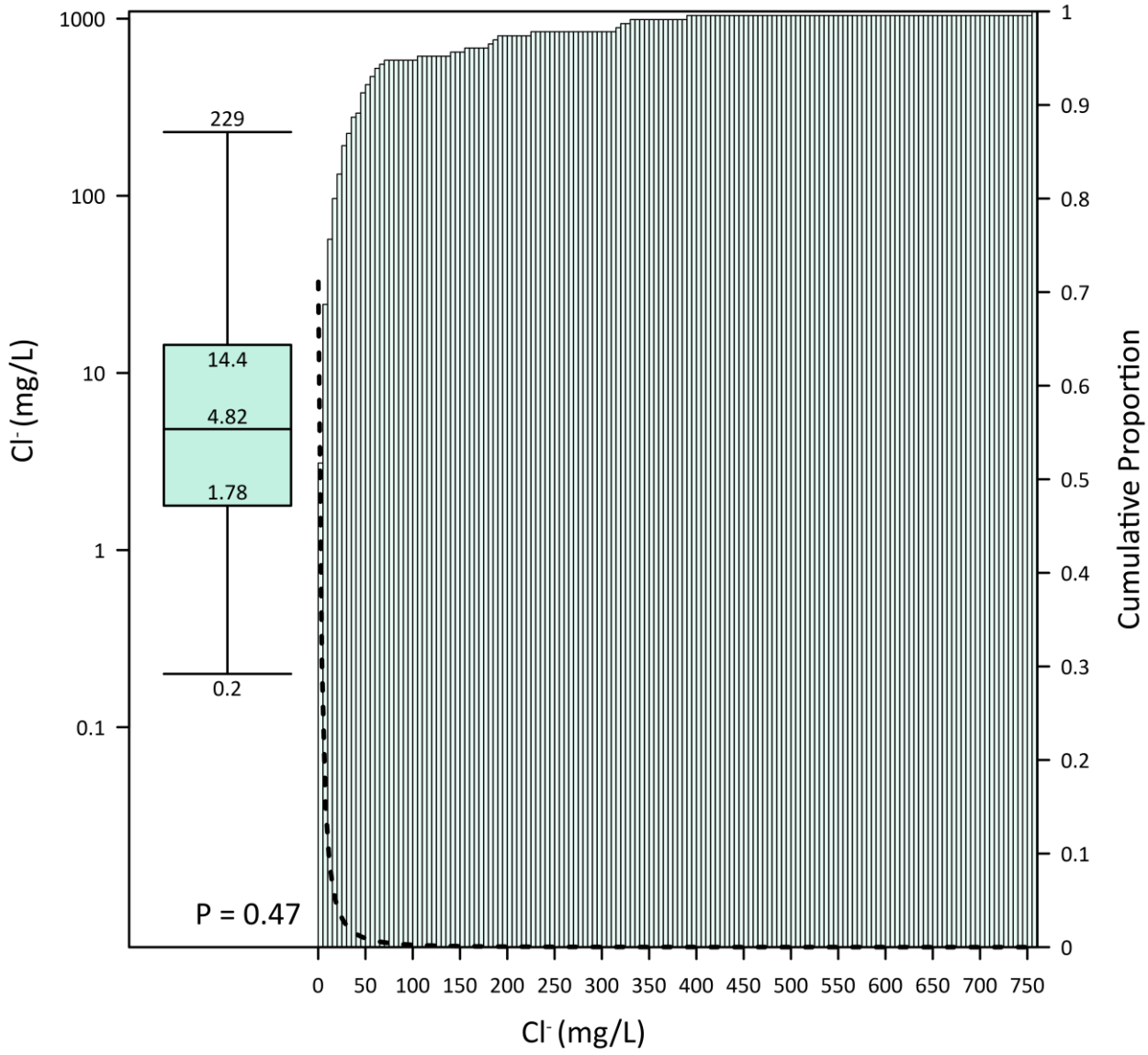

Figure C-8: Baseline chloride concentrations in groundwater in the bedrock. The boxplot shows the median concentration on the centerline. Whiskers mark the 97.5th and 2.5th percentiles. Chloride concentrations are exponentially distributed, with a p-value of 0.47.

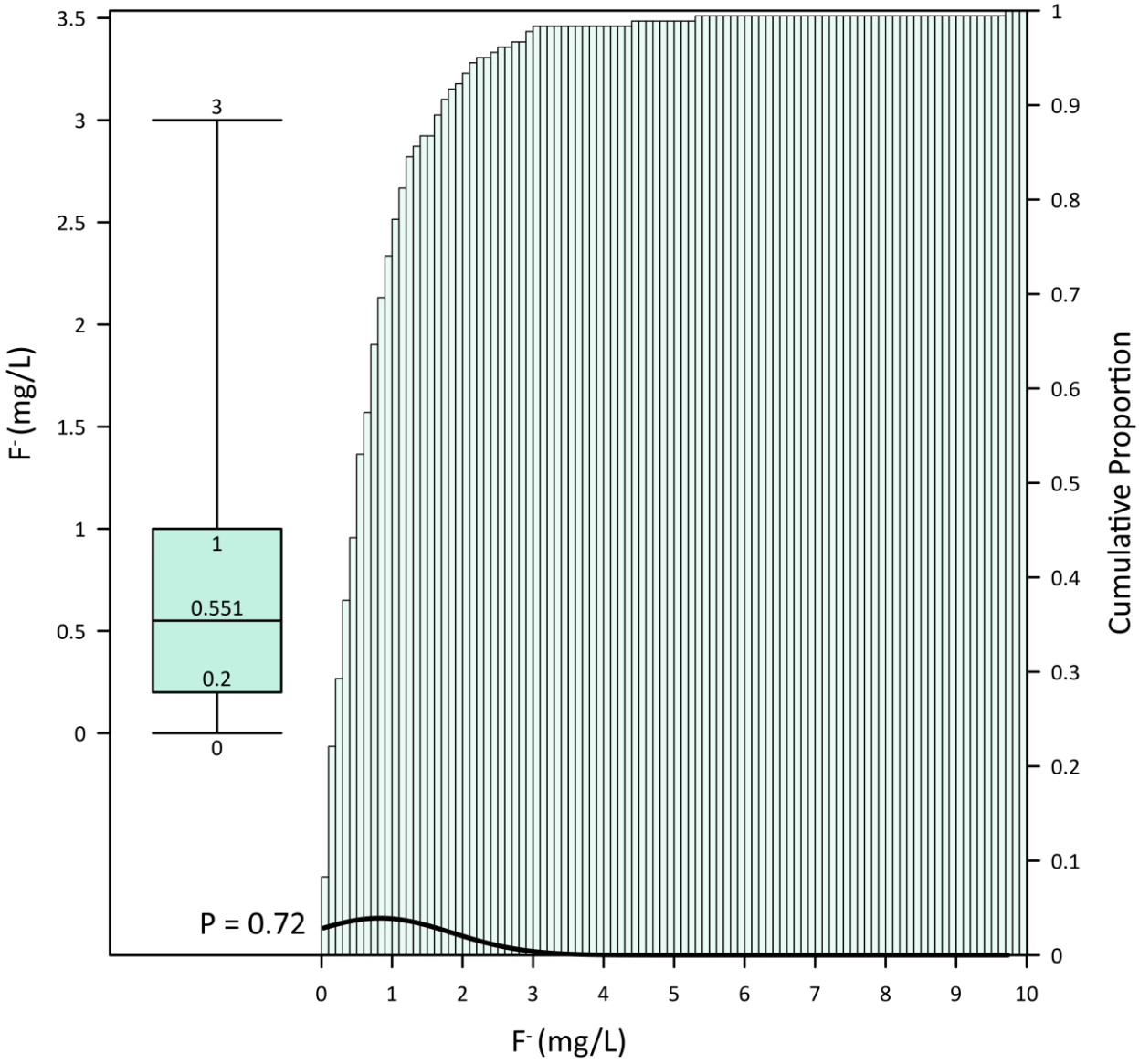

Figure C-9: Baseline fluoride concentrations in groundwater in the bedrock. The boxplot shows the median concentration on the centerline. Whiskers mark the 97.5th and 2.5th percentiles. fluoride concentrations are log-normally distributed, with a p-value of 0.72.

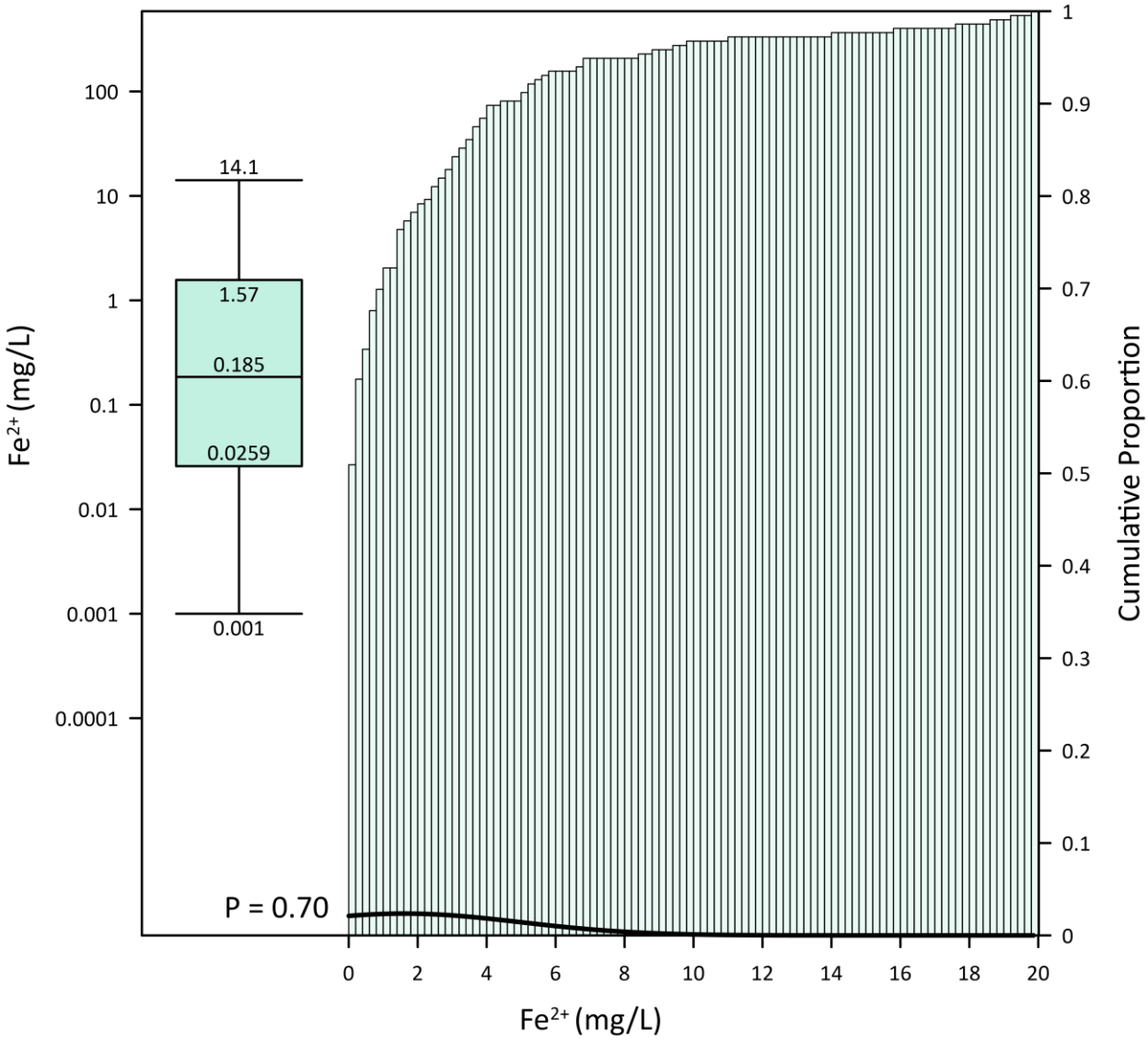

Figure C-10: Baseline ferrous iron concentrations in groundwater in the bedrock. The boxplot shows the median concentration on the centerline. Whiskers mark the 97.5th and 2.5th percentiles. Iron concentrations are normally distributed, with a p-value of 0.70.

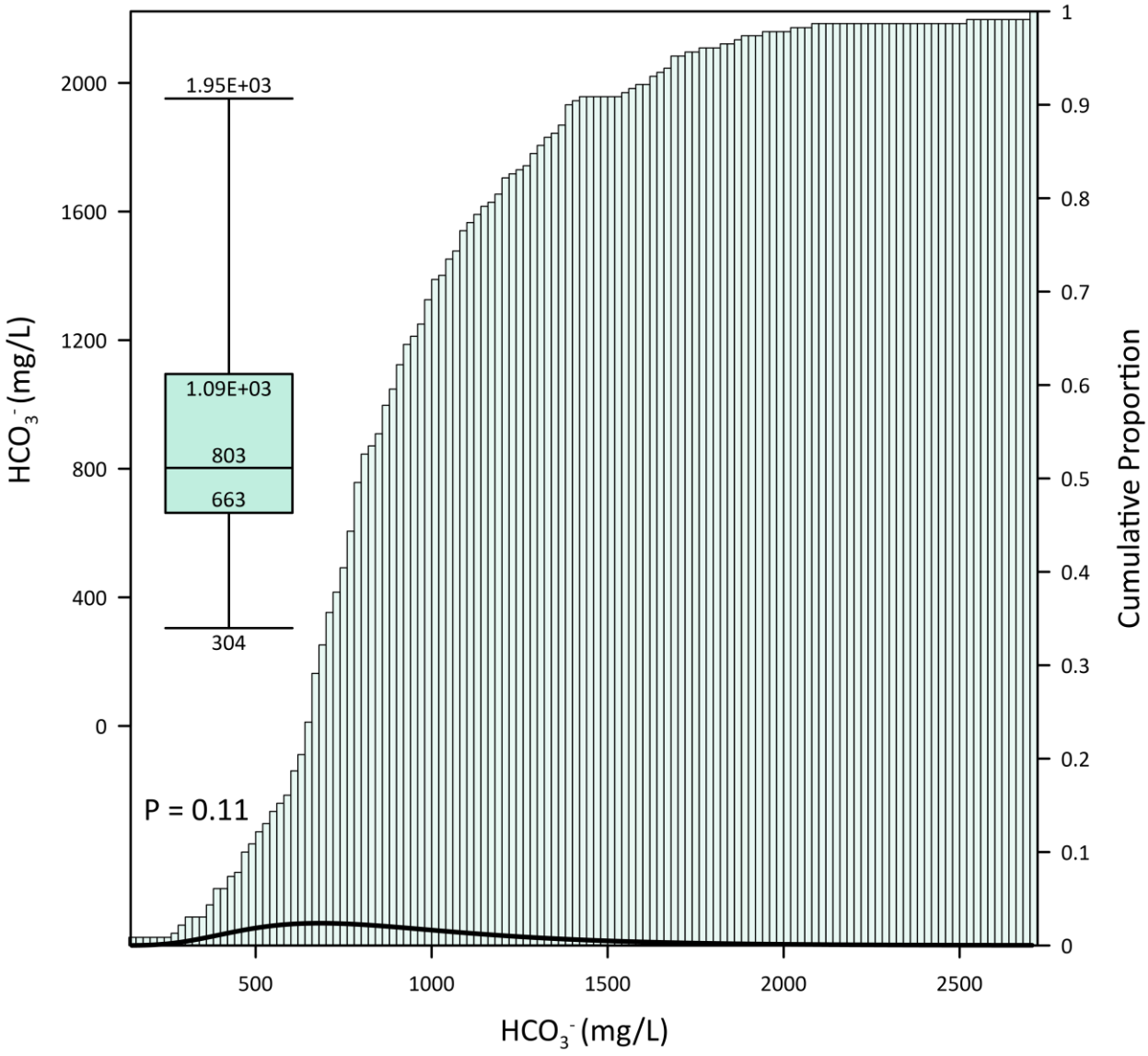

Figure C-11: Baseline bicarbonate concentrations in groundwater in the bedrock. The boxplot shows the median concentration on the centerline. Whiskers mark the 97.5th and 2.5th percentiles. Bicarbonate concentrations are log-normally distributed, with a p-value of 0.11.

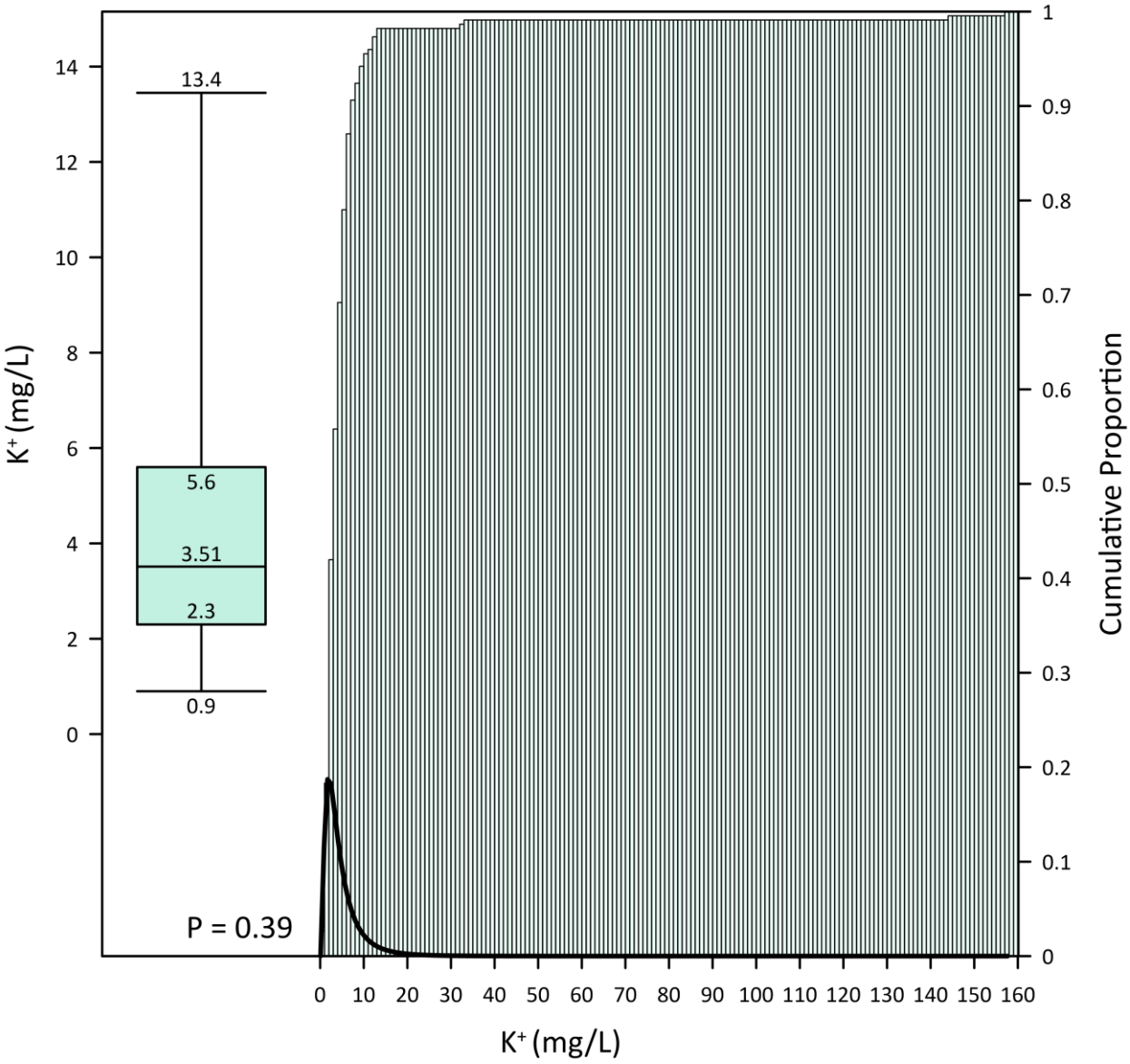

Figure C-12: Baseline potassium concentrations in groundwater in the bedrock. The boxplot shows the median concentration on the centerline. Whiskers mark the 97.5th and 2.5th percentiles. Potassium concentrations are log-normally distributed, with a p-value of 0.39.

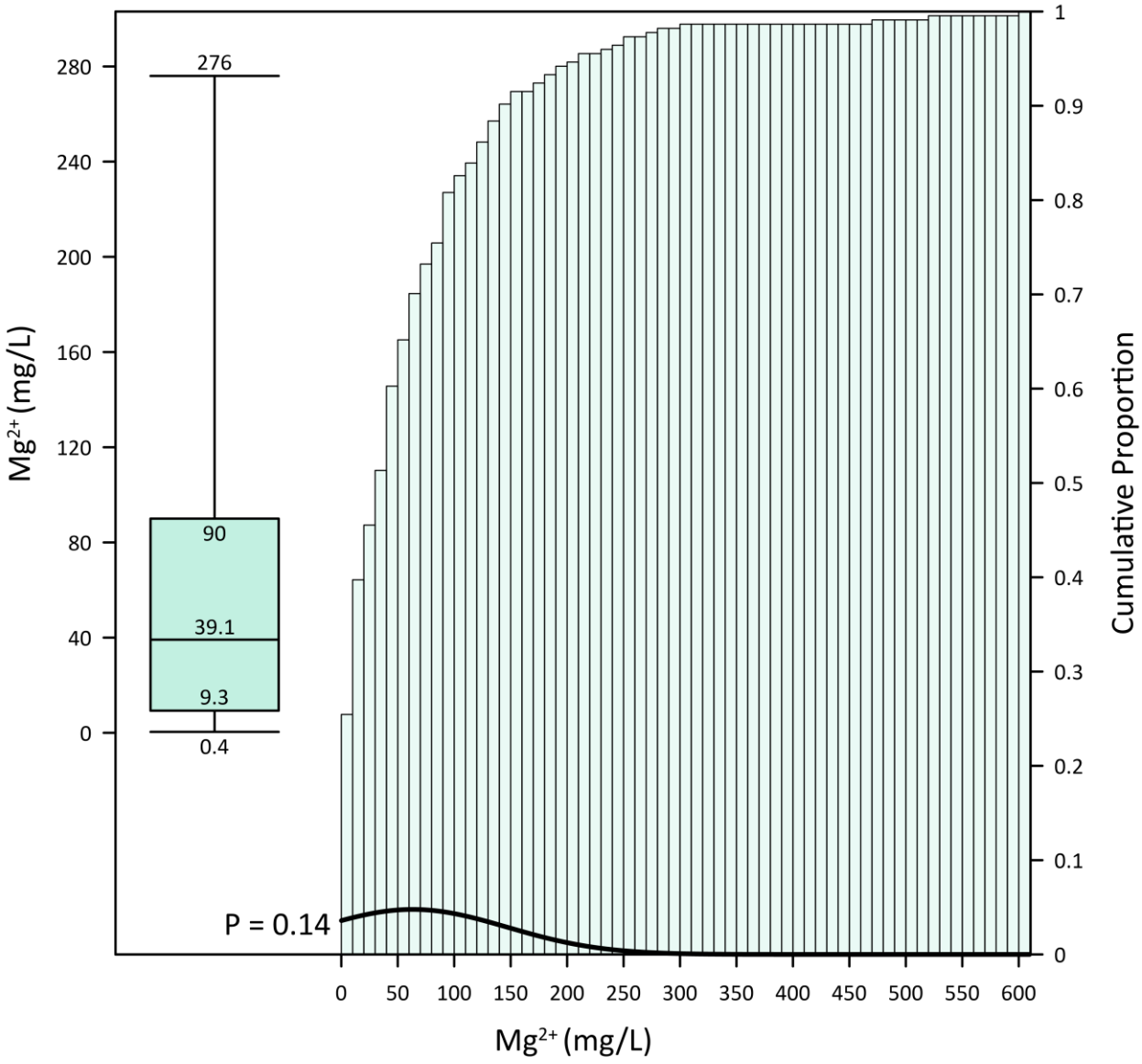

Figure C-13: Baseline magnesium concentrations in groundwater in the bedrock. The boxplot shows the median concentration on the centerline. Whiskers mark the 97.5th and 2.5th percentiles. Magnesium concentrations are normally distributed, with a p-value of 0.14.

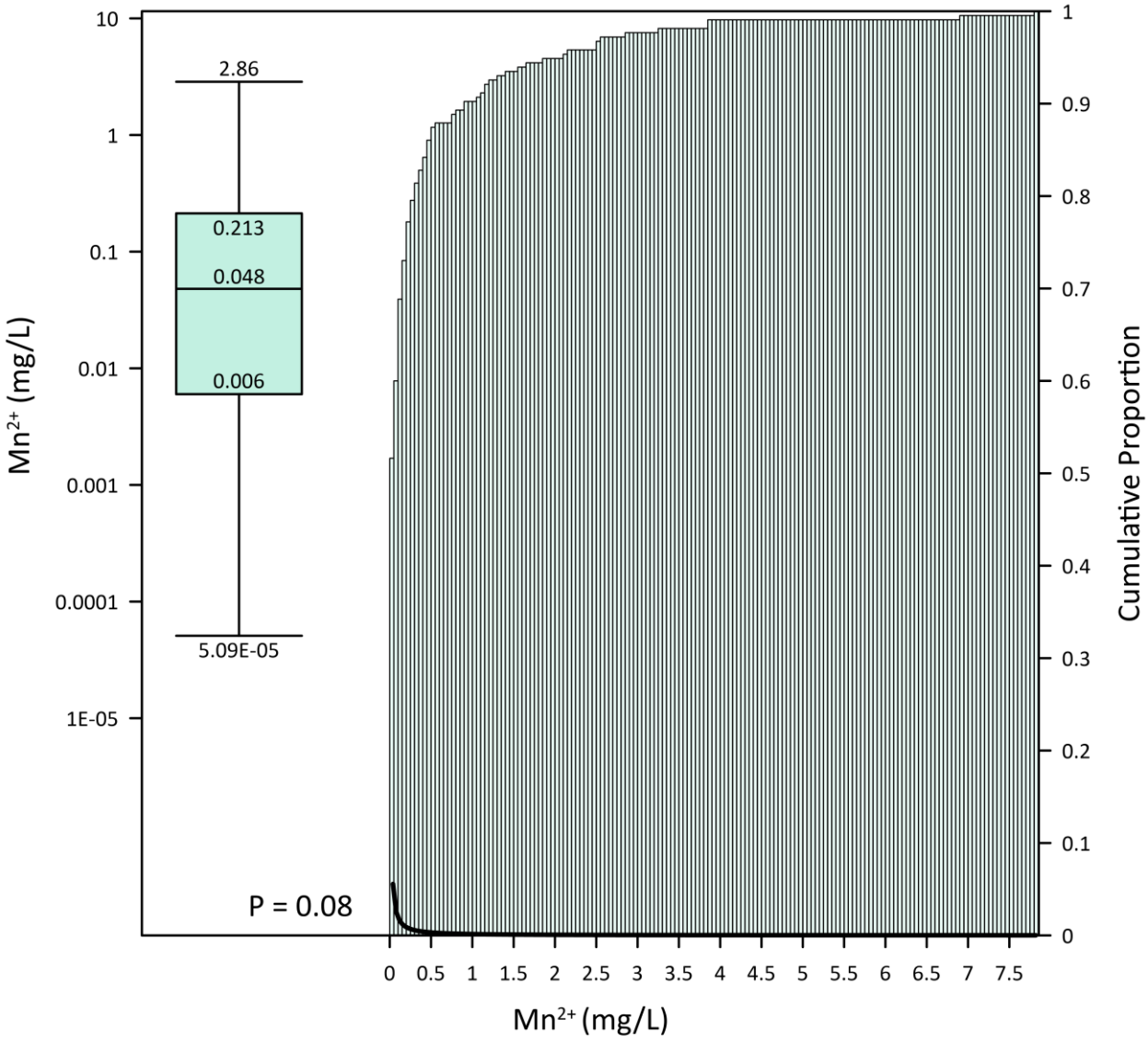

Figure C-14: Baseline manganese(2+) concentrations in groundwater in the bedrock. The boxplot shows the median concentration on the centerline. Whiskers mark the 97.5th and 2.5th percentiles. The distribution of manganese concentrations are follows a power function, with a p-value of 0.08.

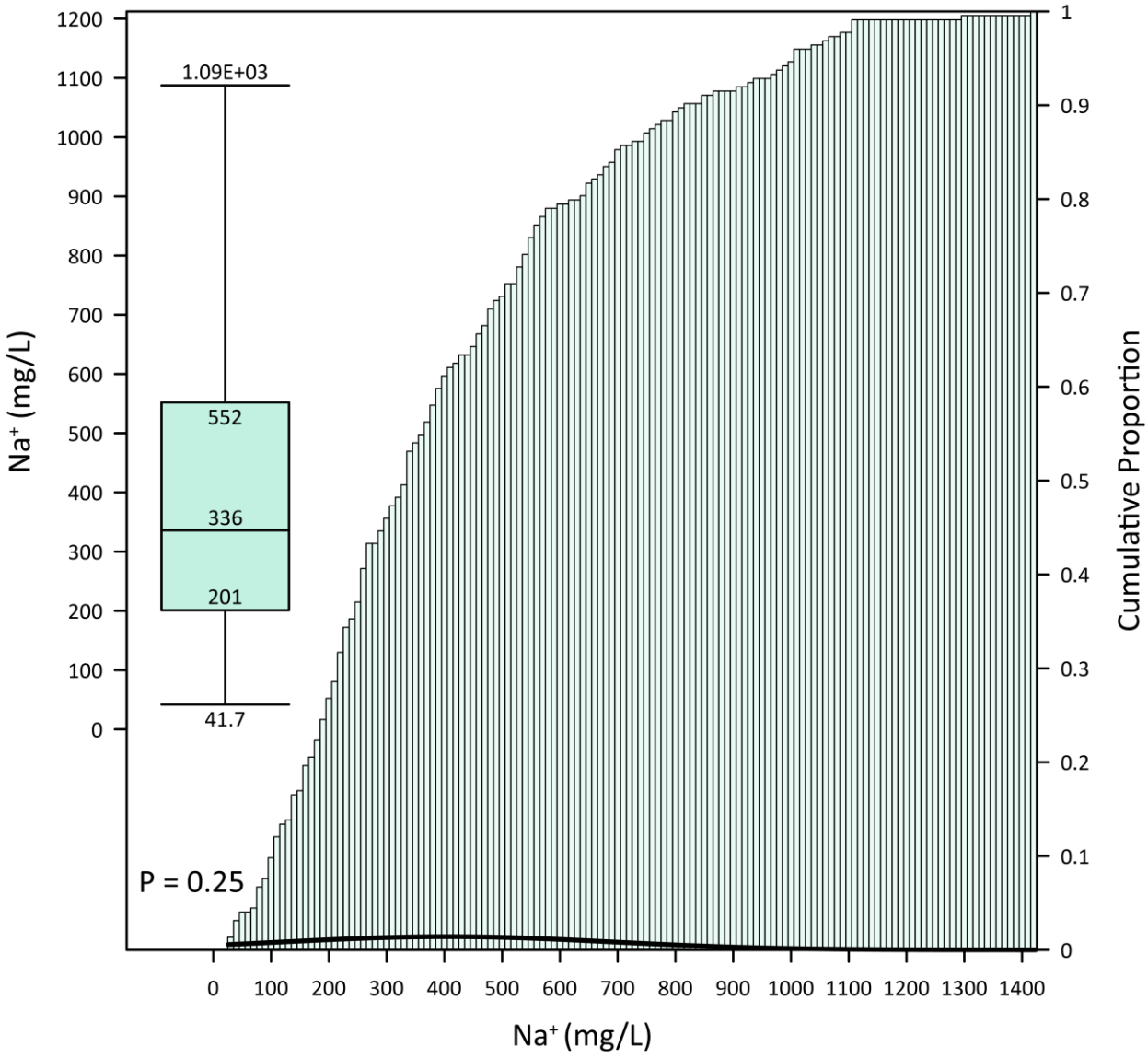

Figure C-15: Baseline sodium concentrations in groundwater in the bedrock. The boxplot shows the median concentration on the centerline. Whiskers mark the 97.5th and 2.5th percentiles. Sodium concentrations are normally distributed, with a p-value of 0.25.

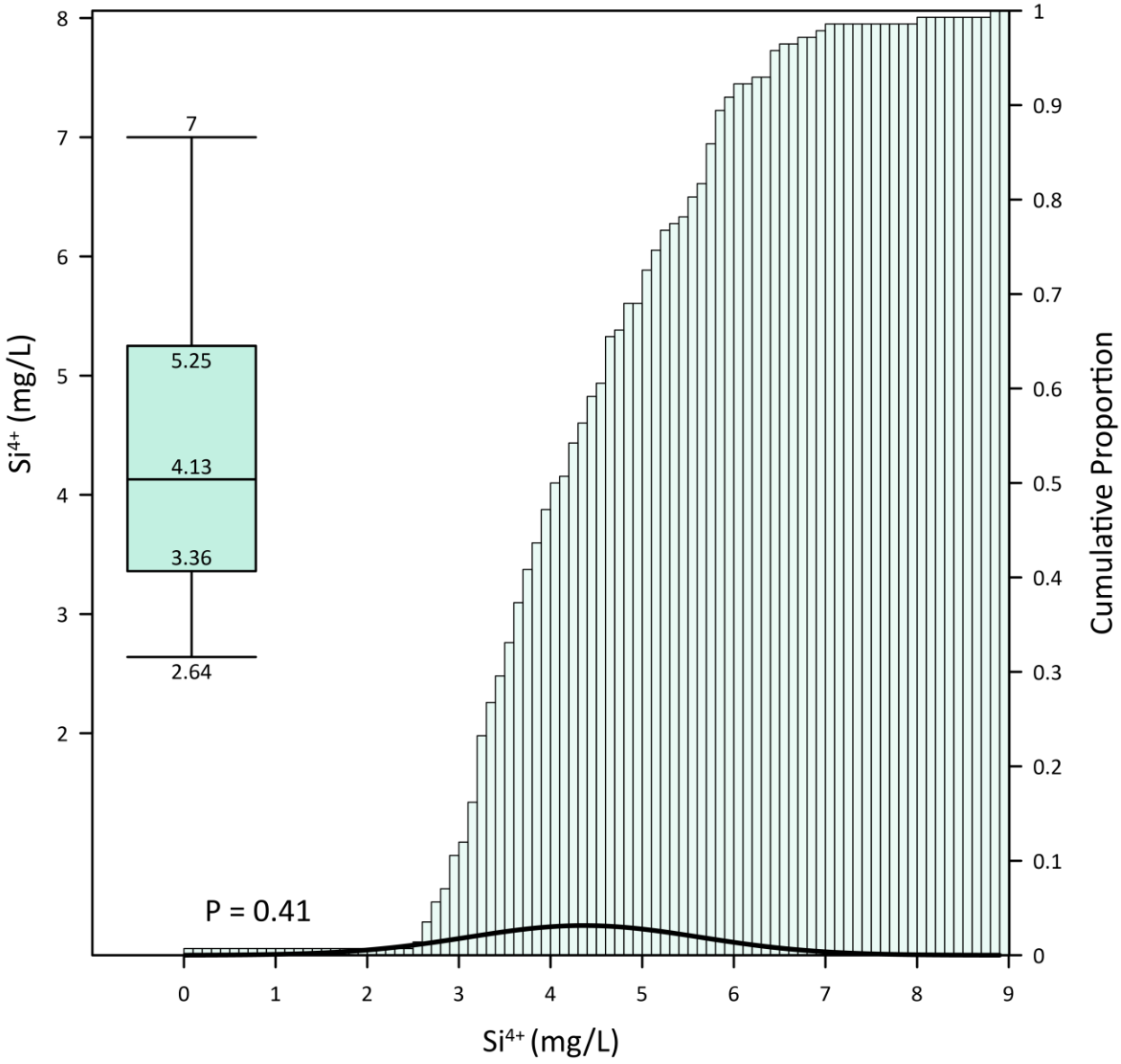

Figure C-16: Baseline silica concentrations in groundwater in the bedrock. The boxplot shows the median concentration on the centerline. Whiskers mark the 97.5th and 2.5th percentiles. Silicon concentrations are normally distributed, with a p-value of 0.41.

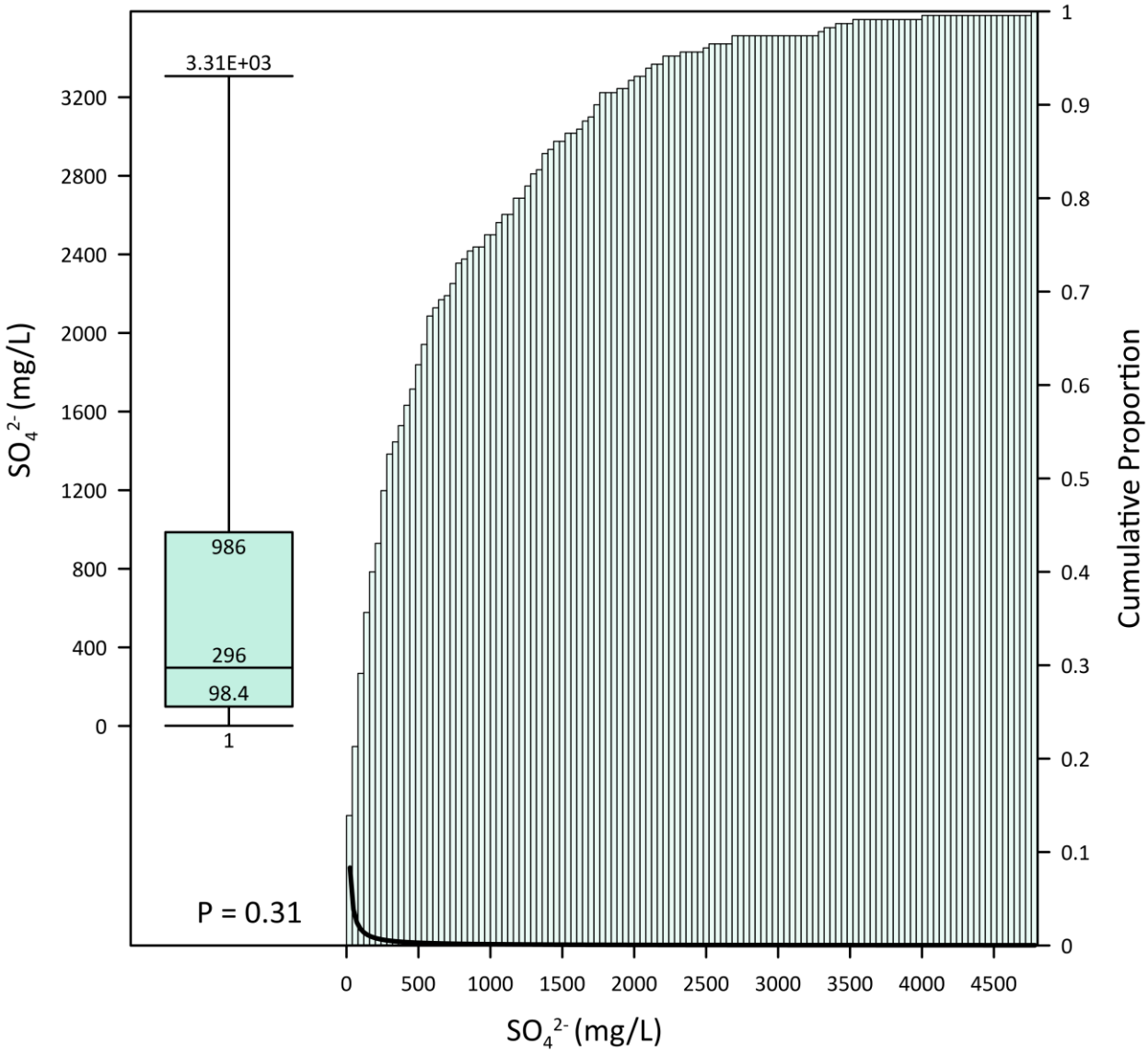

Figure C-17: Baseline sulphate concentrations in groundwater in the bedrock. The boxplot shows the median concentration on the centerline. Whiskers mark the 97.5th and 2.5th percentiles. The distribution of sulphate concentrations follow a power function, with a p-value of 0.31.

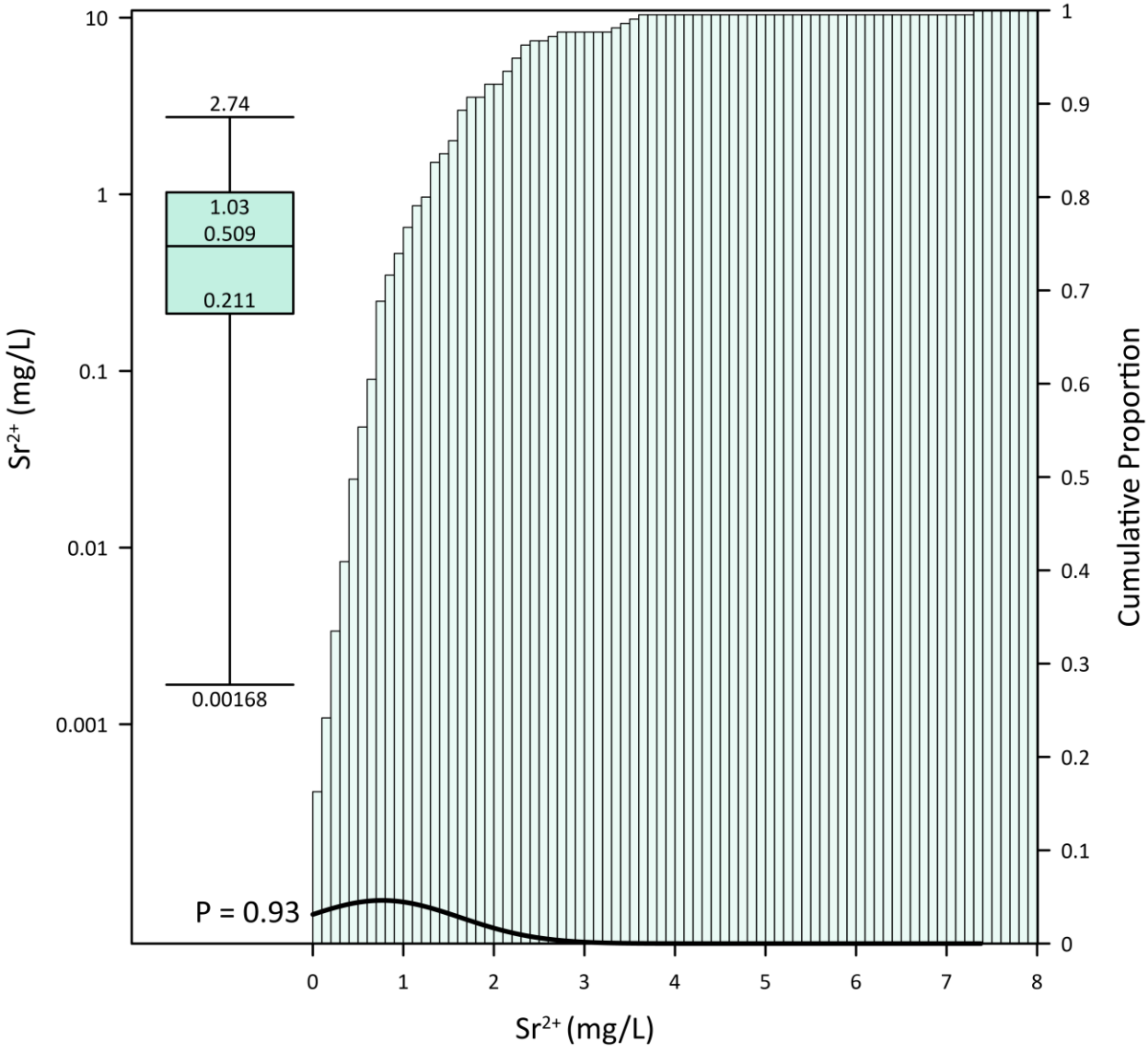

Figure C-18: Baseline strontium concentrations in groundwater in the bedrock. The boxplot shows the median concentration on the centerline. Whiskers mark the 97.5th and 2.5th percentiles. Strontium concentrations are normally distributed, with a p-value of 0.31.

15.3. Isotopic Composition

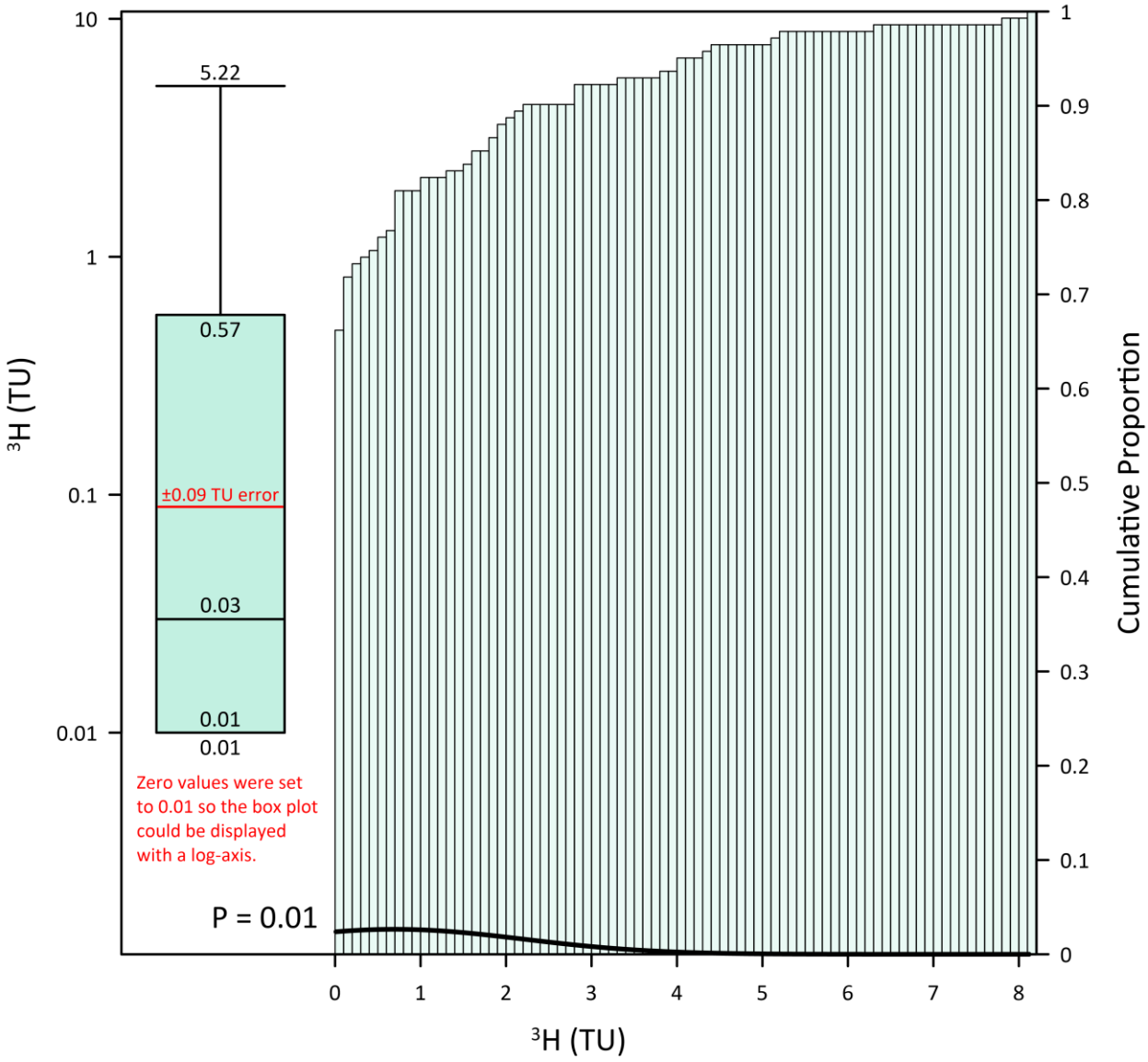

Figure C-19: Baseline tritium concentrations in groundwater in the bedrock. The scale of the boxplot is logarithmic, and the median concentration is shown on the centerline. Zero values were set to 0.01 so that the boxplot axis could be set to log-scale. Whiskers mark the 97.5th and 2.5th percentiles. Tritium concentrations are poorly normally distributed, with a p-value of 0.01. The red line marks the median error in tritium concentrations.

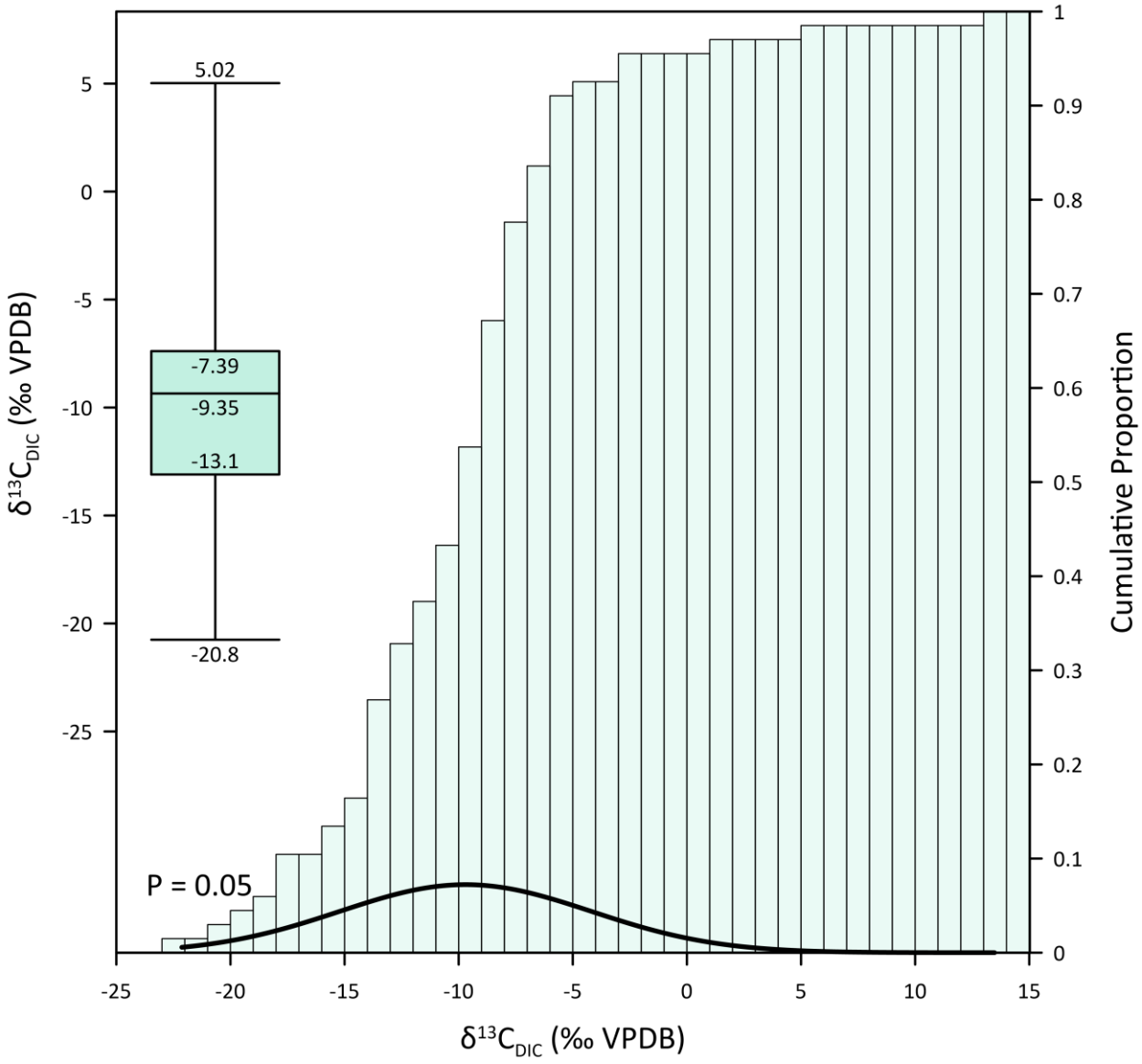

Figure C-20: The baseline $\delta^{13}C_{DIC}$ composition of groundwater in the bedrock. The boxplot shows the median value on the centerline. Whiskers mark the 97.5th and 2.5th percentiles. $\delta^{13}C_{DIC}$ values are normally distributed with a p-value of 0.05.

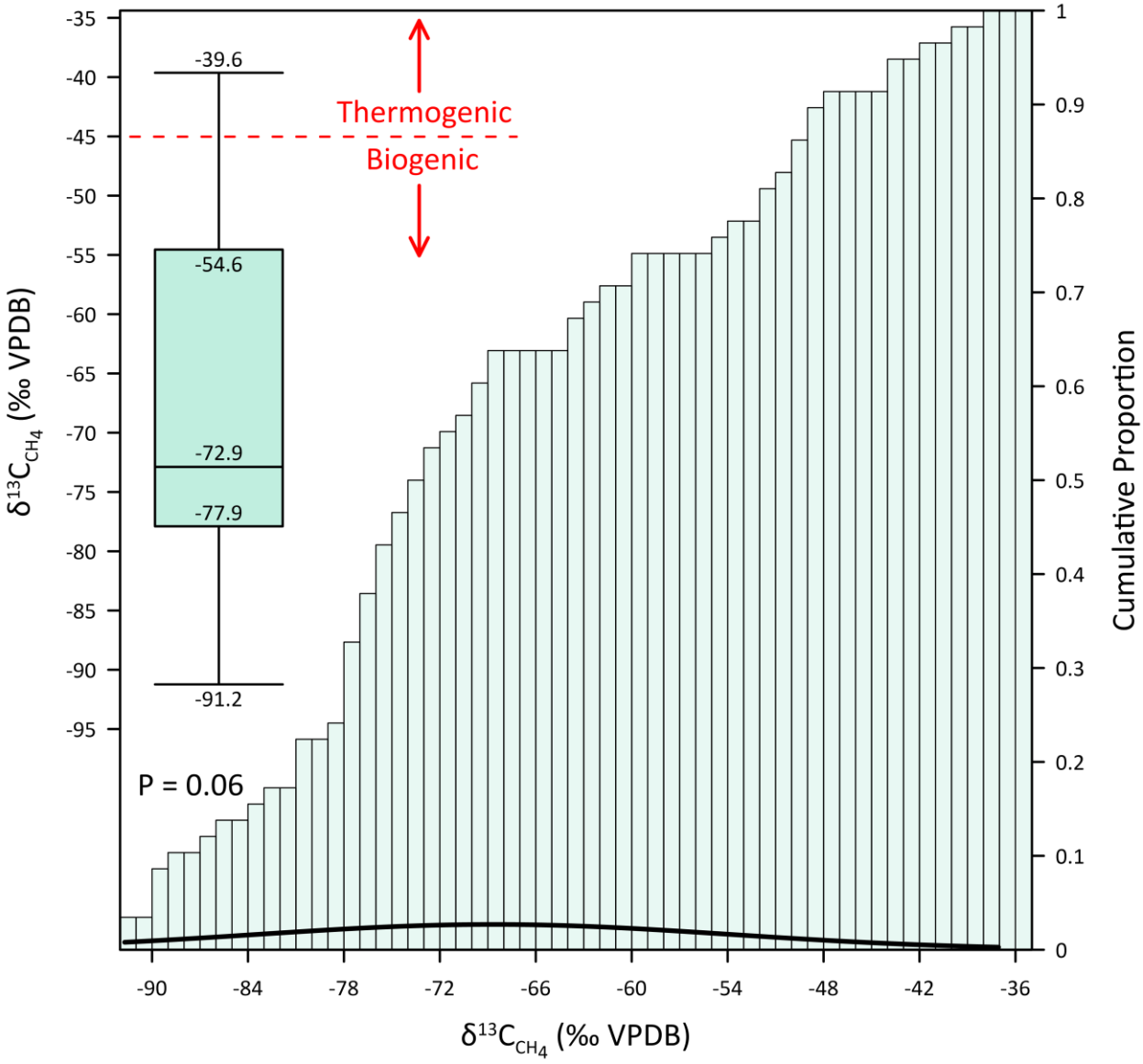

Figure C-21: The baseline $\delta^{13}C_{CH4}$ composition of groundwater in the bedrock. The boxplot shows the median value on the centerline. Whiskers mark the 97.5th and 2.5th percentiles. $\delta^{13}C_{CH4}$ values are normally distributed, with a p-value of 0.06. The red dashed line marks the boundary of thermogenic and biogenic $\delta^{13}C_{CH4}$ methane values. However, there is cross-over between the values, so the boundary is approximate.

15.4. Gas Composition

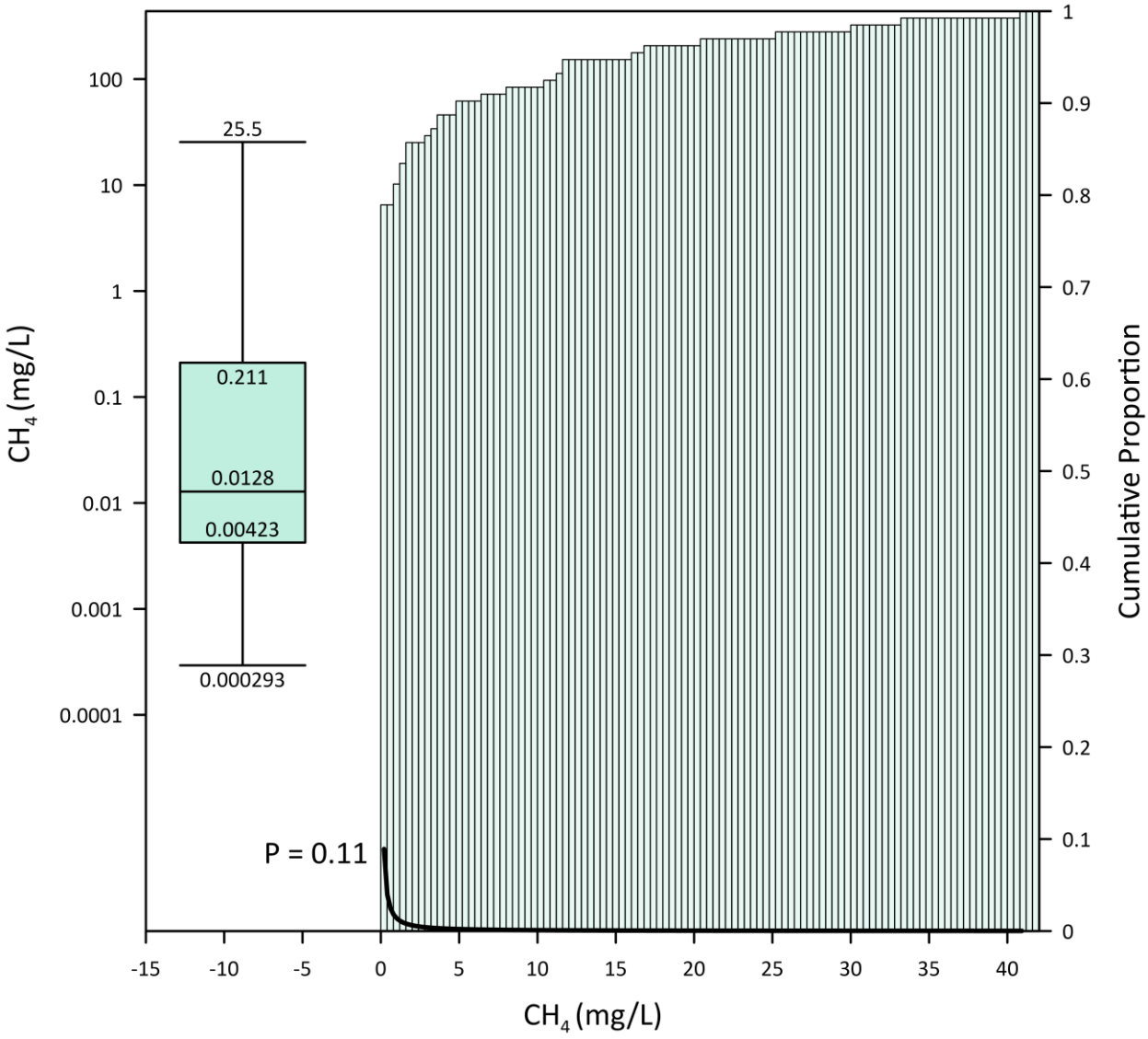

Figure C-22: Baseline methane concentrations in groundwater in the bedrock. The boxplot shows the median concentration on the centerline. Whiskers mark the 97.5th and 2.5th percentiles. The distribution of methane concentrations follows a power function, with a p-value of 0.11.

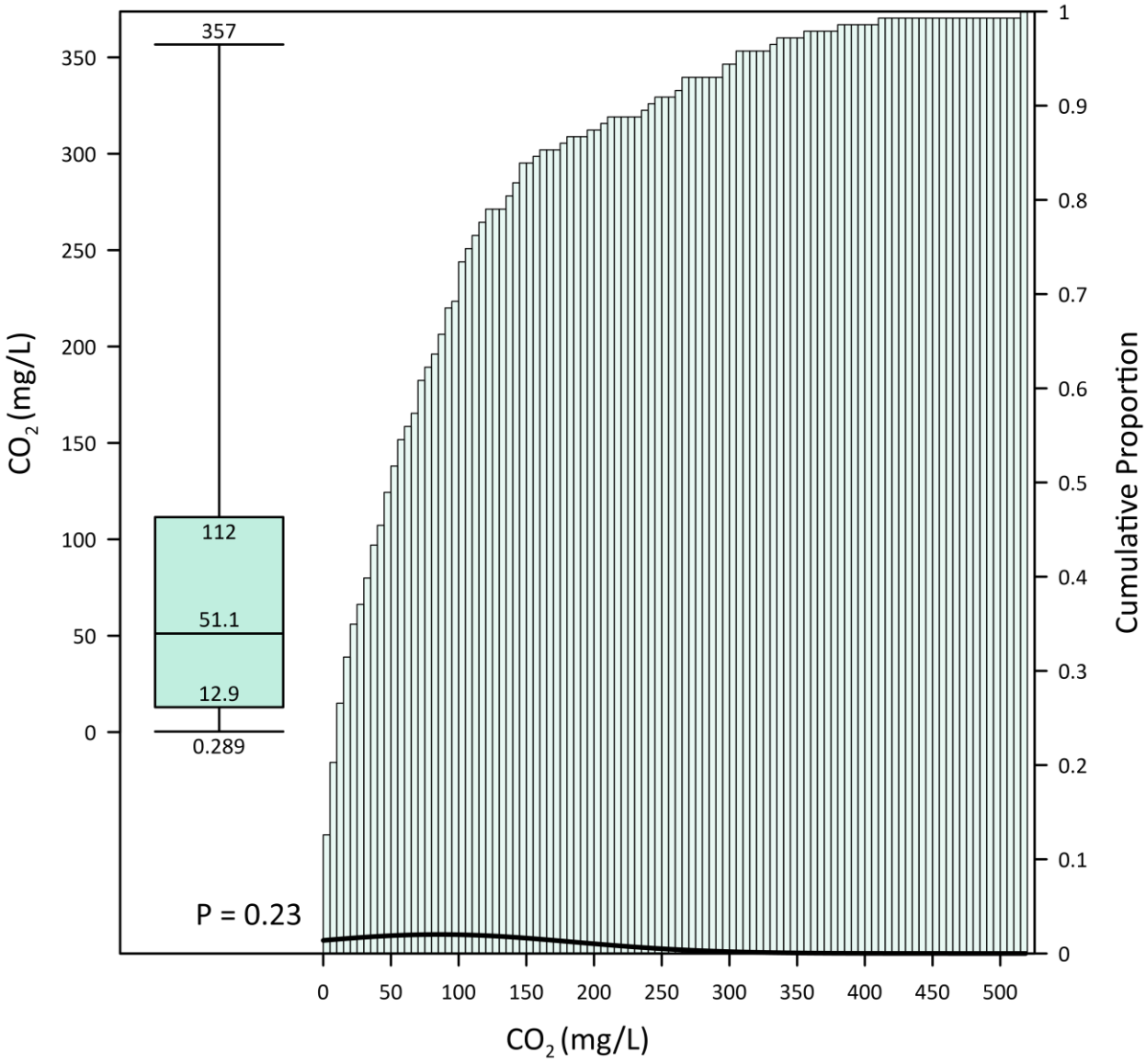

Figure C-23: Baseline carbon dioxide concentrations in groundwater in the bedrock. The boxplot shows the median concentration on the centerline. Whiskers mark the 97.5th and 2.5th percentiles. Carbon dioxide concentrations are normally distributed, with a p-value of 0.23.